The Pennsylvania State University
The Graduate School
College of Engineering

DEVELOPMENT OF ALGORITHMS FOR ROBUST ONLINE OPTIMAL PERIODIC CONTROL IN THE PRESENCE OF PLANT PARAMETER UNCERTAINTY

A Dissertation in
Mechanical Engineering
by
Mohammad Ghanaatpishe

Submitted in Partial Fulfillment
of the Requirements
for the Degree of

Doctor of Philosophy

December 2017

The dissertation of Mohammad Ghanaatpishe was reviewed and approved* by the following:

Hosam K. Fathy
Associate Professor of Mechanical Engineering
Dissertation Advisor, Chair of Committee

Crsitopher D. Rahn
Professor of Mechanical Engineering

Bo Cheng
Associate Professor of Mechanical Engineering

Constantino Lagoa
Professor of Electrical Engineering

Karen A. Thole
Professor of Mechanical Engineering
Department Head of Mechanical and Nuclear Engineering

*Signatures are on file in the Graduate School.

Abstract

This dissertation furnishes a framework addressing the challenges of designing online algorithms for optimal periodic control (OPC). The proposed framework aims to expand the use of the OPC discipline, moving beyond the traditional offline optimization of periodic control trajectories for plants with known dynamics, and instead focusing on the online and stable periodic optimal control of plants whose dynamics are not fully known a priori. More specifically, the design objective of this online framework is to discover, achieve, and maintain the best cyclic performance level of a given engineering system, despite the potential open-loop instabilities of the underlying dynamics and unknown plant model parameters.

This dissertation is motivated by the exciting applications of the OPC theory in nature and engineering. This research area has been studied for nearly 6 decades. The literature has developed mathematical tests for properness: a condition under which there is a periodic trajectory that in average outperforms the best equilibrium point of a given dynamic system. Necessary and sufficient conditions have also been developed to analyze the optimality of a candidate periodic trajectory. Furthermore, researchers have proposed direct and indirect algorithms for the numerical computation of the OPC problem solutions. However, a common limitation of the existing OPC research lies in the fact that traditional OPC has been applied to the offline optimization of trajectories for systems with known dynamics. This stands in contrast both to the goal of this dissertation and to several examples of OPC practices that are observed in nature.

This dissertation seeks to address the above limitations by proposing an adaptive framework that enables engineering systems to achieve robust online periodic optimal control. The steps leading to the development of the online framework are illustrated/validated on an insect flight model, a benchmark drug delivery application problem from the OPC literature, and a vehicle suspension example. The first two of these application problems are known to benefit from OPC, while the oscillatory behavior is enforced on the last application through a periodic road roughness profile. The work of this dissertation builds on established techniques

in control theory including variational calculus methods, direct optimal control, indirect adaptive control, Floquet stability, Lyapunov stability, and feedback linearization. However, it combines these tools in a manner that will result in a novel framework for achieving robust online periodic optimality.

The development of algorithms in this dissertation follows a progressive trend towards the end framework. This is also reflected through the organization of the dissertation as explained below.

- **Chapter 2** introduces a properness test from the OPC literature to determine whether periodic operations can offer any advantage over the best steady-state performance. The application of this tool is demonstrated on a flapping flight model of the fruit fly.

- **Chapter 3** incorporates variational calculus methods to discover the structure of the solution trajectory of the periodic drug delivery application, once OPC properness is established. Also, a discretization approach based on the discovered structure is shown to reduce the computational requirements of solving the OPC problem offline.

- **Chapter 4** develops an adaptive controller to achieve online OPC for the drug delivery application in the presence of unknown plant parameters. This controller is dependent on the innate open-loop stability of the drug absorption dynamics and the local convergence of the closed loop scheme is shown using Floquet analysis.

- **Chapter 5** designs a novel adaptive tracking algorithm grounded in principles of feedback linearization theory. A Lyapunov stability analysis establishes global convergence to a target trajectory dependent on unknown plant parameters. A numerical active vehicle suspension example is employed to showcase the performance of the algorithm.

- **Chapter 6** finally presents the online OPC framework of this dissertation with the adaptive tracking controller of Chapter 5 incorporated at its heart. The performance of the closed-loop scheme is demonstrated on the benchmark drug delivery application.

The proposed online OPC framework (i) provides an online estimate of the uncertain plant parameters, (ii) efficiently solves for and employs a family of precalculated optimal periodic solutions indexed by the plant parameter estimates, and (iii) offers an input adaptation mechanism which enables asymptotic and stable tracking of a dynamically-changing target trajectory constructed from this family of optimal solutions. These tasks collectively are shown to enable stable and global convergence of the closed loop system towards its optimal periodic path.

Table of Contents

List of Figures

List of Tables

Acknowledgments

First and foremost, I need to thank my family for their unconditional love and support for me. My father, Hossein, has always been the greatest advocate of my academic success. Without his never-ending encouragement, I would not be the person I am today. My mother, Gity, is the embodiment of self-sacrifice. If I show patience when facing difficulties in life and have the self-confidence to overcome the challenges on my path, it is all thanks to her. I would not be exaggerating to say that my loving sister, Bahare, is the best there is in the universe. I am so lucky to have her self-less and endless support. Her dedication to conquering what she sets her mind to have always inspired me. Last not but the least, I thank my smart little brother, Ali, for all the help and advice he has provided me in my journey towards my academic goals. There is not a single person in the whole that gets me as much as he does and I am blessed to have him in my life.

Furthermore, I would like to express my sincere gratitude to my advisor Dr. Hosam Fathy not only for his technical support and superb mentorship, but also for believing in me and being a source of inspiration and a role model for me. I am very honored for having the opportunity to work under his supervision, and will always brag about being a member of his research group, as his students keep producing work that revolutionizes the optimal control practices in energy storage and management areas. I would also like to thank my esteemed committee members, Dr. Chris Rahn, Dr. Bo Cheng, and Dr. Constantino Lagoa for sharing their invaluable input, and critical feedback. Their willingness to share their expertise has substantially improved the quality of this dissertation.

I owe a big thank you to my amazing fellow labmates in the COOL, too. I could not have asked for a better research lab to be a member of. Not only my smart labmates helped me grow intellectually with their stimulating discussions and insightful feedback, we also had a lot of fun and became very close friends. I need to specially thank my labmates Donald, Abdullah, Sergio, and Ji for how much their friendship helped me grow as an individual during my graduate studies.

I also met many other great people here at PennState, without whom I would

not have enjoyed grad school nearly as much. My dear friends Behzad and Hamed are among these wonderful friends, and we shared so many wonderful memories together. There is so much I learned from them and they were of great help in motivating me to push through the bottlenecks I would face in my work every now and then. My fantastic pseudo-labmates, Wahba and Nicolas, are other examples of friends for life that PennState has gifted me.

Finally, I would like to acknowledge the National Science Foundation for their financial support during my time as a graduate student.

Chapter 1
Introduction

1.1 Motivation

This dissertation aims to address the challenge of designing robust algorithms for online optimal periodic control (OPC) by proposing an online framework grounded in the principles of optimal control, adaptive control, and feedback linearization theory. The presented framework intends to expand the application horizon of the OPC discipline, moving beyond the traditional offline optimization of periodic control trajectories for plants with known dynamics, and instead focusing on the online periodic optimal control of plants whose dynamics and disturbances are not fully known *a priori*. The developed algorithms will be validated on a benchmark application problem from the OPC literature that is known to benefit from OPC, but requires the ability to adapt to varying plant models.

Optimal periodic control theory has various exciting applications in nature and engineering. The optimal control of certain chemical processes is periodic, for instance: a fact that has been recognized for decades and motivated some of the earliest contributions to OPC [1–6]. The optimal harvesting of ecosystems with periodic dynamics, such as fisheries, has also been examined using the tools of OPC [7–10]. In hypersonic flight, the speed for maximum engine efficiency is usually different from the speed for minimum drag. Consequently, periodic optimal flight has been shown to improve overall airplane fuel efficiency compared to steady flight [11–15]. Fuel economy in vehicle cruise has also been studied as an OPC problem [16]. The "pulse and glide" cruising strategies for improving fuel economy for cars with continuously varying [17] and step-gear [18] transmission

systems are among other important engineering applications of OPC. The tools of optimal periodic control have been used for finding energy-minimizing, open-loop stable periodic gait trajectories for a walking robot [19–21]. These tools have additionally been employed in studying economic systems [22, 23], and maximizing energy harvesting in airborne wind turbines [24, 25]. Optimal periodic control has also been used for designing the acceleration, braking, and gear shift policy for a test automobile to maximize the average speed with which it is able to periodically traverse a test track [26]. Finally, the idea of glider dynamic soaring and exploitation of wind gradients for nearly powerless flight has gained the attention of researchers as an application of the OPC theory [27]. This idea is inspired by the study of flight of birds such as albatross [28].

1.2 Literature Review

A formal statement of a deterministic time-invariant optimal periodic control problem is usually given as follows.

$$\max_{x,u,T} \left\{ J = \frac{1}{T} \int_0^T L(x,u)\, dt \right\}$$

$$\begin{aligned} &\text{subject to:} \\ &x(0) = x(T) && \textit{(Periodicity Constraint)} \\ &\dot{x} = f(x,u) && \textit{(System Dynamics)} \\ &g(x,u) \leq 0 && \textit{(Input/State Constraints)} \\ &\int_0^T h(x,u)\, dt \leq 0 && \textit{(Integral Constraints)} \end{aligned} \tag{1.1}$$

where u is a piecewise continuous function of time, f is Lipschitz continuous in x and continuous in u, and L is the instantaneous performance index (*a.k.a* Lagrangian) for the problem.

The existing literature on periodic optimal control has studied the solution characteristics of, and developed solution algorithms for different variations of the above OPC problem. The literature spans over 6 decades and includes three historical phases of investigation and discovery [29–46]:

Phase 1–*Optimality Conditions and Properness:* Much of the OPC literature builds on Bailey and Horn's pioneering examination of chemical production

processes [2]. They showed that periodic cycling of some chemical reaction's temperature gives a performance superior to the best constant temperature treatment [2]. Bailey and Horn's work motivates two intertwined directions of study in the literature. First, researchers use the calculus of variations to prove the existence and uniqueness of solutions to different benchmark periodic optimal control problems, and derive necessary and sufficient conditions for their optimality [29–33]. Second, researchers also examine the conditions for "properness" in periodic optimal control [34–36]. A periodic optimal control problem is *proper* if its periodic solution is superior to its optimal steady state (OSS) solution. A subset of proper problems is the set of *locally proper* problems, where there exists a weak variation of OSS that improves the performance. Seminal work by Bittanti *et al.* presents the π test for whether or not a periodic optimal control problem is locally proper [34]. Further work by Bernstein and Gilbert establishes regularity conditions that must be met in order for the π test to be valid [35, 36].

Phase 2–*Offline Solution of Periodic Optimal Control Problems:* By the mid-1980s, the community's understanding of (i) the necessary/sufficient conditions for periodic control optimality and (ii) the conditions under which a OPC problem is proper had matured [29–36]. However, there was still a gap in the literature: given a proper periodic optimal control problem, how does one solve this problem computationally?

The literature provides several approaches for solving periodic optimal control problems numerically. One can classify these approaches into direct versus indirect methods. Direct methods for solving optimal control problems proceed by discretizing the problems' underlying feedback gains and/or time-varying signals (*e.g.*, state variables, co-state variables, input variables, etc.). This makes it possible to reformulate the optimal control problems as nonlinear programs, then solve them using the classical tools of nonlinear programming. Varga and Pieters' research provides one optimization approach: they use a gradient-based search to directly optimize the time-dependent feedback gains in a periodic optimal output feedback problem [37]. Chen *et al.*'s work provides another example of direct optimization: they parameterize the input trajectory over a sinusoidal and a piecewise-constant function basis, and solve the problem numerically using analytically found Jacobians of the objective and cost functions [38]. In an indirect optimal control method, one typically begins by deriving necessary conditions for control optimality

using a tool such as the Pontryagin Maximum Principle (PMP). This furnishes a "two-point boundary value" problem that one then solves to obtain candidate optimal trajectories. Evans *et al.*, for instance, derive necessary and sufficient conditions for periodic optimal control, then solve the resulting two-point boundary value problem using an asymptotic series approach [39]. Similarly, Speyer and Evans develop a shooting method that uses some of the optimality conditions to construct and traverse through a one-parameter family of closed orbits in search of the optimal solution [40]. Val Noorden *et al.*'s work provides another example of indirect optimization, where they utilized an efficient Newton-Picard shooting method to obtain closed state and adjoint trajectories. A gradient descent rule is then used to modify the input trajectory and climb these orbits towards the optimal solution [41].

Phase 3–*Online Solution of Periodic Optimal Control Problems:* The above literature on the computational solution of OPC problems is important, but suffers from at least two weaknesses. First, the computational burden of solving OPC problems can be prohibitive, particularly for systems with many state and input variables. Second, the optimal control policies furnished by most of the above methods are open-loop, and lack the robustness to modeling errors that one would ideally seek in a periodic optimal controller. Only recently has the literature begun tackling these two challenges. Specifically, recent research by Varigonda *et al.* exploits differential flatness to reduce the computational complexity of OPC significantly, for the first time [42, 43]. Varigonda *et al.*'s work focuses on offline control optimization, but it has inspired more recent research on online periodic optimal control by Guay *et al.* [44, 45]. In this work, Guay *et al.* consider a differentially flat dynamic system whose periodic optimal control is desired [44, 45]. Like Varigonda *et al.*, they find flat system outputs and discretize these outputs trajectories using truncated Fourier series to enable direct control policy optimization. However, their work departs from Varigonda *et al.*'s in its use of extremum-seeking control to optimize the Fourier basis function weights online [44, 45]. More recent work by Höffner *et al.* extends this research by construction and parameterization of a Hamiltonian reference model. The parameterized limit cycle of the Hamiltonian model is then optimized using an extremum-seeking algorithm and back-stepping is employed to ensure that the resulting periodic trajectory is tracked in a stable manner [46]. Finally, Azzato and Krawczyk employ stochastic

dynamic programming to develop feedback laws *a priori* to optimize the ensemble average performance in a stochastic OPC problem [47]

The fact that researchers are beginning to explore online OPC strategies underscores the importance of the proposed work. However, a common limitation of existing OPC research lies in the fact that traditional OPC has been applied to offline optimization of trajectories for systems with known dynamics and disturbances. This stands in contrast both to the research objective of this dissertation and to several examples of OPC that are observed in nature. The existing OPC literature is specifically weak in terms of its potential for applicability to online optimization problems.There are at least five manifestations of this weakness:

- Most existing OPC work focuses on offline optimization using indirect optimal control (*e.g.*, Pontryagin methods), and fails to offer a framework for implementing the resulting solutions online.

- The few papers that do explore online OPC consistently use direct optimal control methods: they express the optimal state and input trajectories in terms of Fourier series, then optimize the coefficients of these series using nonlinear programming. While this strategy certainly has its appeal, it misses an opportunity to exploit indirect methods (*e.g.*, Pontryagin methods) to guide the choice of control policy discretization.

- Existing online OPC methods typically assume the optimal control policies' time periods to be known. This is reasonable in the context of problems where plant dynamics and disturbances are themselves periodic, with known time periods (*e.g.*, periodic treatment of diabetes). However, this assumption is not reasonable for problems where the period of the optimal control policy is not known *a priori*, and may change based on plant and disturbance parameters (*e.g.*, periodic energy-harvesting flight).

- The majority of the existing online OPC literature assumes that the underlying plant dynamics are known exactly, and offers no guarantees of the robust achievement of optimal periodic orbits in the presence of plant modeling uncertainties. In the very few bodies of work that do consider stochasticity, the controllers do not attempt to estimate and adapt to the unknown dynamics of the plants.

- Most existing online OPC algorithms assume open-loop stable plant dynamics. In these works, with the application of the optimal periodic periodic input trajectory, the optimal solution orbits are essentially considered to be limit cycles with a global region of attraction. This assumption is however rarely met in nonlinear dynamic systems, where adaption of the control parameters can instigate instability issues.

1.3 Contributions

Inspired by the need in several engineering applications to execute periodic optimal control in the presence of changing conditions, the overarching goal of this dissertation is to offer a computationally efficient framework that enables achievement of robust online periodic optimal control. The algorithms developed in this dissertation build on established tools in control theory including variational calculus methods, direct optimal control, indirect adaptive control, Floquet stability, Lyapunov stability, and feedback linearization. However, these tools are combined in a manner that will result in a novel framework for achieving robust online periodic optimality.

This dissertation first incorporates the π test for assessing the relative efficiency of revolving and flapping wings in insect hovering flight models. While the OPC literature already includes numerous examples to which the π test has been applied, the novelty of the work mostly stems from its exciting application problem. Tackling an OPC problem before establishing its properness is a futile effort. Hence, this contribution also acts as stepping stone and constitutes a foundation for the main body of this dissertation. The insect flight literature already offers extensive experimental [48–51] and simulation-based [52–55] comparative studies on the effectiveness of the insect flapping flight and rotary flight as the standard engineering mechanism for controlled hovering flight. A collective conclusion from all the above studies is that the potential advantages of flapping flight is influenced by many factors such as insect size, wing morphology, kinematic flight constraints, aerodynamic efficiency metrics, etc. This, combined with the design complexities of experimental setups and computational power requirements of numerical approaches, has hindered the advancement of bio-inspired micro air vehicles. We address this issue by proposing the application of the π test from the OPC theory as

a simple tool to analyze the impact of local periodic perturbations around an optimized rotary flight trajectory. While this test does not quantify the extent of improvement achievable via flapping flight, its result can be used to identify the salient aerodynamic effects and influential flight parameters for a given study, thus reducing the subsequent experimentations and/or computational efforts needed. We also solve for the optimal lift-power Pareto fronts of the two flight regimes, confirming the results predicted by the π test.

This dissertation next examines the shaping of nicotine's delivery to maximize its long-term cardio-accelerating effects. This application problem has been extensively examined in the existing OPC literature [44–46, 56, 57]. Previous research: (i) furnishes a pharmacokinetic-pharmacodynamic (PKPD) model of this drug's metabolism [58]; (ii) shows that the drug delivery problem is proper, meaning that its optimal solution is periodic [56]; (iii) shows that the underlying PKPD model is differentially flat [56]; and (iv) exploits differential flatness to solve the problem by optimizing the coefficients of a truncated Fourier expansion of the flat output trajectory [56]. The work in this article provides insight into the structure of the theoretical solution to this offline OPC problem. First, we argue for the existence of a bijection between feasible periodic input and state trajectories of the problem. Second, we exploit Pontryagin's maximum principle to show that the optimal periodic solution has a bang-singular-bang structure. Building on these insights, our work also proposes two efficient discretization methods for offline solution of this OPC problem. One method uses nonlinear programming to optimize the states at which the optimal solution transitions between the different solution arcs. The second method approximates the control input trajectory as piecewise constant, and optimizes the discrete values of the input sequence.

While the existing solution methods [44–46,56,57] depend on the exact knowledge of the drug's model, the human body's metabolism varies from one patient to another, affecting the shape of the maximum efficacy trajectory. This creates a need for online solution methods for the drug delivery problem, which can handle unknown plant parameters. Our work addresses this issue by developing a self-tuning regulation scheme that assumes the structure of the system dynamics is known, but takes parameter uncertainty into account. The uncertain parameters are estimated using gradient based methods and the estimates are used to adapt the shape of the input according to a bank of optimal solution trajectories. The

controller converges very quickly, and its local convergence to the optimal solution is shown using Floquet stability analysis. While simulation results demonstrate the effectiveness of this controller in achieving online OPC, it lacks any active tracking mechanism and its convergence heavily relies on the asymptotic stability of the Linear, Time-Invariant (LTI) dynamics of the drug delivery. An approach for generalization of the scheme to the class of convergent nonlinear dynamic systems is also outlined. However, the asymptotic stability property remains a critical to the stability of the controller.

In an attempt to relax the above open-loop stability requirement, the dissertation next develops an adaptive control synthesis technique for tracking output target trajectories which are potentially dependent on unknown parameters in the plant model. The proposed tracking algorithm is designed for a class of state feedback linearizable systems, for which the strict uncertainty matching condition is met. The literature already offers well-established regulation and tracking algorithms which exploit feedback linearization techniques and account for parametric uncertainties in the plant dynamics. These algorithms either rely on static feedback based on the certainty equivalence principle [59–62], or employ dynamic feedback rules based on back-stepping techniques [63–67]. However, all these algorithms assume that the given reference output trajectory and/or the desired reference model dynamics are independent of the uncertain plant model parameters. This assumption limits the performance of the existing adaptive feedback linearizing controllers in a large number of important practical examples. The proposed adaptive tracking algorithm, in contrast, allows for the appearance of unknown plant parameters in the reference output trajectory (or the reference dynamic model). The algorithm presented is shown to always achieve bounded and asymptotic tracking of an estimate of the target trajectory. Additionally, when the signals used in the algorithm's estimation law are persistently exciting, Lyapunov analysis guaranties asymptotic convergence to the true target trajectory. The performance of the proposed algorithm is demonstrated by employing it in a numerical simulation of an active vehicle suspension system.

Lastly, this dissertation proposes an online adaptive control framework for tracking optimal periodic trajectories of feedback linearizable plants with unknown parameters. As explained earlier, the existing online OPC algorithms either assume perfectly known plant models and ensure robust tracking of the optimal solution,

or allow for the appearance of unknown parameters in the plant model, but rely on the plant's open-loop stability for implementation of the optimal solution. This dissertation, in contrast, develops an adaptive feedback linearizing algorithm to simultaneously estimate and track the optimal orbit solving the OPC problem. Inheriting the stability properties of the adaptive tracking algorithm, the system trajectories under this framework always remain bounded and asymptotically approach the periodic solution corresponding to an estimate of the unknown plant parameter vector. Furthermore, when the regressor vector of the parameter estimation law is persistently exciting, global convergence to the true periodic solution trajectory is guaranteed. The dissertation also includes a numerical implementation of the proposed framework on the benchmark periodic drug delivery application.

The above contributions follow a progressive trend towards the ultimate goal of this dissertation: an adaptive framework for online and stable OPC in the presence of plant parameter uncertainties. This is also reflected through the organization of the remainder of the dissertation as described below.

- **Chapter 2** introduces a properness test from the OPC literature to determine whether periodic operations can offer any advantage over the best steady-state performance. The application of this tool is demonstrated on a flapping flight model of the fruit fly.

- **Chapter 3** incorporates variational calculus methods to discover the structure of the solution trajectory of the periodic drug delivery application, once OPC properness is established. Also, a discretization approach based on the discovered structure is shown to reduce the computational requirements of solving the OPC problem offline.

- **Chapter 4** develops an adaptive controller to achieve online OPC for the drug delivery application in the presence of unknown plant parameters. This controller is dependent on the innate open-loop stability of the drug absorption dynamics and the local convergence of the closed loop scheme is shown using Floquet analysis.

- **Chapter 5** designs a novel adaptive tracking algorithm rooted in the principles of feedback linearization theory. A Lyapunov stability analysis establishes

global convergence to a target trajectory dependent on unknown plant parameters assuming persistence of excitation. A numerical active vehicle suspension example is employed to showcase the performance of the developed tracking algorithm.

- **Chapter 6** presents the online OPC framework of this dissertation with the adaptive tracking controller of Chapter 5 incorporated at its heart. The performance of the closed-loop scheme is demonstrated on the benchmark drug delivery application problem.

The remainder of this dissertation highlights the contribution of this work to the OPC literature in the order specified above. Finally, Chapter 7 provides a summary of these contributions and some concluding remarks.

Chapter 2
Rotary vs. Flapping Flight: An Application Study for Optimal Periodic Control Theory

2.1 Introduction

This chapter proposes the application of the π test from the OPC literature as a systematic procedure for comparing the aerodynamic efficiency of rotary wings (as the steady-state hovering mechanism) and flapping wings (as the unsteady periodic hovering mechanism) in insect flight models. At their extremely small size compared to commercial aircrafts, flying insects experience air flow regimes with low Reynolds numbers. This results in a significant enhancement of viscous effects and reduction of the aerodynamic efficiencies to the extent of rendering the steady-state means of lift generation insufficient for sustained hovering flight. Consequently, the bio-inspired insect flapping flight has recently gained a great amount of interest in the design of Micro Air Vehicles (MAVs) capable of controlled hovering flight.

The unsteady lift force mechanisms exploited by flying insects has been investigated by many researchers [48,68,69]. The literature also offers extensive studies on the identification, characterization, and even optimal harvesting of these unsteady phenomena, which offers the possibility of performance improvement via flapping flight used by various insects. The research contributions in this regard can be categorized into experimental and numerical studies.

- The experimental works involve direct measurements of instantaneous aerodynamic forces on actual insect wings or aerodynamically-scaled robotic wings. For instance, Dickinson *et al.*'s setup consists of a scaled robotic wing submerged inside an oil tank to represent aerodynamics of the fruit fly [48]. Using a two-dimensional force sensor mounted at the base of the wing, they characterize delayed stall, rotational circulation, and wake capture as three major unsteady mechanism enhancing aerodynamic performance in flapping flight. The same setup is used in [49] to shape the flight kinematics for maximization of average lift force through these unsteady effects. Lentink and Dickinson, however, show that a sinusoidally flapping fruit-fly wing has significantly lower efficiency compared with a steady revolving wing motion in the range of Reynolds number (Re) between 110 and 14000 [50]. Additionally, Mayo and Leishman surveyed several types of MAV concepts and compared them against the hovering flight of avian and entomological fliers using power loading and effective disk loading as performance metrics [51]. They concluded that conventional rotor systems have higher hovering efficiencies relative to the existing bio-mimetic flapping fliers, but are similar or less efficient than birds and insects capable of hovering flight.

- The numerical contributions to the literature in contrast rely on simplified empirical models or complex first-principle models for their analysis. Berman and Wang, for example, investigate hovering flight of the fruit fly, bumblebee, and hawkmoth using a quasi-steady two dimensional model obtained for a free falling plate model from blade element theory [52]. They minimize the mass-specific power consumption for these insects assuming an elliptical wing geometry with sinusoidal and hyperbolic stroke and pitch angle trajectories. Nabawi and Crowther also use a quasi-steady hovering flight model to maximize the average lift force and minimize the power consumption in insect flapping flights. They show that for their model flapping wing becomes most efficient when it approaches the rotary wing motion [53]. In another example, Pesavento and Wang employ solve the Navier-Stokes (NS) equations and show that an optimized two-dimensional flapping wing motion can save up to 27% of the power required for the optimal steady flight by taking advantage of wing-wake interactions near stroke reversal [54]. Zheng *et al.* take a

multi-fidelity modeling approach towards this problem [55]. They use NS simulation results of a hovering hawkmoth to calibrate a quasi-steady model based on blade element theory. This simple empirical model is next used to optimize aerodynamic efficiency assuming sinusoidal stroke angle and wing elevation angle profiles and a hyperbolic expression for the pitch angle. These actual performance of these optimized trajectories is then analyzed using the high-fidelity NS model. Another work by the same researchers also uses the NS-based hovering hawkmoth model and show that the flapping wing configuration is only efficient for low Reynolds number kinematics ($Re < 300$), while the exact cross-point highly depends on the definition of the Reynolds number and the dimensionless force and power coefficients [70].

The above examples and many other contributions to the literature collectively suggest that there are many factors affecting the effectiveness of flapping and rotary wing motions including insect size, wing geometry and structural flexibility, kinematic constraints, and the definition of flight fitness metric. Under different circumstances, the result of comparative studies on aerodynamic efficiencies of the two flight maneuvers are different and sometimes even conflicting. This, combined with the challenges associated with the design of experimental setups that allow for instantaneous measurement of aerodynamic forces, or the heavy computational needs of accurate flow simulations and optimization schemes of the numerical approaches are among the major challenges encountered in bio-inspired MAV design realm. The work of this chapter aims to address these challenges by proposing the application of the π test developed by Bittanti *et al.* in [34]. The π test is a simple tool from the OPC theory that can be used to analyze the effect of local periodic perturbations around an optimal steady-state solution. While the application of this test does not predict the extent of improvement which can be achieved via flapping flight, its result can be used to identify the most relevant aerodynamic effects and influential flight parameters for a given application study. This helps substantially reduce the subsequent experimentations and/or computational efforts needed for determining the optimal flapping flight kinematics.

Broadly speaking, the problem of building a robust online periodic optimal controller boils down to these questions. First, is the optimal control problem at hand proper, in the sense that it can benefit from periodic control? Second, what is the structure of the optimal periodic controller? Third, how does one implement

this periodic optimal controller online in a stable manner in the presence of plant parameters/model uncertainties? The content of this chapter can be viewed as a review of the literature's existing answer to the first of these three questions with a specific focus on an exciting application problem that has not been examined using the π criterion before.

The remainder of this chapter proceeds as follows. Section 2.2 presents the π test from the OPC literature and describes how it can be used as a standard tool for comparing optimality of flapping and rotary flight configurations for a given insect model. In Section 2.3, a quasi-steady aerodynamic flight model of the fruit fly is introduced and lift generation and power consumption are selected as optimality metrics. Next, the Pareto front of optimal rotary flight solutions is found and the π test is applied at points across the set of optimal solutions (Section 2.4). Lastly, Section 2.5 formulates and solves the optimal flapping flight problem and compares its set of optimal solutions against the steady-state Pareto front of the rotary flight.

2.2 Properness and the π Test

This section formulates a standard OPC problem typically encountered in insect flight optimization problems, defines properness in the context of OPC theory, introduces the π test for assessing local properness of a problem, and finally explains how this test can be used as a tool to systematically compare the optimality of rotary and flapping flights for a given insect flight model.

An OPC problem concerns with shaping the periodic operation of a dynamic system for maximizing a time-averaged performance index and can be formulated as follows:

$$\max_{\vec{x},\vec{u},T} \left\{ J = \frac{1}{T} \int_0^T L(\vec{x},\vec{u})\, dt \right\}$$

subject to:

$$\begin{aligned}
&\dot{\vec{x}} = f(\vec{x},\vec{u}) && \textit{(System Dynaimcs)} \\
&\vec{x}(0) = \vec{x}(T), T \geq 0 && \textit{(Periodicity Constraint)} \\
&\frac{1}{T}\int_0^T h_i(\vec{x},\vec{u}) = 0, 1 \leq i \leq p && \textit{(Equality Constraints)} \\
&\frac{1}{T}\int_0^T g_i(\vec{x},\vec{u}) \leq 0, 1 \leq j \leq q && \textit{(Inequality Constraints)}
\end{aligned} \tag{2.1}$$

where $\vec{u} \in \mathbf{R}^m, \vec{x} \in \mathbf{R}^n$ represent the control input and state vectors of the dynamic system, respectively. Note that the time period of the system, T, is also among the optimization variables.

The solutions to $f(\vec{x}, \vec{u}) = \vec{0}$ constitute the set of equilibria of the system and are by definition periodic. Therefore, the elements of this set of steady state solutions are feasible to the above OPC problem, when they satisfy the integral equality/inequality constraints of Eq. (2.1) . Denote by OSS = $(\vec{x}_{oss}, \vec{u}_{oss})$ the member that maximizes the performance index within this feasible set of steady state solutions and let J_{oss} represent its corresponding objective function value. Also, let J_{opc} be the optimal objective function value of the OPC problem and hence $J_{oss} \leq J_{opc}$. The above OPC problem is said to be proper, when there is a feasible periodic trajectory with an average performance level superior to that of the OSS (i.e., $J_{oss} < J_{opc}$). Moreover, when it is also possible to improve the performance through feasible "weak" variations around the OSS solution, the OPC problem is called locally proper [34].

The literature offers different tools for analyzing optimality of the OSS solution, before solving an OPC problem. For instance, Bailey and Horn use a relaxed steady state analysis to derive a condition for superiority of a rapidly switching control input over the OSS solution [29]. Hudon *et al.* focus on nonsingular OPC problems from a geometric perspective and utilize the Pontryagin Maximum Principle (PMP) and Morse theory to develop necessary conditions for existence of extremal homoclinic orbits [57]. Bittanti *et al.* derive the π test as a necessary and sufficient condition for existence of a weak perturbation around an interior OSS solution which improves the time-averaged performance [34]. Bernstein and Gilbert derive additional constraint qualification conditions for the results of the π test to hold true [35]. Later on, Colonius generalizes the π test results to OPC problems with active state constraints [71].

In light of the OPC problem stated in Eq. (2.1), this chapter focuses on the original derivation of the π test as developed by Bittanti *et al.* in [34]. As explained above this test can determine the local properness of this OPC problem and proceeds as follows. First, the scalar-valued Hamiltonian function for Eq. (2.1) is defined as:

$$H(\vec{x}, \vec{u}, \vec{\lambda}, \vec{\mu}) = L(\vec{x}, \vec{u}) + \vec{\lambda}^T f(\vec{x}, \vec{u}) + \sum_{i=1}^{p} \mu_i h_i(\vec{x}, \vec{u}) \tag{2.2}$$

where $\vec{\lambda} \in \mathbf{R}^n \vec{\mu} \in \mathbf{R}^p$ are the vector of constant Lagrange multipliers for adjoining the state equations and the average equality constraints, respectively. Then, the following set of equations must be met at the OSS solution [34].

$$\begin{aligned} H_x(\vec{x}_{oss}, \vec{u}_{oss}, \vec{\lambda}, \vec{\mu}) + \sum_{j=1}^{q} \nu_j g_{j_x}(\vec{x}_{oss}, \vec{u}_{oss}) = 0 \\ H_u(\vec{x}_{oss}, \vec{u}_{oss}, \vec{\lambda}, \vec{\mu}) + \sum_{j=1}^{q} \nu_j g_{j_u}(\vec{x}_{oss}, \vec{u}_{oss}) = 0 \end{aligned} \tag{2.3}$$

where for any $\nu_j, j \in \{1, \cdots, q\}$ represent the Lagrange multipliers of the inequality constraints and must satisfy the complimentary slackness conditions given below:

$$\begin{aligned} g_j(\vec{x}_{oss}, \vec{u}_{oss}) = 0, \nu_i \leq 0 \\ g_j(\vec{x}_{oss}, \vec{u}_{oss}) < 0, \nu_i = 0 \end{aligned} \tag{2.4}$$

Also, x and u as subindices denote partial differentiation with respect to $\vec{x}$ and $\vec{u}$, respectively. Next, the frequency-dependent $\Pi \in \mathbf{C}^{n \times n}$ matrix of the OPC problem is defined as follows:

$$\Pi(\omega) = G^T(-j\omega)PG(j\omega) + Q^T G(j\omega) + G(-j\omega)^T Q + R \tag{2.5}$$

where $j^2 = -1$ and the constant matrices of the above equation are calculated according to the following:

$$\begin{aligned} P = H_{xx}(\vec{x}_{oss}, \vec{u}_{oss}, \vec{\lambda}, \vec{\mu}) \\ Q = H_{xu}(\vec{x}_{oss}, \vec{u}_{oss}, \vec{\lambda}, \vec{\mu}) \\ R = H_{uu}(\vec{x}_{oss}, \vec{u}_{oss}, \vec{\lambda}, \vec{\mu}) \end{aligned} \tag{2.6}$$

and $G(s) = (sI - A)^{-1}B$ is the transfer function of the system dynamics linearized around the OSS with:

$$\begin{aligned} A = f_x(\vec{x}_{oss}, \vec{u}_{oss}) \\ B = f_u(\vec{x}_{oss}, \vec{u}_{oss}) \end{aligned} \tag{2.7}$$

Now, the OPC problem stated in Eq. (2.1) is locally proper, if and only if, there exists a frequency $\omega_p > 0$ for which $\Pi(\omega_p)$ is not a negative definite matrix. Roughly

speaking, $\Pi(\omega)$ is the Hessian matrix of the performance index at the OSS for weak sinusoidal periodic variations of period $T = 2\pi/\omega$ in the u_{oss}. Hence, when the OPC problem is not locally proper, the OSS solution is a maximum and the Hessian matrix $\Pi(\omega)$ is negative definite for any given positive perturbation frequency.

Note that when the linearized state matrix A has a pole of the form $s = j\omega_N$ on the imaginary axis, the expression for the Π matrix in Eq. (2.5) becomes undefined at $\omega = \omega_N$. A periodic perturbation at the system's natural frequency induces resonance behavior and violates the periodicity condition. Therefore, such variations of the control input are not permissible and the π test is still applicable to those problems.

The shaping of insect flight trajectory for optimization of a desired flight metric such as average lift force or consumed power can be posed as an OPC problem. The OSS solution to this OPC problem is the optimum within the set of rotary flight trajectories with fixed angle of attack and stroke velocity. The properness of this OPC problem determines whether flapping flight can outperform the best rotary flight pattern. If a simple application of the π test establishes that the problem is indeed proper, then the more difficult OPC problem can be solved to show the degree to which performance improvement is possible via flapping. The π test can additionally be used as an extra step in assessing the validity of insect flight models. For instance, when experiments show that flapping flight is superior why the π test does not, it may suggest that some significant mechanisms governing the interactions between the wings and the surrounding fluid have not been captured by the model at hand.

2.3 Flapping Flight Model

Similar to any other submersed object, the fluid flow around an insect wing can be adequately described by the incompressible Navier-Stokes equations [72]. Due to the difficulties associated with solving full Navier-Stokes equations for the highly complicated insect flapping maneuver, however, flight models based on quasi-steady assumptions are of significant practical utility in the literature [72]. These models typically use parameterized analytic expressions to capture various force generation and body-fluid interaction mechanisms. The models then use data from computational fluid dynamics analysis [73, 74], or experiments on actual insect

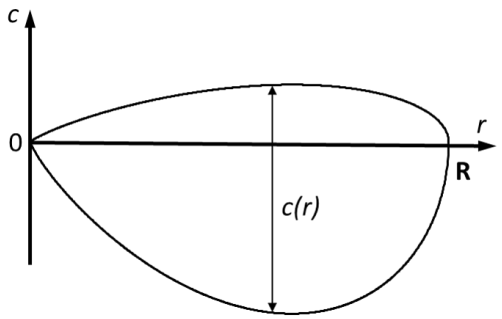

Figure 2.1. Schematic geometry of the fruit fly wing. The cord length (c) is characterized as a function of the spanwise distance from the root of the wing (r).

wings [75–77] or dynamically-scaled robotic flapping wings [48, 49, 78, 79], to find the set of model parameter values which provide the best match.

This chapter uses a semi-empirical, quasi-steady aerodynamic flight model for *Drosophila melanogaster* (commonly known as the fruit fly) adapted from [80] and [81]. Instantaneous forces on a single insect wing, in this model, is determined through a combination of the blade element theory for inviscid flows and empirical formulations assuming a rigid and thin wing structure [48, 49, 80]. The insect model used in this chapter is constrained to a two-dimensional wing motion in the stroke plane and wing elevation effects are ignored. The net instantaneous aerodynamic force acting on each wing can be divided into four different components as follows [80].

$$F_{inst} = F_{trans} + F_a + F_{rot} + F_{wc} \tag{2.8}$$

In the above equation, F_{trans} is the steady-state force generated as a consequence of the linear translation of the wing in the surrounding fluid; F_a is the additional force required for the acceleration of the virtual fluid mass moving with the wing; F_{rot} is the force component due to wing rotations and is also known as the Kramer effect; and finally F_{wc} is the component capturing the wing-wake interactions, or more specifically, the force generated by the flotation of the wing on the wake(s) created during previous half-strokes.

The F_a, F_{rot}, and F_{wc} terms are the force elements representing the unsteady effects in the model. Under the quasi-steady assumption, the added-mass force component F_a and the rotational force F_{rot} are both expressed as a "memoryless"

function of the current wing kinematics. In contrast, F_{wc} is highly dynamic and depends on the entire wing kinematics and fluid flow history. Although, wake capture is of critical importance for insect flight, the literature is yet to derive an accurate, quasi-steady or unsteady formulation of this force component. Therefore, this force component is omitted from our analysis, which leads to an underestimation of the unsteady forces in the resulting quasi-steady aerodynamic model. Consequently, the problem of optimal shaping of the flapping flight of the fruit fly studied in this chapter is conservative in exploitation of the unsteady effects. Yet, our results in Section 2.4 and 2.4 indicate that flapping flight outperforms the best rotary flight for this insect.

The above aerodynamic forces have a strong dependency on the specific shape of the insect wing. Figure 2.1 provides a schematic representation of the wing geometry used for the derivation. The wing morphology is characterized according to a beta distribution from [81] expressing dimensionless chord length as a function dimensionless distance from the root of the wing. Table 2.1 lists the numerical values used as the physical parameters of the flapping flight model. The values of different dimensionless moments of area for the assumed wing geometry are listed in Table 2.2. The remainder of this section provides expressions relating the individual quasi-steady force components to the flight kinematics and the wing geometry. These expressions are then used to calculate the instantaneous lift force generated and power consumed during the wing's flapping motion.

Table 2.1. Physical parameter values of the flapping flight model

Parameter	Value	Description
R	2.02 [mm]	wingspan
$\bar{c}$	0.1	mean chord length
$\hat{c}_{rot}$	0.25	normalized distance of RA from LE
ρ	0.6	air density
v	16.97 [μm^2/s]	air density
m_b	1.1 [μg]	air kinematic viscosity
P_{lim}	40 [W/kg]	body mass specific power

Table 2.2. Dimensionless wing geometry parameters

Parameter	Value
$\int_0^1 \hat{c}(\hat{r})^2\, d\hat{r}$	1.14
$\int_0^1 \hat{r}\hat{c}(\hat{r})^2\, d\hat{r}$	0.65
$\int_0^1 \hat{r}^2\hat{c}(\hat{r})\, d\hat{r}$	0.39
$\int_0^1 \hat{c}(\hat{r})^3\, d\hat{r}$	1.36
$\int_0^1 \hat{c}(\hat{r})^4\, d\hat{r}$	1.58
$\int_0^1 \hat{r}\hat{c}(\hat{r})^3\, d\hat{r}$	0.79
$\int_0^1 \hat{r}^2\hat{c}(\hat{r})^2\, d\hat{r}$	0.42
$\int_0^1 \hat{r}^3\hat{c}(\hat{r})\, d\hat{r}$	0.26

2.3.1 Translational Force

The quasi-steady estimate for the translational lift and drag can be obtained through simple empirical expressions for a thin airfoil integrated over the wing span as follows.

$$F_{trans,L} = \frac{1}{2} C_L(\alpha) \rho R^3 \bar{c} \dot{\phi} |\dot{\phi}| \int_0^1 \hat{r}^2 \hat{c}(\hat{r}) d\hat{r} \tag{2.9}$$

$$F_{trans,D} = \frac{1}{2} C_D(\alpha) \rho R^3 \bar{c} \dot{\phi} |\dot{\phi}| \int_0^1 \hat{r}^2 \hat{c}(\hat{r}) d\hat{r} \tag{2.10}$$

where ρ denotes the density of the fluid medium (air), R is the wingspan, $\bar{c}$ is the mean chord length, and ϕ, α are the stroke and pitch angles, respectively. Also, $\hat{r} = r/R$ is defined as the dimensionless wing position and $\hat{c}(\hat{r}) = c(r)/\bar{c}$ is the dimensionless chord length.

The lift and drag coefficients, C_L and C_D, for Drospholia are adopted from [80] and are represented as:

$$C_L = 1.8 \sin(2\alpha) \tag{2.11}$$

$$C_D = 1.9 - 1.5 \cos(2\alpha) \tag{2.12}$$

2.3.2 Added-Mass Force

The added-mass term for each infinitesimal blade element is estimated using the potential flow theory [82]. For a two-dimensional wing motion, this term can be

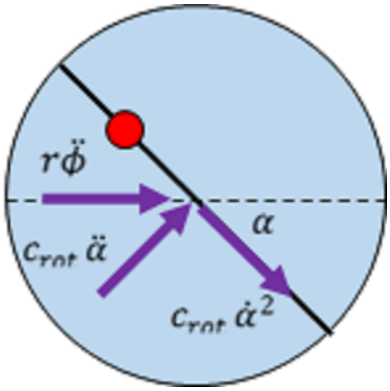

Figure 2.2. Different components of the added-mass force acting on an infinitesimal blade element. The red circle denotes the wing's RA.

integrated over the wingspan to obtain the overall force generated due this effect. Consider a disc of fluid attached to an infinitesimal wing element as sketched in Fig. 2.2, where the Rotation Axis (RA) of the wing is located at a distance equal to $\bar{c} \times \hat{c}_{rot}$ from its Leading Edge (LE). The mass center of this fluid disc experiences three different acceleration components due to its translational and rotational motions as sketched in Fig. 2.2. The translational acceleration of the wing and the angular acceleration of the wing around its RA results in two differential inertial force components acting normal to the wing. By integrating these differential forces over the wing span, the normal component of the added-mass force can be computed as:

$$\begin{aligned} F_{a,n} = \rho\frac{\pi}{4}R^2\bar{c}^2\left(\ddot{\phi}\sin(\alpha) + \dot{\phi}\dot{\alpha}\cos(\alpha)\right)\int_0^1 \hat{r}\hat{c}^2(\hat{r})d\hat{r} \\ + \rho\frac{\pi}{4}R\bar{c}^3(0.5 - \hat{c}_{rot})\ddot{\alpha}\int_0^1 \hat{c}^3 d\hat{r} \end{aligned} \tag{2.13}$$

where $\hat{c}_{rot}$ is assumed to be constant across the wing span. The centripetal acceleration of the fluid disc mass center around its axis of rotation leads to another added-mass force component tangential to the wing surface. The total tangential force due to this effect can be expressed as the following integral.

$$F_{a,t} = \rho\frac{\pi}{4}R\bar{c}^3(0.5 - \hat{c}_{rot})\dot{\alpha}^2\int_0^1 \hat{c}^3 d\hat{r} \tag{2.14}$$

The formulation of the added-mass force in [80] is essentially equivalent to Eq. (2.13) and lacks the tangential component of Eq. (2.14). However, the added-mass effect always produce a conservative force and the net work done by this force must be path-independent and zero over a full flapping cycle. Eq. (2.13), alone, does not amount to a conservative inertial force and leads to an erroneous work expression that is path-dependent. Section 2.3.6 shows that by including the tangential force component of Eq. (2.14) the net added-mass-related momentum exchange between the wing and the fluid is guaranteed to be zero over a full flapping cycle. Lee *et al.*'s model also includes an expression similar to Eq. (2.14) as a second rotational force component [74].

2.3.3 Rotational Force or Kramer Effect

For derivation of this force component, it is assumed that Kutta-Jukowski theory holds for high angle of attack flows experienced in insect flights. Using a theoretical approach, Sane *et al.* estimate the rotational lift coefficient and experimentally validate the resulting expression [80]. The magnitude of this force component is obtained as:

$$F_{rot} = (0.75 - \hat{c}_{rot})\,\rho R^2 \bar{c}^2 |\dot{\phi}|\dot{\alpha} \int_0^1 \hat{r}\hat{c}^2(\hat{r}) d\hat{r} \tag{2.15}$$

Assuming that the wing thickness is negligible, this rotational force component acts normal to the wing area [80].

2.3.4 Rotational Damping Effect

None of the force components formulated above create any damping effects, when the wing rotates at constant velocity without any translational motion. Whitney and Wood in [81] derive a damping torque expression assuming a linear dynamic pressure profile caused due to the rotation of the wing around AR. This rotational damping torque is given by:

$$M_{rd} = -\frac{1}{2}\rho C_{rd} \bar{c}^4 R \hat{Y}_{rd} \dot{\alpha}|\dot{\alpha}| \tag{2.16}$$

where C_{rd} is the rotational damping coefficient, $\hat{Y}_{rd}$ is the nondimensional effective moment arm averaged over the wingspan, and the negative sign is used to denote

that this moment always opposes the rotational motion. A rotational damping coefficient of $C_{rd} = 5.0$ is reported to achieve a good agreement with experimental results in [81]. Also, numerical integration over the geometry of the wing yields $\hat{Y}_{rd} = 0.17$.

2.3.5 Total Instantaneous Lift Force

The individual force components derived above may be projected onto the direction normal to the stroke plane to provide the total lift force generated for any given set of wing kinematic trajectories. Taking the orientation of each force component into account, the total lift force expression reads as follows:

$$FL = F_{trans,L} + \cos(\alpha)\left(F_{a,n} + F_{rot}\right) - \sin(\alpha)F_{a,t} \tag{2.17}$$

where the individual force component are substituted from Eq.(2.9)-(2.15). For notational convenience, we reformulate the above equation by lumping the physical parameters together and introducing a set of lift force coefficients as shown below:

$$\begin{aligned} FL &= K_t \sin(2\alpha)\dot{\phi}|\dot{\phi}| + K_{a3}\sin(\alpha)\dot{\alpha}^2 \\ &+ \cos(\alpha)\left(K_{a1}(\ddot{\phi}\sin(\alpha) + \dot{\phi}\dot{\alpha}\cos(\alpha)) + K_{a2}\ddot{\alpha} + K_r|\dot{\phi}|\dot{\alpha}\right) \end{aligned} \tag{2.18}$$

where subindices t, a, and r stand for translational, added-mass, and rotational, respectively. For hovering flight, the magnitude of the lift force needs to overcome the insect's weight. Therefore, the average net lift force over each flapping cycle and for each wing must not fall below $FL_{min} = 0.5 m_b g$, where g is the gravitational acceleration and m_b is the insect's mass from Table 2.2.

2.3.6 Total Instantaneous Power Consumption

The power needed for generating a given flapping flight trajectory can be calculated for each infinitesimal blade element by taking the inner product of the net aerodynamic force acting on the element and the velocity of its center of action (approximated to coincide with the center of the element). In other words, the power needed to implement a given flight trajectory can be derived as:

$$PW = \int_0^R d\vec{F}_{inst}(r).\vec{V}(r)\ dr \tag{2.19}$$

where $\vec{V}$ is the element's center velocity vector. Again, for notational convenience, we lump the model's physical parameters together, introduce some power coefficients (*e.g.*, T_{t_1}, T_{t_2} etc.), and obtain the following formulation for power consumption.

$$PW = P_t + P_a + P_{rd} + P_r \tag{2.20}$$

where

$$P_t = (T_{t1} - T_{t2}\cos(2\alpha))\dot{\phi}^2|\dot{\phi}| \tag{2.21}$$

$$\begin{aligned} P_a = {} & T_{a1}\dot{\phi}\sin(\alpha)\left(\ddot{\phi}\sin(\alpha) + \dot{\phi}\dot{\alpha}\cos(\alpha)\right) + \sin(\alpha)(T_{a2}\dot{\phi}\ddot{\alpha} + T_{a3}\ddot{\phi}\dot{\alpha}) \\ & + T_{a4}\cos(\alpha)\dot{\phi}\dot{\alpha}^2 + T_{a5}\dot{\alpha}\ddot{\alpha} \end{aligned} \tag{2.22}$$

$$P_{rd} = T_{rd}\dot{\alpha}^2|\dot{\alpha}| \tag{2.23}$$

$$P_r = T_r\sin(\alpha)\dot{\alpha}\dot{\phi}|\dot{\phi}| \tag{2.24}$$

In the power expression due to the added-mass effects, $T_{a2} = T_{a3} = T_{a4}$. Hence, the right hand side of Eq. (2.22) can be reformulated as the time-derivative of a potential function given by:

$$\Psi(\phi, \alpha, \dot{\alpha}) = \frac{T_{a1}}{2}(\dot{\phi}\sin\alpha)^2 + T_{a2}\dot{\phi}\dot{\alpha}\sin\alpha + \frac{T_{a5}}{2}\dot{\alpha}^2 \tag{2.25}$$

Therefore, the work done by the added-mass force over the time interval $[0, T]$ equals $\Psi(T) - \Psi(0)$ and is path-independent.

The insect's wing muscles are limited in the amount of power they can deliver for extended periods of time. In this chapter, the average power consumed by each wing of the fruit fly over a cycle is not to exceed $PW_{max} = 0.5m_bP_{lim}$, where P_{lim} is the insect's body mass specific power rate from Table 2.2. Section 2.4 takes the average of these lift and power expressions over one flapping cycle and use them to formulate an OPC problem for comparing the optimality of rotary and flapping flights.

2.4 Optimal Rotary Flight: The OSS Solution

From the aerodynamic energy efficiency perspective, an optimal flapping flight trajectory is one that generates the maximum average lift force under certain power constraint, or one consuming the minimum amount of energy over a full cycle given certain lift requirement. The lift force and the associated aerodynamic power have been reported in the literature as the most common metric for comparing the relative performance of the rotary and flapping flight configurations [55]. In mathematical terms, the objective is to maximize FL and minimize PW among the set of all periodic pitch and stroke angle trajectories respecting the average lift and power constraints. Rotary flight with a constant pitch angle and a constant stroke velocity is the steady state solution of this optimization problem. In this section, we first use the lift and power expressions derived in Section 2.3 and solve a bi-objective flight optimization problem under the steady-state assumption. Next, we use the π test to analyze the local optimality of the resulting rotary flight trajectories within the larger class of all periodic flapping flight trajectories.

2.4.1 OPC Problem Formulation

Maximization of lift force and minimization of power consumption are two conflicting objectives in nature. As a consequence, there is not a single flight trajectory that outperforms all others in both the objectives. There rather exist a set of nondominated optimal solutions, which offer a trade-off between these conflicting objectives. The optimization literature refers to this set as the"Pareto front" of the problem, and the members of the set are known as "Pareto-optimal" solutions.

The power-lift Pareto front of the flapping flight problem of this chapter is the solution set to the following problem:

$$\begin{aligned} &\max_{\phi,\alpha,T}\{\tfrac{1}{T}\textstyle\int_0^T FL\,dt, -\tfrac{1}{T}\int_0^T PW\,dt\} \\ &\text{subject to:} \\ &\tfrac{1}{T}\textstyle\int_0^T FL\,dt \geq 0.5 m_b g \\ &\tfrac{1}{T}\textstyle\int_0^T PW\,dt \leq 0.5 m_b P_{lim} \end{aligned} \tag{2.26}$$

where ϕ, α and their first two time-derivatives are $T-$periodic for some $T > 0$.

Moreover, *FL* and *PW* are static functions of $\dot{\phi}, \ddot{\phi}, \alpha, \dot{\alpha}, \ddot{\alpha}$ as given by Eq. (2.18) and Eq. (2.20)-(2.24).

2.4.2 OSS Solutions

This section first finds the steady-state, power-lift Pareto front of the flapping flight problem given by Eq. (2.26). Each point across this front is representative of a nondominated rotary flight trajectory. The translational lift and drag are the only force elements present in rotary flight. Moreover, we scalarize the bi-objective optimization problem by maximizing a convex combination of the conflicting objectives as follows:

$$J_{oss}(\gamma) = \max_{\dot{\phi}_{oss}, \alpha_{oss}} \{(1-\gamma)F_{trans,L} - \gamma P_t\} \tag{2.27}$$

where $\gamma \in (0,1)$ is the scalarization parameter determining the relative importance of each objective.

The following state-space representation governs the relationship between the kinematic flight variables of the model.

$$\dot{\vec{x}} = \begin{bmatrix} 0 & 0 & 0 \\ 0 & 0 & 0 \\ 0 & 1 & 0 \end{bmatrix} \vec{x} + \begin{bmatrix} 1 & 0 \\ 0 & 1 \\ 0 & 0 \end{bmatrix} \vec{u} \tag{2.28}$$

with $x_1 = \dot{\phi}, x_2 = \dot{\alpha}, x_3 = \alpha$ and $u_1 = \ddot{\phi}, u_2 = \ddot{\alpha}$. Note that at any equilibrium point of the above equation $x_1 = \dot{\phi}$ and $x_3 = \alpha$ are both constant. Therefore, any steady-state solution is indeed a rotary flight trajectory and vice versa. By differentiating Eq. (2.27) with respect to $\dot{\phi}_{oss}$ and α_{oss}, one concludes that the optimal stroke velocity is always a solution to the following equation:

$$0.5\cos(2\alpha_{oss})^2 - 1.9\cos(2\alpha_{oss}) + 1 = 0 \tag{2.29}$$

Therefore, $\alpha_{oss} \approx 0.43 rad$ (25.4°) regardless of the scalarization parameter γ. In contrast, the optimal stroke velocity is a function of γ according to the following equation.

$$\dot{\phi}_{oss} = \frac{K_t(1-\gamma)}{T_{t2}\tan(2\alpha_{oss})\gamma} \tag{2.30}$$

Figure 2.3 shows the variations of the optimal stroke velocity with γ. By substitution of the OSS solution in the translational lift and power expressions, one can construct the steady-state, power-lift Pareto front depicted in Fig. 2.4. By imposing the minimum lift and maximum power limits of Eq. (2.26), the allowable range of the scalarization parameter is obtained as $0.226 \leq \gamma \leq 0.281$. The infeasible regions in Fig. 2.3 and 2.4 are highlighted with gray. Additionally, the power-lift Pareto front is traced from the left to the right as γ increases.

2.4.3 π Test Results

The Hamiltonian function for the problem is calculated as:

$$H(\vec{x}, \vec{u}, \vec{\lambda}, \gamma) = (1-\gamma)FL - \gamma PW + \lambda_1 u_1 + \lambda_2 u_2 + \lambda_3 z_2 \tag{2.31}$$

The vector of Lagrange multipliers $\vec{\lambda}$ may be obtained as a function of γ by solving the system of optimality equations given in (2.3). However, due to the linearity of the system dynamics, the Π matrix as a second-order perturbation test is not affected by $\vec{\lambda}$ for this problem. Also, the transfer function of these linear system

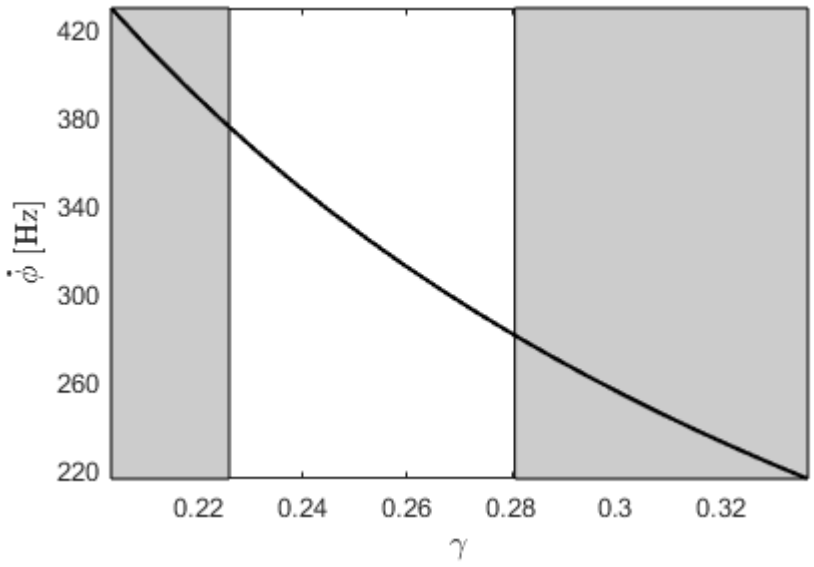

Figure 2.3. Optimal revolution frequency in rotary flight.

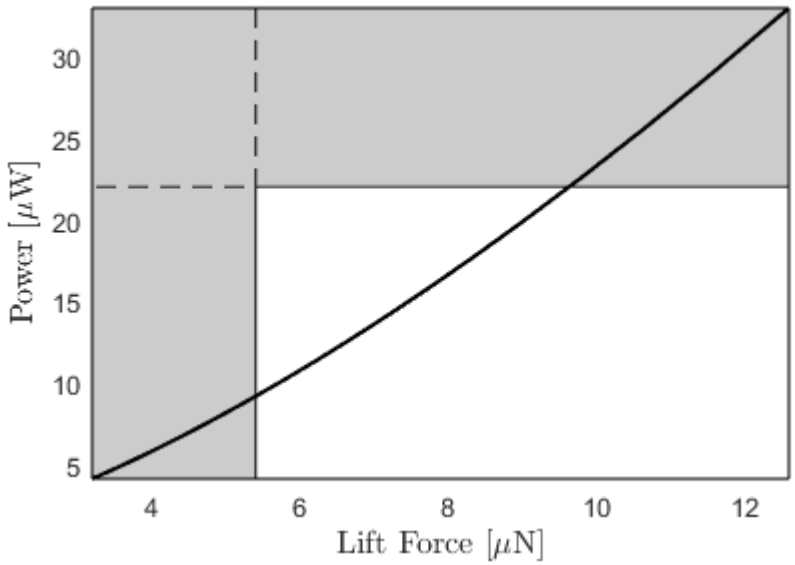

Figure 2.4. Optimal power-lift Pareto front in rotary flight.

dynamics is readily calculated as:

$$G(s) = \begin{bmatrix} \frac{1}{s} & 0 \\ 0 & \frac{1}{s} \\ 0 & \frac{1}{s^2} \end{bmatrix} \tag{2.32}$$

The second-order partial derivatives of the Hamiltonian function are a convex combination of the Hessian matrices of the total lift force from Eq. (2.18) and net consumed power from Eq. (2.20)-(2.24). It is easy to verify that the resulting Q matrix is of the following structure:

$$Q = H_{xu} = \begin{bmatrix} Q_{11} & Q_{12} \\ 0 & 0 \\ Q_{31} & Q_{32} \end{bmatrix} \tag{2.33}$$

and also that $R = H_{uu} = \mathbf{0_{2\times 2}}$. From Eq. (2.5), the complex-valued symmetric $\Pi(\omega)$ matrix is therefore calculated as:

$$\Pi(\omega, \gamma) = \begin{bmatrix} \frac{P_{11}}{\omega^2} & \frac{(P_{12}-Q_{31})\omega - j(P_{13}-Q_{12}\omega^2)}{\omega^3} \\ \frac{(P_{12}-Q_{31})\omega + j(P_{13}-Q_{12}\omega^2)}{\omega^3} & \frac{(P_{22}-2Q_{32})\omega^2 + P_{33}}{\omega^4} \end{bmatrix} \tag{2.34}$$

where P_{ij}, Q_{ij} are the elements of the P, Q matrices expressed as a function of the flight kinematics at the OSS and lift and power coefficients. Table A.1 in Appendix A provides a summary of all these expressions.

Hence, the characteristic equation of the $\Pi(\omega)$ matrix becomes the following:

$$\omega^6 s^2 + \beta_1(\omega)s + \beta_2(\omega) = 0 \tag{2.35}$$

with

$$\begin{aligned}\beta_1(\omega,\gamma) &= (2Q_{32} - P_{11} - P_{22})\omega^4 - P_{33}\omega^2 \\ \beta_2(\omega,\gamma) &= -Q_{12}^2\omega^4 + \Big(P_{11}P_{12} - 2P_{11}Q_{32} + 2P_{13}Q_{12} - (P_{12} - Q_{31})^2\Big)\omega^2 \\ &\quad + P_{11}P_{33} - P_{13}^2\end{aligned} \tag{2.36}$$

Note that $\beta_2(\omega,\gamma)$, the constant term of the above quadratic characteristic equation, is a second-order polynomial in ω^2 with a negative number (i.e., $-Q_{12}^2$) multiplying its highest power term. As a result, for any given value of γ, there exists a perturbation frequency $\omega_p(\lambda)$ large enough to make $\beta_2(\omega,\gamma)$ a negative number. Hence, the characteristic equation of $\Pi(\omega,\gamma)$ will have a positive root for this potentially large $\omega_p(\lambda)$ value. This means that the flapping flight is always superior to rotary flight and the OPC problem is always proper regardless of the scalarization parameter value.

A numerical computation of the Hessian matrices shows that $\beta_1(\omega,\gamma)$ is always positive for the insect flight model of this chapter. Moreover, any sinusoidal perturbation faster than the positive root of $\beta_2(\omega,\gamma)$ makes this coefficient negative. Consequently, this positive root yields a critical perturbation frequency, $\omega_{cr}(\gamma)$, above which $\Pi(\omega \geq \omega_{cr},\gamma)$ is not negative-definite.

To clarify this point further, pick an $\omega_p \geq \omega_{cr}$. Then, the π test result guarantees that (i) $\Pi(\omega_p,\gamma)$ has an eigenvector $\vec{V}_p^*$ such that $\vec{V}_p^{*\,T}\Pi(\omega_p,\gamma)\vec{V}_p < 0$ where $*$ denotes the convex conjugate operator, and (ii) there exists a weak input perturbation of the form $\delta\vec{u} = \epsilon(\vec{V}_p e^{j\omega_p t} + \vec{V}_p^* e^{-j\omega_p t})$ with $\epsilon > 0$ leading to a differential improvement over the OSS solution (i.e., $\delta J > 0$). Figure 2.5 depicts the variations of ω_{cr} with γ.

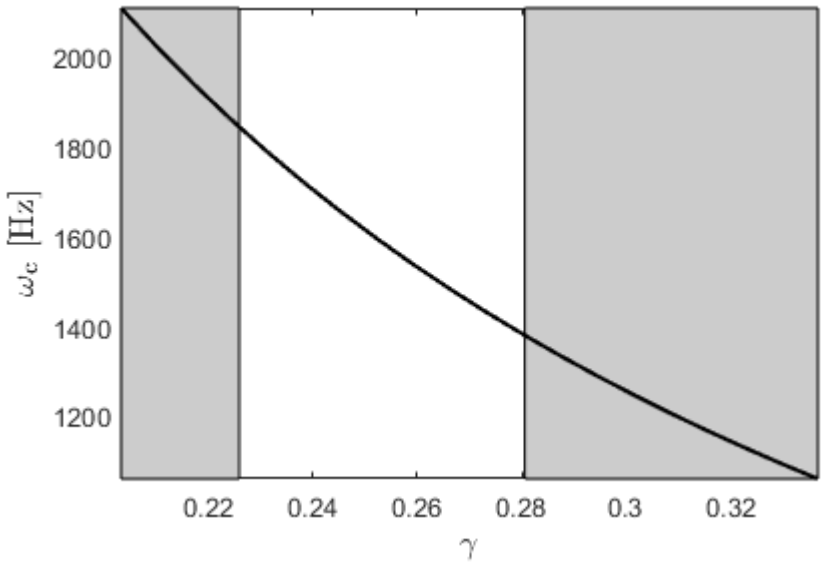

Figure 2.5. Minimum perturbation frequency for properness.

Define the Reynolds number for an optimal rotary flight trajectory as follows:

$$Re = \frac{R\dot{\phi}_{oss}}{v} \tag{2.37}$$

where v is the kinematic viscosity of air given in Table 2.1. Then, it can be seen that the dimensionless minimum perturbation frequency defined as $\hat{\omega}_{cr} = \omega_{cr}/\dot{\phi}_{oss}$ depends linearly on the stroke velocity which is proportional to the Reynolds number. The value of $\hat{\omega}_{cr}$ can be thought of as the minimum number of wing flaps per one full wing rotation, needed to surpass the best rotary flight performance. The following equation illustrates this linear relationship and essentially summarizes the entire plot of Fig. (2.5) by a single dimensionless equation.

$$\hat{\omega}_{cr} = 4.91Re \tag{2.38}$$

Also, the feasible range of the scalarization parameter maps to a feasible range for the flow Reynolds number. This permissible range is specified by $108 \leq Re \leq 215$, where a higher Reynolds number means higher lift generation at the expense of more power consumption.

2.5 Flight Trajectory Optimization

Having established that the periodic flight problem is proper, this section relaxes the steady-state assumption of Section 2.4 and solves for a set of nondominated flapping flight trajectories that optimize the two conflicting objectives of the problem. A comparison of the steady-state and dynamic Pareto fronts reveals the degree to which improvement is achieved via flapping wing flight.

The hinge structure attaching an insect wing to the thorax allows for only a limited range of stroke and pitch angels, as a freely rotating joint introduces a physical barrier for the vascular and the nervous system [55]. Therefore, the following bound constraints are additionally imposed on the optimal control problem statement in Eq. (2.26) to reflect this limitation.

$$\begin{aligned} 0 \leq \phi(t) \leq \pi \\ 0 \leq \alpha(t) \leq \pi \end{aligned} \tag{2.39}$$

for every $t \in [0, T]$.

We now transcribe optimal flapping flight problem using the Legendre Pseudospectral Method (LPM) presented in [83]. This transcription method introduces the change of time variable $\tau = 2t/T - 1$, so that the new time variable varies between -1 and 1. Next, the temporal stroke and pitch trajectories are approximated with an N_{th}-order polynomial as follows:

$$\begin{aligned} \phi(\tau) = \sum_{k=0}^{N} \phi(\tau_k) L_k(\tau) \\ \alpha(\tau) = \sum_{k=0}^{N} \alpha(\tau_k) L_k(\tau) \end{aligned} \tag{2.40}$$

where τ_k, L_k with $k \in [0, N]$ are the Legendre-Gauss-Lobatto (LGL) points, and the N_{th}-order Lagrange interpolating polynomials defined by the LGL points, respectively [83]. By assuming a polynomial shape for the pitch and stroke trajectories, the infinite-dimensional optimal control problem is approximated by a finite-dimensional Nonlinear Programming (NLP) problem in terms of the time period T and values

of the independent variables at the discretization points $\phi(\tau_k), \alpha(\tau_k)$.

Due to the polynomial expansion of Eq. (2.40), the time derivative of the stroke and pitch angle are also lower-order polynomials in time. The values of these time derivatives at the discretization points is simply obtained by premultiplying the LPM differentiation matrix $D_{(N+1)\times(N+1)}$ by the angle values at these points [83]. The average lift and power forces are also calculated as weighted summation of the lift and power at the discretization points with weights $(w_k, k = 0, \cdots, N)$ computed according to the LGL quadrature rule [83]. As an example, with this transcription, the stroke acceleration at the first discretization point is computed as $\ddot{\phi}(t = \frac{T}{2}(\tau_0 + 1)) \approx \frac{T}{2}[1, 0, \cdots, 0]D^2[\phi(\tau_0) \cdots \phi(\tau_N)]^T$, and the average lift force over one flapping cycle is estimated as $\frac{1}{T}\int_0^T FL(t)dt \approx \frac{1}{2}\sum_{k=0}^{N} FL(\tau = \tau_k)$. More details on the LPM transcription of optimal control problems can be found in reference [83].

The LPM method directly includes the endpoints of the time interval as the discretization points, which significantly facilitates the enforcement of the periodicity condition. The transcribed flapping flight optimization problem may now be written as follows:

$$\max_{\vec{\phi}_{0:N}, \vec{\alpha}_{0:N}, T} \{\frac{1}{2}\sum_{k=0}^{N} FL(\tau = \tau_k), -\frac{1}{2}\sum_{k=0}^{N} PW(\tau = \tau_k)\} \tag{2.41}$$

where $\vec{\phi}_{0:N} = [\phi(\tau_0) \cdots \phi(\tau_N)]^T, \vec{\alpha}_{0:N} = [\alpha(\tau_0) \cdots \alpha(\tau_N)]^T$ and the NLP is subject to the following constraints.

1. Periodicity Constraints:

$$\begin{aligned} [1, 0, \cdots, 0]\vec{z} &= [0, \cdots, 0, 1]\vec{z} \\ [1, 0, \cdots, 0]D\vec{z} &= [0, \cdots, 0, 1]D\vec{z} \\ [1, 0, \cdots, 0]D^2\vec{z} &= [0, \cdots, 0, 1]D^2\vec{z} \end{aligned} \tag{2.42}$$

   where D is the LPM differentiation matrix and $\vec{z}$ should be replaced with $\vec{\phi}_{0:N}, \vec{\alpha}_{0:N}$ to ensure the periodicity of stroke and pitch trajectories and their first two time derivatives.

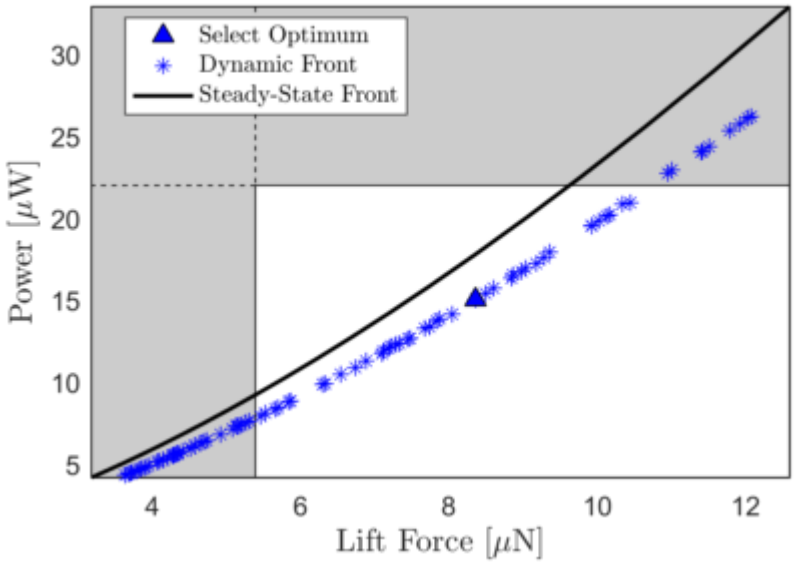

Figure 2.6. Steady state vs. dynamic Pareto front.

2. Average Constraints:

$$\begin{aligned} \sum_{k=0}^{N} FL(\tau = \tau_k) &\geq m_b g \\ \sum_{k=0}^{N} PW(\tau = \tau_k) &\leq m_b P_{lim} \end{aligned} \tag{2.43}$$

3. Bound Constraints:

$$\begin{aligned} 0 \leq \vec{\phi}_{0:N} &\leq \pi \\ 0 \leq \vec{\phi}_{0:N} &\leq \pi \end{aligned} \tag{2.44}$$

The dimension of the problem is further reduced by using the periodicity constraints in Eq. (2.42), to solve for the last three discretized values of the ϕ, α trajectories in terms of their first $N + 1 - 3$ discretized values. Therefore, the resulting NLP problem includes only a total of $2 \times (N-2)+1$ optimization variables.

Concavity is necessary for properness of an OPC problem [22]. As a result, gradient-based NLP solvers may get trapped at a local extremum, specifically when initialized at the OSS solution. To ensure global optimality of the solution, this chapter uses a differential evolution algorithm for solving the optimal flapping flight

problem. This solution method also allows us to conveniently treat the problem as a genuine bi-objective optimization problem, therefore eliminating the need for scalarization of the two objectives.

The transcribed flapping flight problem was numerically solved with $N = 5$ and a population of 250 members, 20% of which was initialized using OSS solutions uniformly distributed across the stead-state Pareto front. Figure 2.6 illustrates the optimization search results after 50 generations of the initial population with blue stars. The corresponding Pareto front is seen to be superior to that of the rotary flight as predicted by the π test. Figure 2.7 shows the periodic stroke and pitch angle trajectories for a select optimized solution marked by a blue triangle on the Pareto front of Fig. 2.6. The small red circles in Fig. 2.7 represent the optimized values at the discretization points. Finally, Fig. 2.8 provides a visualization for the optimal flapping and revolving wing flight regimes. Each bar in this figure depicts

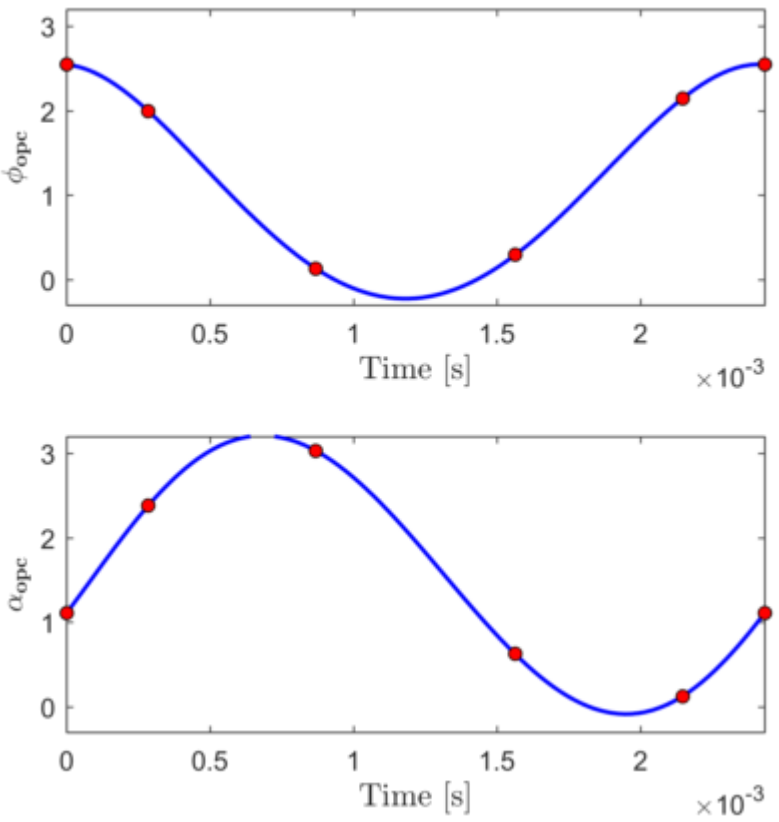

Figure 2.7. Optimal flapping flight stroke and pitch trajectories.

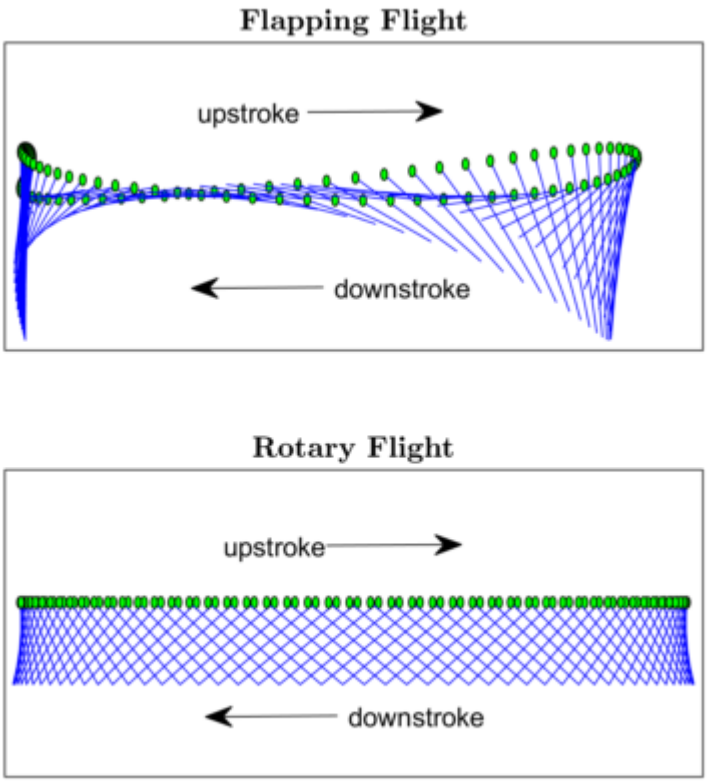

Figure 2.8. Optimal flight patterns for flapping and revolving wings. The green dots and red dots denote the wing's leading edge.

a side view of the positioning of the wing tip at a given moment in time. The green dots at the top endpoints of these bars denote the leading edge. The time span between the consecutive snapshots of the wing locations is fixed. Therefore, the spacing between the bars is a representative of the rate of change of stroke and pitch angles. As seen from Fig.2.7 and 2.8, in contrast to the rotary flight, the stroke velocity and the wing's angle of attack change very dynamically during the course of each flapping cycle. The wing travels with low angle of attack values and relatively fast speed during mid-stroke to minimize the drag forces. Then, stroke reversal occurs at a rapid pitch rate to decrease the angle of attack for the next half-stroke.

2.6 Conclusions

This chapter introduces a framework for analyzing the relative optimality of flapping and revolving wing motions in insect flight models. Due to the small scale of flying insects, the viscous effects are substantially amplified, reducing the aerodynamic efficiency of steady-state rotary flight. The flapping flight however exploits additional unsteady lift generation mechanisms by dynamically interacting with the surrounding air flow. The flapping flight optimization problem is posed in this chapter as an OPC problem whose steady-state solution is the best rotary flight configuration. The π test is then incorporated to assess the impact of periodic perturbations around this optimal steady-state solution. An application of the π test to a quasi-steady fruit fly model shows that best flapping trajectory always outperforms the optimal revolving wing flight. The chapter concludes with obtaining the unsteady optimal lift-power Pareto front using a pseudospectral transcription of the optimal flapping flight. The superiority of this Pareto front compared to its steady-state counterpart for rotary flight confirms the predictions of the π test results.

Chapter 3
On the Structure of the Optimal Solution to a Periodic Drug Delivery Problem[1]

3.1 Introduction

This chapter examines the problem of optimizing a drug's delivery schedule in order to maximize its time-averaged efficacy. The particular drug considered here is nicotine, and the optimization goal is to exploit its long term cardio-accelerating effect as much as possible. This problem is introduced to the literature by Varigonda *et al.* [56], building on a Pharmacokinetic/Pharmakodynamic (PKPD) model of nicotine's metabolism by Porchet *et al.* [58]. Varigonda *et al.* show that this is an interesting optimal control problem because it is "*proper*", meaning that its optimal periodic solution is superior to the best achievable steady-state solution.

Properness of the above drug delivery problem has an important physical explanation. The human body accumulates a tolerance or resistance to nicotine over time. When nicotine is administered at a fixed rate, this tolerance builds up, and the drug loses its long-term efficacy. Periodic drug delivery can avoid this tolerance buildup issue as follows: one begins by administering the drug aggressively in order to maximize its benefits while resistance is low. As resistance builds up, the subject is weaned off the drug partly because additional drug administration is

[1]The work of this chapter has been published in journal of Dynamic Systems, Measurement and Control, 2017 [84].

not effective, and partly in order to attenuate the buildup of drug resistance. Once drug resistance has been attenuated, the aggressive administration of the drug resumes. This results in a periodic delivery strategy superior to the best achievable steady-state strategy.

The problem of drug resistance is very common in pharmacology: a fact that suggests the work in this chapter may be of value to delivery problems for drugs other than nicotine. The nicotine drug delivery problem has already been extensively studied in the scientific literature. Specifically, Porchet *et al.*'s PKPD model captures the dynamics of drug resistance by (i) treating nicotine as an agonist, (ii) modeling tolerance as the result of a hypothetical antagonist with first-order dynamics whose buildup depends on nicotine concentration, and (iii) modeling drug efficacy as a function that grows with agonist concentration but diminishes with antagonist concentration.

Varigonda *et al.*'s work uses this model to formulate the optimal drug delivery problem as an application for OPC theory. Using the π test, Varigonda *et al.* show that this problem is proper. They also explain that the underlying PKPD dynamics are differentially flat with the agonist's concentration serving as a flat output. Building on these insights, Varigonda *et al.* find the optimal solution to this problem by expressing the temporal trajectory of the flat output as a truncated Fourier series and optimizing the coefficients of this series.

More recent research examines the online solution of this drug delivery problem. The focus, in this research, is on developing algorithms capable of improving a parameterized drug delivery trajectory using gradient descent update rules. Guay *et al.* solve this problem by using extremum-seeking control to adjust the trajectory of the flat output online [45]. Höffner *et al.* propose an alternative online solution where the optimal drug delivery trajectory is related to the limit cycle of a Hamiltonian oscillator. Höffner *et al.*'s algorithm optimizes the parameters of this limit cycle, then uses back-stepping control to track this limit cycle in a stable manner [46]. Hudon *et al.* solve this problem assuming a time-switching input trajectory alternating between full and no treatment periods [85]. They then use a gradient-descent based model predictive control algorithm to find the optimal duration of the no treatment periods. Finally, the work in Chapter 4 focuses on discovering the optimal drug delivery trajectory adaptively, for patients whose underlying PKPD dynamics may not be exactly known *a priori* and the

corresponding publications can be found in [86, 87].

In all of the above research, one fundamental weakness is visible: while it is clear that the optimal drug delivery trajectory is periodic, no further information is available regarding the structure of this periodic trajectory. This motivates the contributions of this chapter. Specifically, this chapter first argues that optimizing just the control input trajectory as a function of time uniquely determines the optimal state trajectory. Secondly, the chapter utilizes PMP to show that the optimal solution to Varigonda's periodic drug delivery problem follows a bang-singular-bang structure. We build on these two insights to develop two numerical algorithms for solving Varigonda's optimal drug delivery problem. The first algorithm uses nonlinear programming to determine the points in the PKPD model's state space where the optimal solution transitions between different solution arcs (bang, singular, bang). The second algorithm uses direct transcription of the control input trajectory. Specifically, it approximates the optimal control input as a piecewise-constant function, and optimizes the different discrete values of this function. Both of these new algorithms find the optimal trajectory more efficiently than the existing approach in the literature. However, the primary benefit of this chapter is not computational, but rather conceptual. In particular, this chapter represents the first work in the literature to utilize variational calculus tools to elucidate the structure of the optimal solution to the periodic drug delivery problem.

Broadly speaking, the chapter illustrates the use of indirect optimal control methods to elucidate the structure of a periodic optimal controller. This is an important stepping stone towards the remainder of this dissertation, where the goal is to examine the online implementation of optimal periodic control policies.

The remainder of the chapter is organized as follows. Section 3.2 presents the optimal drug delivery problem as given in [56]. Section 3.3 investigates the structure of the feasible set of the problem and proves the existence of a bijection between the sets of feasible input and state trajectories of the problem. In Section 3.4, PMP is utilized to derive the necessary conditions of optimality and as a result the optimal solution subarcs of the problem are found. Section 3.5 uses the insights gained in the previous sections and presents two numerical solution methods. Lastly, in Section 3.6, the optimal solutions obtained using each method are given and compared to the existing solution in the literature.

3.2 Problem Formulation

This section restates the optimal periodic drug delivery problem presented in [56]. Because of the periodicity constraint of the problem, it is labeled as an OPC problem. The drug delivery model used in this problem is a compartment model. The PK portion of this model is mathematically formulated as follows.

$$\begin{cases} \dot{c} = -c + u \\ \dot{a} = k_a(c - a) \end{cases} \tag{3.1}$$

where c and a denote the drug's and antagonist's concentrations, respectively. Furthermore, u represents nicotine's infusion rate and $k_a = 0.1$ is a constant determining the relative elimination rate of the two reactions. In addition, the PD effect of the drug on the body is modeled by

$$E(c, a) = \frac{c}{(1 + c)(1 + a/a^*)} \tag{3.2}$$

where E is the drug efficacy, a quantity related to the heart rate, and $a^* = 1$ is a measure of how much the antagonist affects the body compared to the drug.

An ideal treatment regimen always maintains the number of heart beats within the target heart rate range for patients. This target range maps into a desired interval, $[E_1, E_2]$, for the dimensionless drug efficacy variable in this model. All efficacy levels in this range are equally desirable. Therefore, a metric needs to be defined that scores an administration schedule solely based on the time duration for which the induced effects is in the desired range. The smoothed membership function depicted in Fig. 3.2 is selected for this reason. This function returns a value of approximately 1 when efficacy level is within the desired range and 0 when it is outside of it.

$$I(E) = \frac{(E/E_1)^\gamma}{(1 + (E/E_1)^\gamma)(1 + (E/E_2)^{2\gamma})} \tag{3.3}$$

where γ is a constant that controls the function's steepness at the boundaries of the desired interval for E. As γ gets large I approaches to the indicator function of the desired efficacy interval. In defining the indicator function, the numerical values of $\gamma = 10, E_1 = 0.3, E_2 = 0.6$ are used in [56].

The performance index, J, for any given periodic treatment cycle of period T,

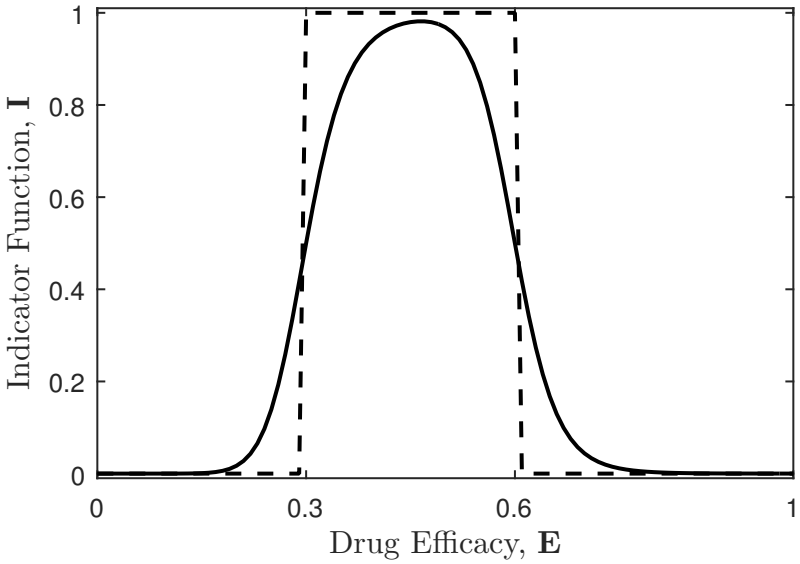

Figure 3.1. State-Space paths taken by application of u^* in Eq. 3.22 for different starting points.

is defined as the time average of the membership function in Eq. (3.3) over the time interval $[0, T]$.

$$J(I,T) = \frac{1}{T}\int_0^T I\Big(E\big(a(t),c(t)\big)\Big)\,dt \tag{3.4}$$

With the model presented in Eq. (3.1) and the performance index defined by Eq. (3.4), the optimal drug delivery problem is formulated as follows.

$$\begin{aligned}
&\max_{a,c,u,T}\Big\{J = \tfrac{1}{T}\textstyle\int_0^T I(t)\,dt\Big\}\\
&\text{subject to:}\\
&a(0) = a(T), c(0) = c(T) \quad \textit{(Periodicity Constraints)}\\
&0 \le u \le u_{max} \quad \textit{(Input Constraints)}\\
&a(t) \ge 0, c(t) \ge 0 \;\; \forall t \in [0,T] \quad \textit{(State Constraints)}
\end{aligned} \tag{3.5}$$

and the dynamic constraints of Eq. (3.5). The nonnegativity constraints on the input and states of the above problem exist to limit the solution space to include only physically meaningful trajectories. Also, u_{max} is the maximum allowable drug dosage beyond which there are toxication hazards.

3.3 Structure of the Feasible Set

This section presents our first set of insights regarding the solution structure for the above periodic optimal control problem. The section focuses on T-periodic state and input trajectories for the drug delivery problem. We say that the drug infusion trajectory, $u(t)$, is T-periodic if $u(t) = u(t+T)\,\forall t$. Similarly, a state trajectory, $\mathbf{x}(t)$, is T-periodic if $\mathbf{x}(t) = \mathbf{x}(t+T)\,\forall T$. Our goal is to answer the following questions: *does every T-periodic input trajectory correspond to a unique T-periodic state trajectory, and vice versa? In other words, is the mapping between the set of all T-periodic input and state trajectories bijective?* The section also presents conditions on the T-periodic input trajectory which, if satisfied, automatically guarantee that the corresponding T-periodic state trajectory meets the nonnegativity constraints in Eq. (5). The insights in this section are important because they make it possible to solve the periodic optimal control problem at hand by simply optimizing a nonnegative period control input trajectory $u(t)$. Not all systems have a bijective relationship between the sets of T-periodic input and state trajectories. For example, a dynamic system where one of the state variables is a pure integral of the input variable will have an infinite number of T-periodic state trajectories corresponding to any given T-periodic input trajectory, and therefore the relationship between these two sets of trajectories will not be bijective.

The analysis in this section proceeds as follows. First, we argue that the state periodicity constraint establishes a bijective mapping between the sets of periodic inputs and closed state trajectories of a general LTI system. The section next proves that meeting the input constraints of the periodic drug delivery problem also ensures satisfaction of the state constraints of the problem. These two facts together imply that a search among the feasible input set of the problem is sufficient for finding the optimal solution.

Consider the following LTI system:

$$\dot{x} = [A]x + [B]u \tag{3.6}$$

where $[B]$ is full column rank. Let u be an arbitrary piecewise continuous $T-$periodic input trajectory. Also, by x_u denote a periodic solution to the system corresponding to u. Finally, define the set of imaginary numbers $R = \{\lambda : \lambda = \frac{2k\pi i}{T}, k \in \mathbb{Z}\}$. Then

the following statements hold.

Statement 1. *x_u, if it exists, is $T-$periodic as long as $[A]$ does not have any imaginary eigenvalues belonging to Λ.*

Statement 2. *x_u exists and is uniquely determined from solving Eq. (3.6) with the initial condition*

$$x_u(0) = (I - e^{[A]T})^{-1} \int_0^T e^{[A](T-t)}[B]u(t)\, dt, \tag{3.7}$$

if and only if, $[A]$ does not have any imaginary eigenvalues belonging to Λ.

Statement 3. *u is the one and only piecewise continuous periodic input trajectory that generates x_u and can be back-calculated as:*

$$u = ([B]^T[B])^{-1}[B]^T(\dot{x}_u - [A]x_u) \tag{3.8}$$

Proofs of the above statements are provided in Appendix B. The statements imply the existence of a one-to-one correspondence between the sets of piecewise continuous periodic input trajectories and periodic state trajectories for a large subset of LTI systems. From Eq. (3.1), it is clear that the drug delivery model is one example of such systems. Note that this bijective mapping does not generally exist for nonlinear dynamic systems. Pavlov *et al.* define convergent systems, as dynamic systems which "forget" their initial condition (see [88] for a formal definition). Each $T-$periodic input trajectory of a nonlinear convergent systems also maps to a unique $T-$periodic state trajectory [88]. However, the converse is not necessarily true.

Reconsidering the OPC problem given in Eq. (3.5), we can further argue that the *feasible* periodic input and state trajectories of the model are also bijectively mapped to each other. Note that the state matrix of the drug delivery is Metzler (see [89] for a definition), and the input matrix is element-wise nonnegative. As a result, the model is a monotone control system and the convolution integral in Eq. (3.7) is element-wise nonnegative for any nonnegative periodic input [90]. In addition, the Metzler state matrix of the model is triangular and strictly Hurwitz. Therefore, $(I - e^{[A]T})^{-1}$ and consequently $x_u(0)$ are seen to be nonnegative. It follows then from the monotonocity of the system that the periodic $x_u(t)$ trajectory will always remain in the nonngative quadrant. Hence, with a nonnegative periodic

nicotine injection policy, the corresponding periodic agonist's and antagonist's concentration trajectories are guaranteed to remain nonnegative.

3.4 Structure of the Optimal Solution Trajectory

This section draws our second sets of insights by characterizing the shape of the problem's solution arcs through through exploiting PMP. The analysis derives necessary conditions for optimality of a candidate solution and also determines the different pieces of the optimal input trajectory.

First-Order Necessary Conditions

First, the Hamiltonian function of the problem is constructed by adjoining the dynamic constraints of Eq. 3.1 to the Lagrangian of the problem (i.e., integrand of the performance index I). This is done through introducing continuous Lagrange multiplier functions $\lambda_1(.), \lambda_2(.)$. These functions are required to have piecewise continuous derivatives.

$$H(a, c, \lambda_1, \lambda_2, u) = I\Big(E(a, c)\Big) + \lambda_1(-a + u) + k_a\lambda_2(a - c) \tag{3.9}$$

Now, using scalar real Lagrange multipliers μ_1, μ_2 for adjoining the periodicity constraints, the *augmented performance index* becomes

$$\bar{J} = \frac{1}{T}\int_0^T H(a, c, \lambda_1, \lambda_2, u)\, dt + \mu_1(a(T) - a(0)) + \mu_2(c(T) - c(0)) \tag{3.10}$$

Variational calculus performs an arbitrary differential perturbation away from the extremal path, but in the feasible set of the problem, and calculates the associated variation in the augmented performance index. For an extremal path, the first-order variations must be zero. Restricting the domain of perturbation to the feasible set of the problem becomes a challenge when state constraints are present. However, as shown in Section 3.3, the nonnegativity state constraints of the periodic drug delivery problem are never violated and can be safely dropped. Setting the first-order variations equal to zero leads to the following set of equations, wherein variables with asterisks represent elements of the optimal trajectory.

- *Costate Equations:*

$$\begin{aligned}\dot{\lambda}_1^* &= -\left.\frac{\partial H}{\partial a}\right|_{a^*,c^*} = \lambda_1^* - k_a\lambda_2^* - \left.\frac{\partial I}{\partial a}\right|_{a^*,c^*} \\ \dot{\lambda}_2^* &= -\left.\frac{\partial H}{\partial c}\right|_{a^*,c^*} = \qquad k_a\lambda_2 - \left.\frac{\partial I}{\partial c}\right|_{a^*,c^*}\end{aligned} \tag{3.11}$$

- *Dual Periodicity Conditions:*

$$\begin{aligned}\lambda_1^*(T) &= \lambda_1^*(0) = \mu_1^* T^* \\ \lambda_2^*(T) &= \lambda_2^*(0) = \mu_2^* T^*\end{aligned} \tag{3.12}$$

- *Transversality Conditions for T:*

$$H(t = T^*) - J(a^*, c^*, u^*, T^*) = 0 \tag{3.13}$$

- *Input Transversality Conditions:*

$$\begin{aligned}u^*(t) &= \underset{u \in \mathcal{U}}{argmax}\ H(a^*(t), c^*(t), \lambda_1^*(t), \lambda_2^*(t), u) \\ &= \begin{cases} u_{max} & \text{if } \lambda_1^*(t) > 0 \\ 0 & \text{if } \lambda_1^*(t) < 0 \end{cases}\end{aligned} \tag{3.14}$$

where $\mathcal{U} = [0, u_{max}]$ is the set of all admissible control input values.

Speyer and Evans derive the first-order necessary conditions for more general OPC problems in [31]. Therefore, this chapter leaves out the details of derivation and refers interested readers to their work. If $\lambda_1^*(t)$, the coefficient of u in the Hamiltonian, ever becomes zero, Eq. (3.14) fails to yield the optimal input. This is a well known difficulty with the application of PMP to the problems, where the Hamiltonian linearly depends on the control input and its occurrence suggests the possibility of existence of what is known as a *singular arc*.

If the input's coefficient, H_u, in Eq. (3.14) is only momentarily zero, this potentially causes a discontinuity in the optimal input trajectory and is not an issue. A singular arc, in contrast, is created when H_u is zero over a time interval of nonzero measure, and that is the key point to solving singular arc problems.

Along a singular arc H_u is congruent to zero. Therefore, we keep differentiating H_u with respect to time and setting the result equal to zero, until u explicitly appears in the expression. For most singular arc problems, this occurs after finitely many differentiations. In that case, it is shown that u shows up for the first time in an even-order derivative [91]. Half the number of the required differentiation times is, therefore, an integer number and is used to classify different types of singular arcs [92].

Carrying out this process for the optimal drug delivery problem, u first appears in the second time-derivative of H_u as shown below.

$$0 = \ddot{H}_u = -k_a \frac{\partial I}{\partial a} - k_a \frac{\partial I}{\partial c} + \frac{\partial^2 I}{\partial a^2}(-a + u) + k_a \frac{\partial^2 I}{\partial a \partial c}(a - c) \tag{3.15}$$

As a result, by adopting the convention in [92], the associated singular arc is of first order.

Second-Order Necessary Conditions

As opposed to the first-order conditions which are unable to distinguish a maximum from a minimum or a saddle point, second-order conditions concern with local convexity of the objective function about a candidate trajectory. The optimal control literature is rather rich in second order necessary and sufficient conditions of optimality in the case of singular problems [91–94] as well as nonsingular problems [95–98]. But such conditions, for problems where the optimal trajectory contains both singular and nonsingular subarcs, are yet to be developed.

One can, however, apply the necessary second-order conditions to the individual subarcs separately. In a maximization problem and along a nonsingular maximal arc, the Legendre-Clebsch (LC) [97] condition requires

$$\frac{\partial^2 H}{\partial u^2} \leq 0 \tag{3.16}$$

Since H_u is linear in u for the optimal drug delivery problem, this condition is automatically satisfied as an equality. Equivalent of the LC conditions for "totally singular" problems is known as the Generalized Legendre-Clebsch (GLC) condition

and is given below [91].

$$(-1)^q \frac{\partial}{\partial u}\left(\frac{d^q H_u}{dt^q}\right) \leq 0 \tag{3.17}$$

where q is the order of the singular arc. This condition for the optimal drug delivery problem boils down to the following inequality.

$$\frac{\partial^2 I}{\partial a^2} \leq 0 \tag{3.18}$$

Note that the expression in Eq. (3.18) is the coefficient of u in Eq. (3.15). Now, two scenarios are possible:

1. The GLC condition is met strictly. Then Eq. (3.15) can be solved for u to give

$$u_{trans} = \left(k_a \frac{\partial^2 I}{\partial a^2}\right)^{-1}\left[\frac{\partial I}{\partial a} + \frac{\partial I}{\partial c} + \frac{\partial^2 I}{\partial a \partial c}(c-a)\right] + a \tag{3.19}$$

2. Eq. (3.18) holds as an equality. Then, the singular subarc is the solution to the following differential equation system.

$$\begin{cases} \frac{\partial^2 I}{\partial a^2} & = 0 \\ \frac{\partial I}{\partial a} + \frac{\partial I}{\partial c} + \frac{\partial^2 I}{\partial a \partial c}(c-a) & = 0 \end{cases} \tag{3.20}$$

Denote the solution of this system of equations by the pair (a^*, c^*). Then the agonist's dynamic in Eq .(3.1) can be used to find the optimal control over the subarc as follows.

$$u_{trans}(t) = \frac{dc^*(t)}{dt} + c^*(t) \tag{3.21}$$

The expressions found for u_{trans} are essentially nonlinear state-feedback laws for the optimal control of the plant in transitioning from one boundary optimum to another. With having u_{trans} characterized, Eq. (3.14) is updated as follows.

$$u^*(t) = \begin{cases} u_{max} & \text{if } \lambda_1^*(t) > 0 \\ u_{trans}(a^*(t), c^*(t)) & \text{if } \lambda_1^*(t) = 0 \\ 0 & \text{if } \lambda_1^*(t) < 0 \end{cases} \tag{3.22}$$

A control policy of this type is sometimes referred to as *bang-singular-bang* control. As the name suggests, there are two parts to such an optimal control law: 1) a *bang-bang* portion: where the control input instantaneously switches from one extreme to another, 2) a *singular* portion: where there is a smoother transition between the extreme values and along a singular arc.

3.5 Two Numerical Solution Methods

Using the insights obtained on the structure of the feasible set and the optimal solution trajectory, this section proposes two numerical solution approaches. The first approach is an indirect optimization method, where the necessary conditions of optimality are used to construct the optimal solution trajectory of the problem. The second approach, in contrast, transcribes the problem into an NLP and obtains a direct numerical solution to the transcribed problem.

3.5.1 PMP Based Solution

From the PMP results obtained in the previous section, if an optimal periodic administration schedule exists it has to satisfy Eq. (3.11)-(3.13) and Eq. (3.22). This section utilizes these necessary optimality conditions to outline an indirect numerical algorithm for solving our OPC problem.

In theory, the optimality conditions derived in the last section completely specify the optimal solution of the problem. However, the direct use of these optimality conditions to compute the optimal solution trajectory presents at least three challenges. First, it is difficult to determine the specific initial values of the state and co-state variables that would lead to a periodic optimal solution. Second, solving a periodic optimal control problem can also be difficult if the optimal period is unknown *a priori*. Third, it is possible that a numerical solution algorithm may accidentally "skip" the singular arc portion of an optimal control trajectory, even with very fine time discretization levels.

Instead of the direct use of the necessity conditions, we first investigate Eq. (3.22) more carefully to gain more intuition on the structure of the solution. As seen in Eq. (3.22), u^* is a piecewise continuous function composed of three different pieces. Each piece maps into a family of paths in state-space when used to solve Eq. (3.1)

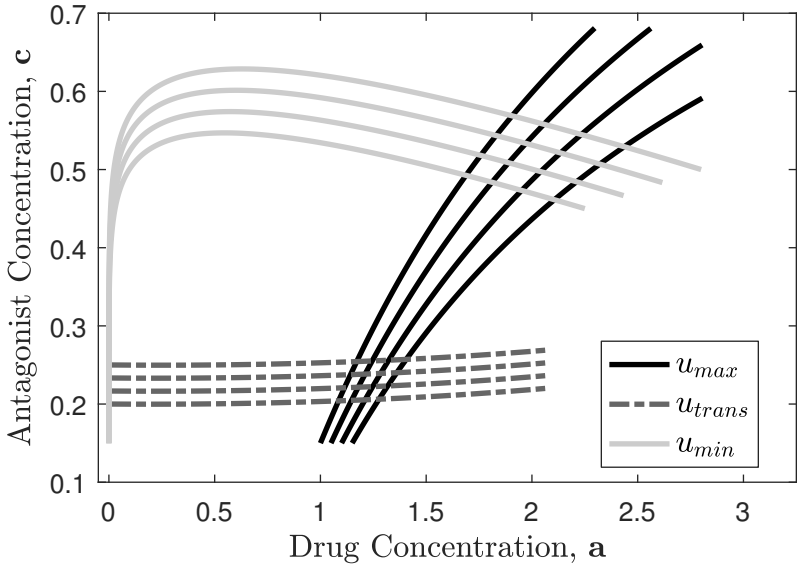

Figure 3.2. State-Space paths taken by application of u^* in Eq. 3.22 for different starting points.

for different starting points. Fig. 3.5.1 depicts a few paths in each family to aid with the visualization of the problem for the same numeric values of k_a, a^*, γ, and u_{max} as those used in [56].

In theory, the optimal solution trajectory can consist of an arbitrary sequence of bang, singular, and bang sections. In this chapter, we conjecture that the trajectory consists of only 3 segments (bang, singular, bang). Given this assumed sequence of three segments, one can determine the optimal control trajectory fully by optimizing the values of state variables at which the transitions between the three solution segments occur. Periodicity constraints simplify this optimization problem by making it possible to characterize the solution trajectory fully in terms of the starting coordinates of the singular arc segment and the time duration of the singular arc. The problem of optimizing these three variables is a simple NLP, and we tackle it using MATLAB's fmincon optimizer. The results of this optimization process agree with the second solution approach presented in this chapter, namely, the direct optimization of a piecewise-constant input trajectory. This provides numerical evidence supporting our conjecture that the optimal solution trajectory does, indeed, consist of only three segments (bang, singular, bang). In situations where the above conjecture does not hold, the problem of determining the optimal

solution trajectory involves finding (i) the sequence of solution segments and (ii) the transition points between the segments. This is a mixed-integer programming (MIP) problem that can be solved using standard MIP solvers, building on the fundamental insights in this chapter.

3.5.2 Piecewise Constant Input Solution

The second solution algorithm uses the insights obtained on the optimal solution's structure to propose a *direct* optimization technique. In these methods, **trajectories** of the system are expanded and parameterized over a proper set of **basis functions**. This simplification transcribes the dynamic optimization problem into an NLP in terms of the parameters used in the expansion of the system's trajectories.

In contrast to Varigonda *et al.* [56]'s indirect solution, here we parameterize the input trajectory rather than a flat output's trajectory. As discussed in Section 3.3, this is possible because there a is bijection between the feasible input set and the set of feasible state trajectories of the problem. Moreover, we choose the set of periodic piecewise constant functions over the Fourier basis for parameterization. The rationale behind this preference is discovery of the discontinuous nature of optimal input trajectory and the fact that it contains constant portions.

Note that the optimal solution of the transcribed problem is an approximation of the true optimal solution and suboptimal to the original problem. The discretization of the input space reduces the original infinite dimensional optimal control problem to an NLP in terms of the height and duration of each constant piece. As the number of pieces over one period increases, the corresponding solution approaches to the true optimal solution. However, for practicality matters, we need to restrict the number of pieces to a finite number. A feasible input trajectory belonging to this parameterization class is shown in Fig. 3.3 over the length of one period.

Paying attention to the following points can greatly simplify the solution of this NLP:

- Looking at the optimal control law obtained in Section 3.4, it is natural to assume that the optimal input trajectory includes a portion of value zero.
- Constrain the height of the first piece of the input trajectory to be positive and the last one to be zero. This prevents needless recalculation of the

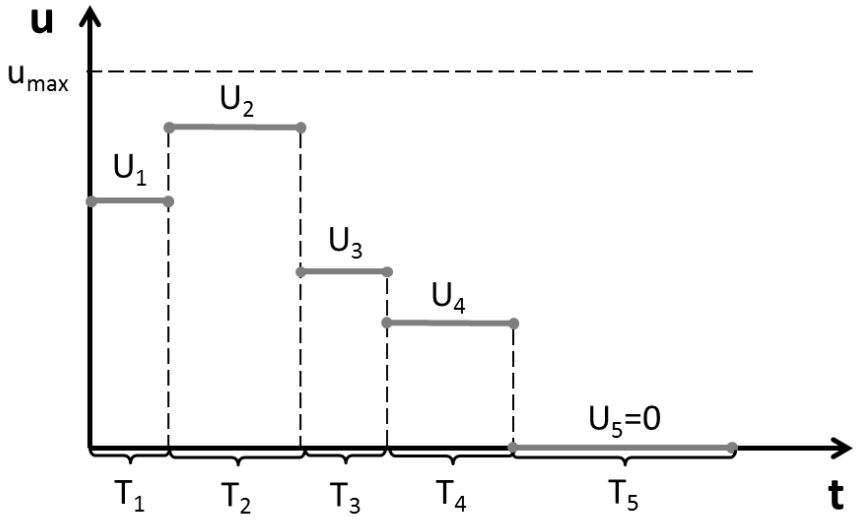

Figure 3.3. A periodic piecewise constant function feasible to the transcribed optimization problem.

performance index for candidate solutions that are just shifted in time.

3.6 Numerical Results

This section employs the two solution methods presented in Section 3.5 to numerically solve the periodic drug delivery problem. The best steady state solution for this problem occurs when $a = c = u = \sqrt{a^*} = 1$ and results in an objective function value of $J_{SS} = 0.139$. Varigonda *et al.* parameterize the flat output's trajectory using the first 20 harmonics of the Fourier expansion. Solving the corresponding 42 variable optimization problem, they obtain an optimal value of $J_{OPC} = 0.3537$.

3.6.1 Results of the Variational Calculus Based Method

First, the auxiliary optimization problem presented in Section 3.5.1 is formulated and solved. The solution offers a candidate optimal trajectory to the periodic drug delivery problem with a performance index of $J_{OPC} = 0.3627$. This is slightly ($\sim 2.5\%$) higher than the optimal value obtained in [56].

Fig. 3.4a plots the path taken by the system in the state space. Next, using Eq. (3.11) the corresponding path in the adjoint state space is found and shown in

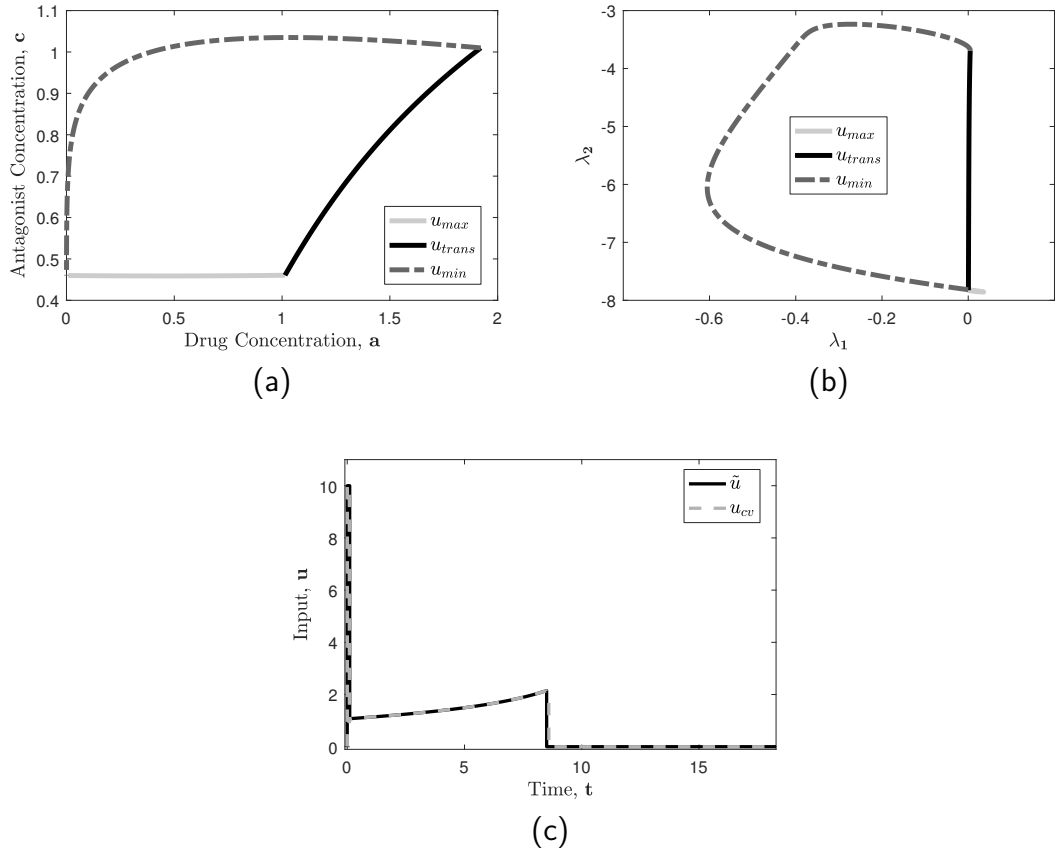

Figure 3.4. (a) and (b) are the optimal phase plots in the state space and adjoint space. (c) is the optimal input trajectories of the drug delivery problem.

Fig. 3.4b. Also, the input trajectory related to the solution of the auxiliary problem, $\widetilde{u}$, is directly calculated from the optimal state trajectories. The input predicted by our PMP results, u_{cv}, is obtained as a function of λ_1 using Eq. (3.14). As shown in Fig. 3.4c, these two input trajectories coincide. Finally, the time length of the solution of the auxiliary problem is found to be $T = 18.28$. Plugging this value into the right-hand side of Eq. (3.13) gives a negligible error of 0.001. Therefore, the optimal solution of the auxiliary problem meets all the necessary optimality conditions derived for the original OPC problem.

3.6.2 Results of Piecewise Constant Input Method

Following the description of the method given in Section 3.5.2, we formulate the transcribed optimization problem for periodic piecewise constant functions.

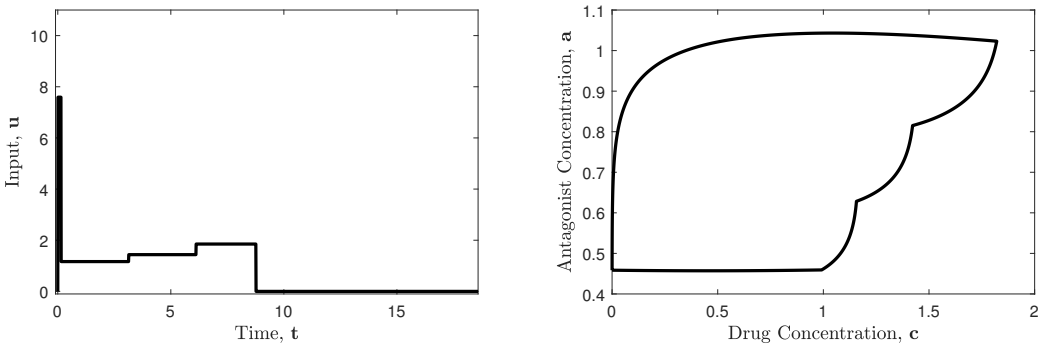

Figure 3.5. (a) A suboptimal piecewise constant input trajectory and (b) its corresponding phase plot for the drug delivery problem.

Furthermore, we limit our optimization search to input trajectories having at most five pieces in each period. Five is the smallest number of pieces required to yield an objective value ($J_{OPC} = 0.3601$) superior to what was achieved in [56]. Lastly, Fig. 3.5b illustrates the path taken by the solution in the system's state space. The proximity of the optimal trajectories from the two methods suggests that the analytical solution found by the first method is indeed the true optimal solution of the problem.

3.6.3 Sensitivity Analysis

While this chapter focuses on the structure of the optimal drug delivery trajectory, research is also needed on implementation of the solution. Our work in Chapter 4 and Chapter 6 develops indirect adaptive control schemes to deal with plant model uncertainties in solving OPC problems (the corresponding publication can be founds in [86, 87, 99]). This section analyzes the sensitivity of the maximum average efficacy in presence of inaccurate model parameters, however, design of an adaptive drug administration policy is beyond the scope of this work.

The parameters used in the PD portion of the drug delivery model and the exponent γ in the definition of the indicator function are all constants defined in earlier research. In contrast, the one parameter of the PK portion, k_a, depends on the specific metabolism of the body and varies from one patient to another. In order to assess the robustness of the solution to uncertainty in k_a, we perform a

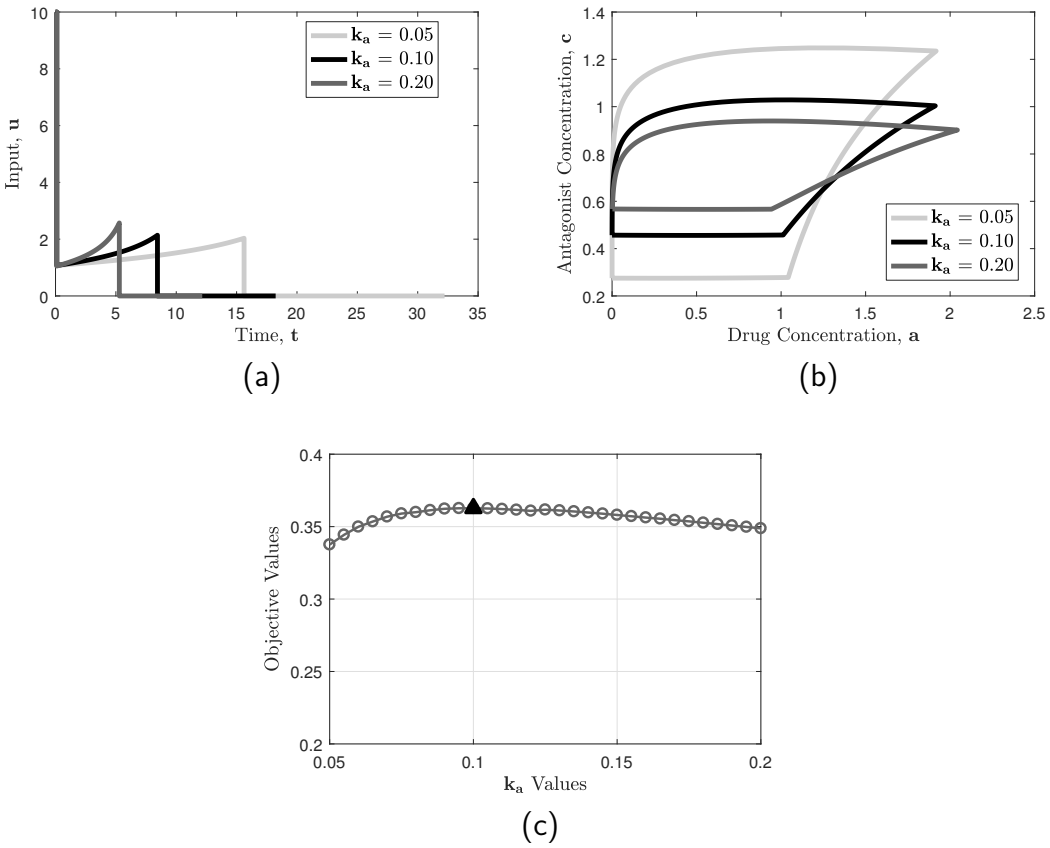

Figure 3.6. Sensitivity of the optimal (a) input trajectory, (b) phase plot, and (c) objective value to to uncertainty in k_a.

sensitivity analysis with respect to the variations in this parameter. Using the first solution method the problem is re-solved for cases where k_a is half and double its nominal value. Fig. 3.6a compares the optimal input trajectories corresponding to the three trajectories. These input trajectories are next applied to the nominal model (i.e., $k_a = 0.1$) and Fig. 3.6b illustrates the response trajectories in the state space. Fig. 3.6c depicts variations of the objective value as a function of k_a as it varies from 0.05 to 0.2. It is clearly seen that although the system trajectories are rather dramatically affected by uncertainty in k_a, the decrease in effectiveness of the drug is very small.

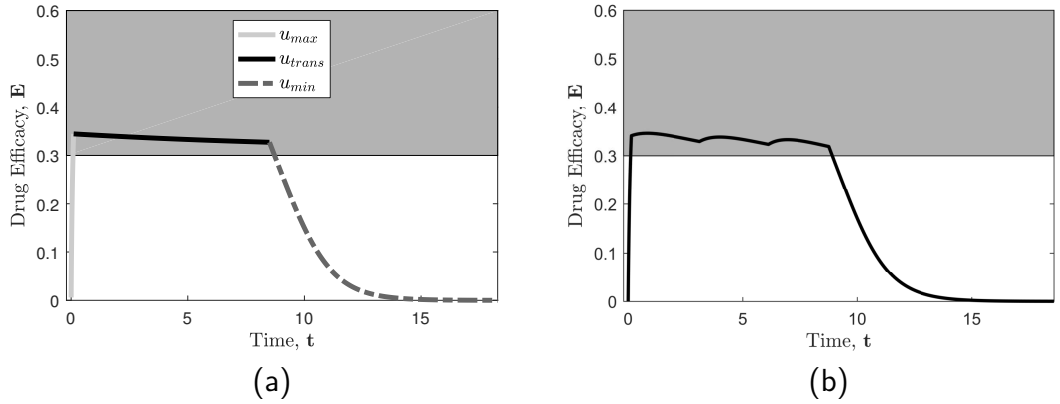

Figure 3.7. Variations of efficacy in the optimal (a) PMP based solution and (b) constant piecewise solution of the drug delivery problem. Gray shaded area is the desired range.

3.6.4 Discussion on Results

The simulation results show that a significant improvement is achieved by relaxing the steady state assumption and solving the drug delivery problem as an OPC problem. Fig. 3.7 shows how drug efficacy changes with time during one period for each solution method. These results can also be used to explain more intuitively why the OPC problem is proper. Fig. 3.8 depicts the surface of problem's Lagrangian function over the state space, as well as, the trajectory that the optimal solution traverses on this surface. The set of all the equilibrium points of the drug delivery model is also depicted. This set is the bisector of the first quadrant in the state space (i.e., the ray $a = c, a \geq 0, c \geq 0$). If the surface attained a maximum over this set, then the optimal steady state solution would be also the optimal periodic solution. However, as was predicted by π test, that is not the case and the optimal solution trajectory has to pass through both convex and concave regions of the Lagrangian's surface.

3.7 Conclusion

This chapter investigates the structure of the optimal solution to a periodic drug delivery problem. Although the literature already offers different solutions to this problem using direct transcription methods, the structure of the solution has remained unstudied. This chapter contributes to the literature by revealing this

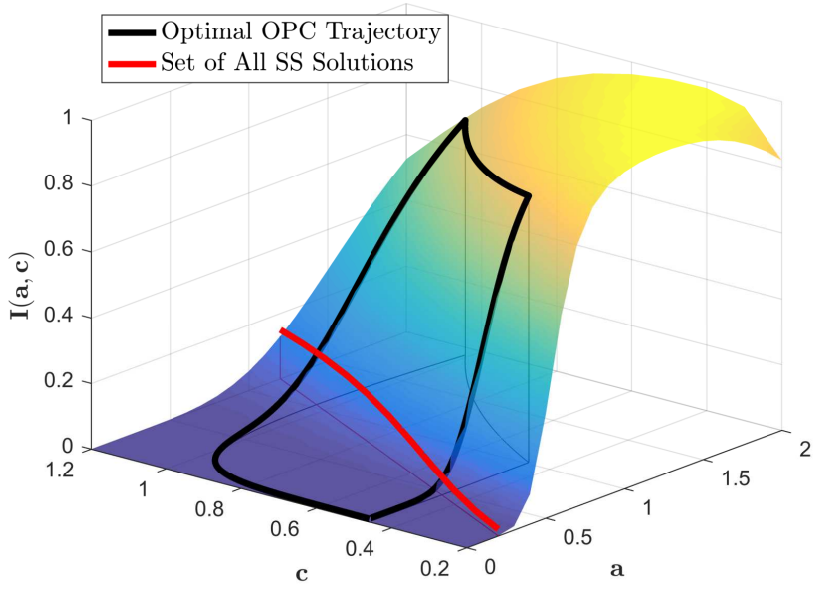

Figure 3.8. Lagrangian function of the drug delivery problem.

structure and employing it in two novel solution methods. First, PMP is employed to reveal that the optimal solution trajectory has a bang-singular-bang structure. Then an NLP problem is formulated to find the optimal transition points between the subarcs of the solution trajectory. Second, the chapter shows there exists a one-to-one correspondence between the feasible input and state trajectories of the problem. Exploiting this relationship the input trajectory is proposed for direct parameterization in a direct solution method. Not only are the two methods computationally more efficient than the literature's existing solution, but also they both show a slight improvement over the existing optimal value. However, we see the most important contribution of the chapter in revealing the optimal solution's structure. Finally, through a sensitivity analysis it is seen that the optimal solution found is also robust to parametric uncertainty.

Chapter 4
Online Shaping of a Drug's Periodic Administration Trajectory for Efficacy Maximization[1]

4.1 Introduction

Having solved the offline problem in Chapter 3, the present chapter examines the problem of online optimization of nicotine's delivery schedule for maximization of its long term cardio-accelerating effects. One common shortcoming, apparent in both the existing offline and online solution methods [45, 46, 56, 85] to this problem, is the reliance of algorithms on exact knowledge of the drug's PKPD model. However, the human body's metabolism in reaction to the nicotine injection varies from one subject to another. This affects the shape of the maximal periodic efficacy trajectory and necessitates use of algorithms capable of handling modeling uncertainties. This chapter focuses on discovering the optimal drug delivery trajectory adaptively, for patients whose underlying PKPD dynamics may not be exactly known *a priori*. We employ a model-reference, self-tuning adaptive control scheme to identify the uncertain parameters of the drug's model and use the estimates obtained for adaptation of the control policy. The chapter employs Floquet analysis to show that the overall closed loop system is asymptotically convergent in a neighborhood of the optimal periodic solution of the problem.

[1]The work of this chapter has been presented in the American Control Conference, 2015 [86] and published in IEEE Transactions on Control Systems Technology, 2017 [87].

The remainder of this chapter proceeds as follows. First, the optimal drug delivery problem is presented again together with an approximate offline solution suitable for online adaptations (Section 4.2). Next, the chapter describes the structure of the self-tuning control scheme and proves its convergence to the optimal solution cycle (Section 4.3). Lastly, Section 4.5 demonstrates the performance of the closed loop control schemes in a numerical simulation, and also compares the results to the existing solutions of the problem in the literature.

4.2 Deterministic Drug Delivery Problem

In this section, a quick review of the nicotine delivery problem is given for ease of access. The problem statement is then followed by an approximate offline solution method suitable for an online implementation.

4.2.1 Drug Delivery Model

The drug delivery problem, as stated by Varigonda in [56], considers the effect of the drug nicotine on the body. The problem uses a PKPD compartment model to capture the drug dynamics. This model is based on Porchet *et al.*'s [58] experimental work, but is adapted and nondimensionalized for control purposes. In the model, the concentration of the drug, c, causes build up in the concentration of an antagonist, a, which represents drug tolerance. The dynamics are modeled by

$$\begin{aligned} \dot{c} &= -c + u \\ \dot{a} &= k_a(c - a) \end{aligned} \tag{4.1}$$

where u is the drug infusion rate and k_a is a rate constant for antagonist elimination. The effect on the body is modeled by

$$E(c, a) = \frac{c}{(1 + c)(1 + a/a^*)} \tag{4.2}$$

where E is the drug efficacy and a^* is a measure of how much the antagonist diminishes the effect of the drug.

The goal of a successful drug delivery schedule is to maintain the drug efficacy level in a desired range, $[E_1, E_2]$. In this work, as in [45, 46, 56, 85], $k_a = 0.1$, $a^* = 1$,

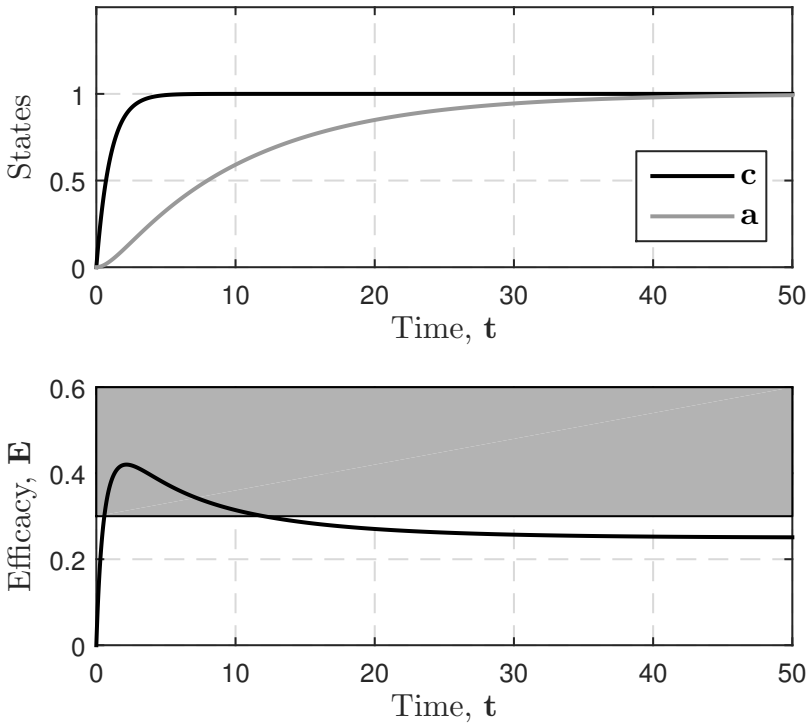

Figure 4.1. The concentration and efficacy trajectories corresponding to the best constant infusion rate (i.e. $u = 1$).

$E_1 = 0.3$, $E_2 = 0.6$.

At steady state, the maximum of the efficacy function in Eq. (4.2) is achieved when $u = a = c = 1$. This results in an efficacy level of $E = 0.25$, which is still not in the desired range. The reason for ineffectiveness of constant drug infusion rates can be seen from in Eq. (4.1) and Eq. (4.2). The presence of nicotine in the blood causes the body to build up a tolerance, which lessens the effect of the drug. Initially, the high drug concentration leads to high efficacy, but soon after, the antagonist builds and counteracts the effect. As a result, the drug is not in the effective range in the long run. Fig. 4.1 confirms this argument by depicting the state and efficacy trajectories of the model for the best time-independent delivery case.

4.2.2 OPC Problem Formulation

Allowing the drug (and the tolerance) concentration time to diminish before injecting additional drug can lead to higher efficacy in the long term. Consequently, a periodic injection pattern can be more effective than the best constant injection rate. Optimal periodic control is used to improve drug efficacy in an average sense: although it is impossible to stay in the target range for all time, it is desirable to stay in the target range for as large a fraction of time as possible.

In order to mathematically formulate the optimal periodic drug delivery problem, the smooth indicator function of Chapter 3 is again used to determine if the drug efficacy lies within the desired range, $[E_1, E_2]$. As explained in Chapter 3, the indicator function, I, is approximately 1 when within the range and 0 when outside the range and is modeled by

$$I(E) = \frac{(E/E_1)^\gamma}{(1 + (E/E_1)^\gamma)(1 + (E/E_2)^{2\gamma})} \tag{4.3}$$

where γ is a constant that controls the function's steepness at the boundary of the desired efficacy range. Similar to [45, 46, 56, 85], we set $\gamma = 10$. Fig. 3.2 demonstrates this smooth indicator function and compares it against the ideal non-smooth indicator function of the desired efficacy range.

Finally, the objective function, J, is defined as the indicator function averaged over the period, T:

$$J(I, T) = \frac{1}{T} \int_0^T I(\tau) d\tau \tag{4.4}$$

The optimal periodic drug delivery problem can now be formulated as follows.

$$\begin{aligned} &\max_{a,c,u,T} \left\{ J = \tfrac{1}{T} \textstyle\int_0^T I(t)\, dt \right\} \\ &\text{subject to:} \\ &a(0) = a(T), c(0) = c(T) \quad \textit{(Periodicity Constraints)} \\ &0 \le u \le u_{max} \qquad\qquad\qquad\quad \textit{(Input Constraints)} \end{aligned} \tag{4.5}$$

and the drug delivery dynamics given by Eq. (4.1). The nonnegativity requirement on the input is imposed to limit the solution space to include only physically meaningful trajectories. Additionally, the injection rate is bounded above by the maximum allowable drug dosage $u_{max} = 10$. As was discussed in analyzing the structure of the problem's feasible set in Chapter 3, the nonnegative input constraint

automatically restricts the state trajectories of the drug delivery model to the first quadrant. Therefore, the state nonnegativity constraint is redundant and has been dropped in the above OPC problem formulation.

4.2.3 Offline Periodic Solution

As discussed before, a constant infusion rate regimen is not very effective and in the best case results in a constant efficacy level of $E = 0.25$. This corresponds to an objective value of $J_{OSS} = 0.14$ as the best steady state solution of the problem. In Varigonda *et al.*'s work, they solve the OPC problem presented in Eq. (4.5) by parameterizing the antagonist's concentration trajectory, using the first 20 harmonics of the Fourier expansion. The input and agonist's trajectories are then obtained in terms of the transcribed flat output's (i.e. antagonist's) trajectory. The choice of the parameterization basis makes all the system trajectories periodic by construction. Finally, they solve a constrained NLP problem to find the optimal values of all the 42 parameters in their expansion, and obtain an optimal objective value of $J_{OPC} = 0.3537$.

The solution method that this chapter proposes is different in its choice of the transcription trajectory and also the way the problem's constraints are handled. It is important to mention that we do not intend to re-solve an already solved problem; the motivation is rather to develop a solution method that is more conducive for online applications. Instead of the antagonist's trajectory, here we directly parameterize the input trajectory. Note that the knowledge of the input trajectory alone is not enough to completely specify the model's state trajectory. However, for any choice of the input trajectory, the state periodicity constraint in Eq. (3.5) must be met. This helps us *uniquely* determine the proper initial state vector for any candidate input trajectory using the following expression.

$$x_u(0) = (I - e^{[A]T})^{-1} \int_0^T e^{[A](T-t)}[B]u(t)\, dt \tag{4.6}$$

where $[A]$ and $[B]$ are, respectively, the state and input matrix of the model from Eq. (4.1); I is the 2-by-2 identity matrix; and $e^{[A]t}$ is the state transition matrix of the system.

Moreover, instead of assuming "hard" constraints, we employ the *interior point* method as a "soft" constraint-handling technique, to transform the problem into an

unconstrained one. Similar to [45, 46, 85], shifted log-barrier functions are added as fictitious costs to the original objective function defined in Eq. (4.4). As a result, the area where the constraints are violated gets penalized and the area where the constraints are met is only minimally affected. The resulting "augmented" objective function is given by Eq. (4.7):

$$\begin{aligned} \bar{\phi}(I, u, t) &= I(t) + \rho_1 \log\left(u(t) + \epsilon_1\right) + \rho_2 \log\left(10 + \epsilon_2 - u(t)\right), \\ \bar{J} &= \frac{1}{T}\int_0^T \bar{\phi}(I, u, t)\, dt \end{aligned} \tag{4.7}$$

where ρ_1, ρ_2, ϵ_1, and ϵ_2, the tuning constants of the log-barrier functions, are small positive real numbers.

Using only the first n harmonics of the Fourier basis functions, the input trajectory is parameterized as follows.

$$u = \alpha_0 + \sum_{k=1}^{n} \left[\alpha_k \cos(k\frac{2\pi}{T}t) + \beta_k \sin(k\frac{2\pi}{T}t)\right] \tag{4.8}$$

Maximizing the unconstrained objective function in Eq. (4.7) with the input transcription given above and $n = 4$, we find a solution trajectory with an original objective value of $J_{OPC} = 0.33$. Fig. 4.2 illustrates the input, state, and the efficacy trajectories of this optimal solution. The difference in the objective value between the literature's solution and ours ensues from the smaller size of our optimization problem, and the fact that the interior point method with constant tuning parameters is not a "constraint-hugging" algorithm. Both these issues can be alleviated through extending the input expansion by use of more harmonics and choosing smaller weights for the log-barrier functions. However, the current formulation of the problem is simple enough for use in an online framework and we are tolerant of the small sacrifice in the optimality of its solution.

As explained before, the nicotine model given by Eq. (4.1) is not universal, and the parameters of the model depends on the specific metabolism of the human body. In the following two sections, we propose two algorithms to find and implement the solution of the periodic drug delivery problem online, each of which designed to handle different levels of uncertainty. These two algorithms build on the offline solution method developed in this section.

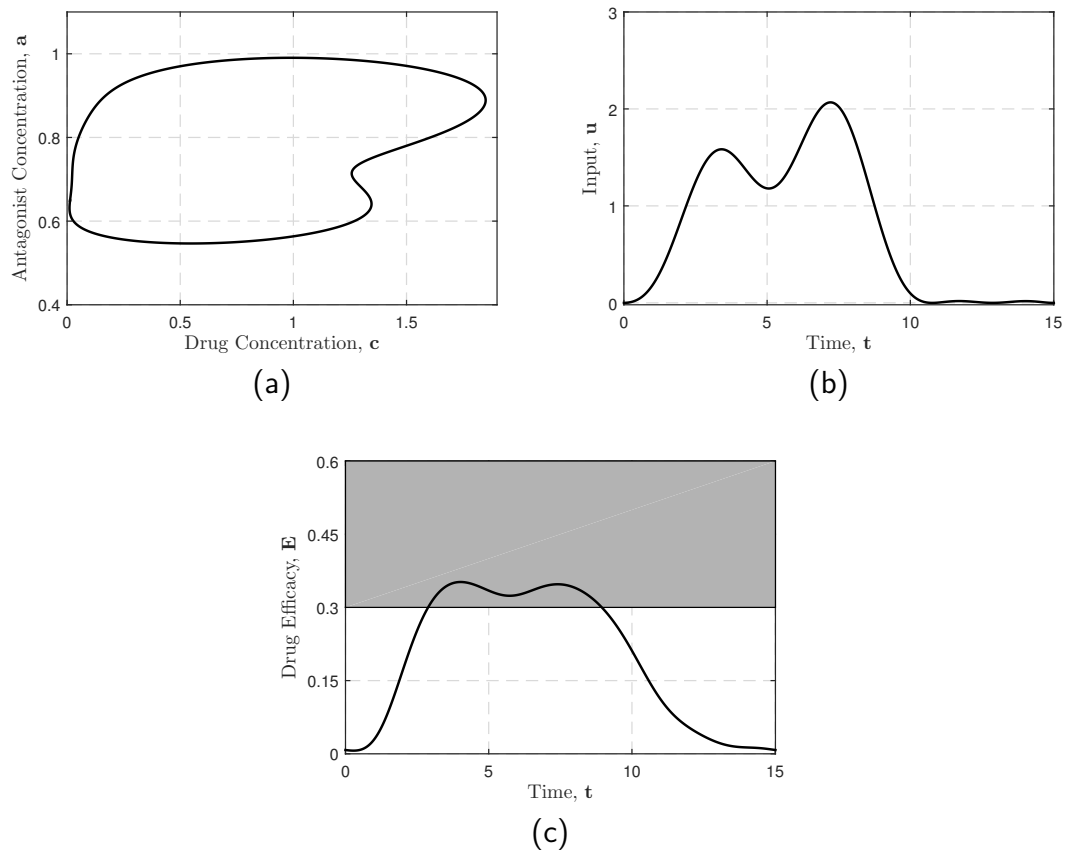

Figure 4.2. Solution trajectories of the offline drug delivery problem: (a) shows the optimal phase plot, (b) and (c) show the optima input and efficacy trajectories, respectively.

4.3 A Self-Tuning Optimal Periodic Controller

This section presents the first of two controllers for optimizing the drug's delivery trajectory online. The Self-Tuning Optimal Periodic (STOP) controller uses some information about the structure of the drug delivery model, but it is flexible in that it allows for parametric uncertainty. Fig. 4.3 schematically depicts the structure of the overall control scheme and how it interacts with the plant under control. This controller is essentially an indirect self-tuning regulator that forces the system to cycle along the optimal periodic trajectory computed online. The controller consists of three parts: (i) an estimator block that analyzes the model's input/output data and gives an approximation of the uncertain parameter(s) in the model; (ii) an adjustment mechanism which is a continuous mapping between the different

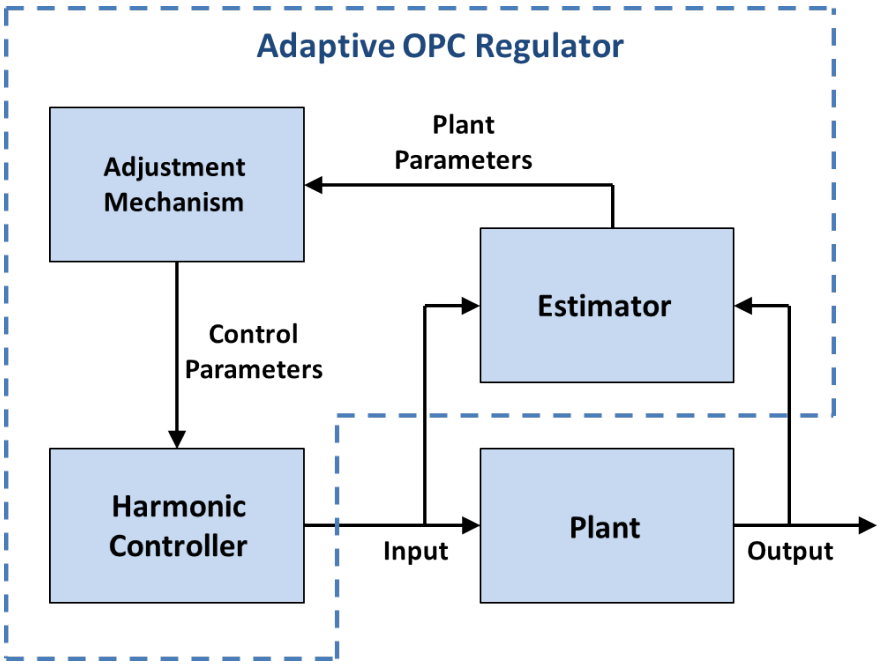

Figure 4.3. Structure of a self-tuning control scheme for optimal periodic control problems.

realizations of the uncertain parameters of the model and the corresponding sets of optimal control parameters (i.e., Fourier coefficients and time period of the input); and (iii) a harmonic oscillator that adjusts the input trajectory to incorporate the change in the control parameters and applies the input to the model. As the drug delivery system runs, the estimator develops more accurate estimates of the unknown model parameters. Then, it implements the drug infusion trajectory (found offline *a priori*) that corresponds to these estimates.

The aforementioned control scheme exploits three ideas that, when integrated together, result in steering the model to its optimal solution trajectory. This section first lays out these ideas and uses them to clarify the structure of the controller. Next, it employs linearization and Floquet theory to rigorously proves local convergence of the overall scheme to the optimal solution.

4.3.1 Details of the Closed-Loop Control Scheme

There are three ideas we exploit in the design of the STOP controller: (i) estimation of the uncertain parameters from analyzing the input-to-output response, (ii) continuous dependence of control parameters on the uncertain parameters, and

(iii) global asymptotic stability of the limit cycle corresponding to any admissible set of control parameters.

(i) Estimation of the uncertain model parameters: The parameters used in the PD portion of the drug delivery model, as well as those used in the definition of the desired efficacy range and its indicator function, are known parameters. ast, the one parameter of the PK portion, k_a, depends on the specific metabolism of the body. This parameter determines the relative decay rate of the antagonist compared to the drug concentration and directly shows up in the dynamics of the model. Here, we assume there is uncertainty in the value of k_a, and formulate an estimation problem to find this unknown value. For notational convenience, we denote by θ the estimate of the unknown parameter k_a, and use θ^* to represent its actual value (i.e. $\theta^* = k_a$). Furthermore, we assume both the agonist and antagonist concentrations (i.e. a, c) are measured. Since only a is affected by k_a, we introduce $\hat{a}$ as its estimate with dynamics similar to the real antagonist concentration dynamics:

$$\dot{\hat{a}} = \theta(c - \hat{a}) \tag{4.9}$$

Next, we define the error between the measured and estimated antagonist concentration trajectories by $e = \hat{a} - a$ and use the following gradient-descent rule to update θ:

$$\dot{\theta} = -\frac{\Gamma}{2}\frac{\partial e^2}{\partial \theta} = -\Gamma \frac{\partial e}{\partial \theta} e \tag{4.10}$$

where Γ is the estimation gain and a positive constant.

Note that $\theta = \theta^*$ is an equilibrium point of the above equation, since it is the minimizer of the error squared term, e^2. Moreover, notice that the real antagonist concentration is independent of the estimated parameter and therefore $\frac{\partial e}{\partial \theta} = \frac{\partial \hat{a}}{\partial \theta}$. The derivative of $\hat{a}$ with respect to θ is itself a time-varying variable. Let $y = \frac{\partial \hat{a}}{\partial \theta}$ denote this derivative, and differentiate both sides of Eq. (4.9) with respect to θ to obtain the following expression.

$$\dot{y} = c - \hat{a} - \theta y \tag{4.11}$$

Equations (4.9), (4.10), and (4.11) together specify the dynamics of the estimator block in Fig. 4.3. As the estimator runs and processes more data, θ continuously varies according to these equation. The most recent value of this estimated variable

can then be used to adapt the control action feeding to the model.

(ii) Continuity of control parameters: The adjustment mechanism and harmonic controller blocks in Fiq. 4.3 work together to realize an intuitive control law: implement the optimal trajectory corresponding to the best available estimate of θ^*. Following this rule requires solving the offline drug delivery problem for different realizations of θ and essentially creating a map between these values and the corresponding sets of optimal control parameters.

Fig. 4.4a and 4.4b illustrate this relationship for select control parameters. The optimal control parameters were obtained from solving the offline drug delivery problem with $\rho_1 = \rho_2 = \epsilon_1 = \epsilon_2 = 0.01$, and for a range of k_a values including its nominal value. The optimization was carried out using the MATLAB interface of the NLP solver SNOPT [100, 101], where the analytic first-order derivatives of the input constraints and the objective function were provided. The control parameters in between the optimized values are found using the natural cubic spline interpolation method.

As seen from Fig. 4.4a and 4.4b, the optimized map of control parameters as a function of the unknown plant parameters is a continuous and smooth spline. If the estimate of θ^* converges to its actual value, then from the continuity argument above, the control parameters also converge to their optimal values. This, in turn, leads to the convergence of our estimate of the optimal control action $u(G(\theta^*))$ to the actual optimal input trajectory for the model.

(iii) Global asymptotic stability of the model: The drug delivery model as presented in Eq. (4.1) has a strictly Hurwitz state matrix. Then, from the linear control theory, for any choice of the control parameters the model has a stable limit cycle and this limit cycle is globally attractive with an exponential convergence rate. Hence, if the accuracy in estimation of the uncertain parameters improves and the control input approaches to its optimal trajectory, then the states of the model will also follow the steps of the input and eventually converge to their optimal trajectory.

4.3.2 Local Convergence of the Overall Scheme

The rough convergence argument made above is entirely contingent upon convergence of the estimation parameter. Here, we rigorously analyze the convergence of

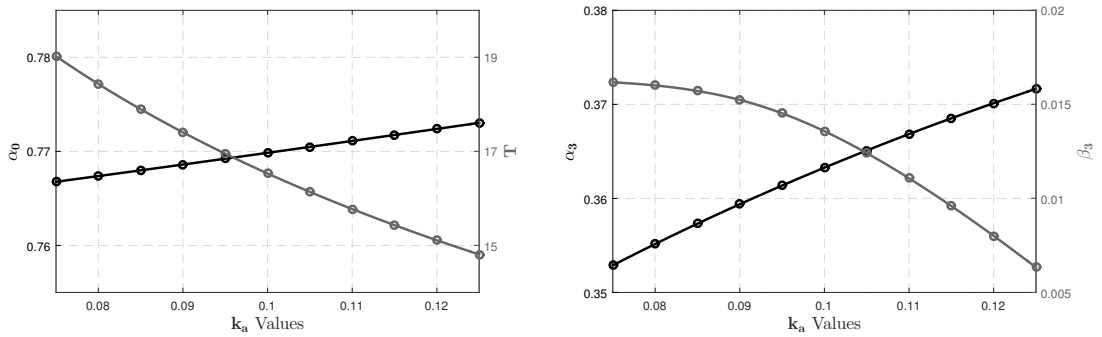

Figure 4.4. Continuous dependence of select control parameters on the uncertain model parameter, k_a.

the closed-loop system and its relation to the choice of the estimation gain Γ.

First, the closed-loop system can be reformulated as an autonomous one by introducing additional state variables that generate the periodic input function. To this purpose, we use the pair (x_{2k-1}, x_{2k}) to construct the $k^{th}-$ harmonic, which then enables us to represent the input signal as follows:

$$\begin{cases} \dot{x}_{2k-1} = -k\omega x_{2k} \\ \dot{x}_{2k} \quad = k\omega x_{2k-1} \end{cases}, k = 1, \ldots, n$$
$$u \quad = \alpha_0 + \sum_{k=1}^{n} \left[\alpha_k x_{2k-1} + \beta_k x_{2k}\right] \tag{4.12}$$

where $\omega = \frac{2\pi}{T}$ is the oscillation frequency of the input.

We augment the state vector of the drug delivery model with the state variables used in the estimator (Eq. 4.9-4.11) and input dynamics (Eq. 4.12) to obtain an autonomous representation of the closed-loop dynamics. Let z be this augmented vector defined as $z = \begin{bmatrix} e & \theta & x_1 & x_2 & \cdots & x_{2n-1} & x_{2n} & c & a & y \end{bmatrix}^T$. It will be seen that the specific ordering of the state variables and use of e instead of $\hat{a}$ simplifies the analysis. Furthermore, use $\bar{z}$ to denote the values of z along the optimal solution trajectory. Finally, define the deviations of the states from the optimal trajectory as $\delta z = z - \bar{z}$. Then, linearization of the system around the optimal trajectories determines the perturbation dynamics as follows.

$$\dot{\delta}z = P(t)\delta z \tag{4.13}$$

where $P(t)$ is the following $T-$periodic function:

$$P = \begin{bmatrix} -\theta^* & \bar{c}-\bar{a} & 0 & 0 & \cdots & 0 & 0 & 0 & 0 & 0 \\ -\Gamma\bar{y} & 0 & 0 & 0 & \cdots & 0 & 0 & 0 & 0 & 0 \\ 0 & -\dot{\omega}\bar{x}_2 & 0 & -\omega & \cdots & 0 & 0 & 0 & 0 & 0 \\ 0 & \dot{\omega}\bar{x}_1 & \omega & 0 & \cdots & 0 & 0 & 0 & 0 & 0 \\ \vdots & \vdots & \vdots & \vdots & \ddots & \vdots & \vdots & \vdots & \vdots & \vdots \\ 0 & -n\dot{\omega}\bar{x}_{2n} & 0 & 0 & \cdots & 0 & -n\omega & 0 & 0 & 0 \\ 0 & n\dot{\omega}\bar{x}_{2n-1} & 0 & 0 & \cdots & n\omega & 0 & 0 & 0 & 0 \\ 0 & s & \alpha_1 & \beta_1 & \cdots & \alpha_{2n-1} & \beta_{2n-1} & -1 & 0 & 0 \\ 0 & 0 & 0 & 0 & \cdots & 0 & 0 & \theta^* & -\theta^* & 0 \\ -1 & -\bar{y} & 0 & 0 & \cdots & 0 & 0 & 1 & -1 & -\theta^* \end{bmatrix}$$

Also, the notation $(.)'$ is used to denote the differentiation with respect to θ, and

$$s = \alpha_0' + \sum_{k=1}^{n} [\alpha_k' x_{2k-1} + \beta_k' x_{2k}]$$

As was explained before and also illustrated in Fig. 4.4a and 4.4b, all the control parameters are differentiable functions of the uncertain parameter. Consequently, s is well-defined and the above linearization is valid.

Floquet theory can be employed to analyze the stability properties of the autonomous and periodic perturbation dynamics. According to this theory, the stability of an autonomous Linear Time-Varying (LTV) system with a periodic state matrix is closely tied to the eigenvalues of its "monodromy" matrix. This matrix is defined as the *principal fundamental matrix solution* of the system evaluated at the time period of the state matrix, $t = T$. The eigenvalues of the matrix are known as the *characteristic multipliers*. The theory states that: (i) for an asymptotically stable system, all the eigenvalues fall inside the unit circle in the complex plane; (ii) if any of the eigenvalues has a magnitude greater than unity, then the system becomes unstable; and (iii) when there is only one eigenvalue of magnitude of one and the rest are inside the unit circle, the system has a periodic solution.

Lemma 1. *Let $A(t)$ be a $T-$periodic, lower block triangular matrix with the square*

A_{11} and A_{22} matrices as the diagonal blocks. Then, the set of the characteristic multipliers of the LTV system $\dot{x} = A(t)x$ equals the union of the characteristic multipliers of the two subsystems $\dot{x}_1 = A_{11}(t)x_1$ and $\dot{x}_2 = A_{22}(t)x_2$.

Proof. Let $\phi(t)$ be the principal fundamental matrix solution of $\dot{x} = A(t)x$. Therefore, from the definition $\dot{\phi}(t) = A(t)\phi(t), \phi(0) = I$, where I is the identity matrix of proper dimension. Assume the lower block triangular matrix A to be partitioned as $A = \begin{bmatrix} A_{11} & 0 \\ A_{21} & A_{22} \end{bmatrix}$. Let $\phi = \begin{bmatrix} \phi_{11} & \phi_{12} \\ \phi_{21} & \phi_{22} \end{bmatrix}$ be a partitioning of ϕ with the same configuration as A. It then follows that $\dot{\phi}_{12} = A_{11}(t)\phi_{12}$ and $\phi_{12}(0) = 0$. As the zero matrix is a solution to this initial value problem, $\phi_{12}(t) = 0$ and ϕ is a block lower triangular matrix as well. Furthermore, it follows from $\phi_{12} = 0$ that $\dot{\phi}_{11} = A_{11}(t)\phi_{11}$ and $\dot{\phi}_{22} = A_{22}(t)\phi_{22}$, which completes the proof. □

Apply the results of the above lemma to Eq. (4.13) two times. It is inferred that the characteristic multipliers of the linearized system are the collection of the characteristic multipliers of three autonomous linear systems with the following state matrices:

$$P_1(t) = \begin{bmatrix} -\theta^* & \bar{c} - \bar{a} \\ -\Gamma\bar{y} & 0 \end{bmatrix}, \; P_3 = \begin{bmatrix} -1 & 0 & 0 \\ \theta^* & -\theta^* & 0 \\ 1 & -1 & -\theta^* \end{bmatrix}$$

$$P_2 = \begin{bmatrix} 0 & -\omega & \cdots & 0 & 0 \\ \omega & 0 & \cdots & 0 & 0 \\ 0 & 0 & \cdots & 0 & -n\omega \\ 0 & 0 & \cdots & n\omega & 0 \end{bmatrix}$$

Let ϕ_1, ϕ_2, ϕ_3 be the principal fundamental matrix solutions corresponding to the state matrices P_1, P_2, P_3, respectively. Using the result of Lemma 1 once again for the lower triangular matrix P_3, the eigenvalues of $\phi_3(T)$ are simply the exponentials of the diagonal elements times the time period, namely $\{e^{-T}, e^{-\theta^* T}, e^{-\theta^* T}\}$. These eigenvalues clearly all fall inside the unit circle. Additionally, viewing ϕ_2 as the state transition matrix of the $T-$ periodic subsystem $\dot{x} = P_2 x$, it must hold that $\phi_2(T) = I_{2n}$. Therefore, $\phi_2(T)$ has $2n$ eigenvalues of 1.

Using the identity matrix I_2 as the initial condition, we numerically integrate $\dot{\phi}_1 = P_1(t)\phi_1$ from 0 to T to obtain its monodromy matrix. It is seen that for

$\Gamma \leq \Gamma_{max} = 0.05$, the two $\Gamma-$dependent characteristic multipliers will also have magnitudes less than one. Note that the formal statement of the Floquet theorem is inconclusive in the case of existence of several characteristic multipliers of magnitude one. However, because of the lower block triangular structure of the matrix $P(t)$, we assert that the solution to Eq. (4.13) is indeed periodic for $\Gamma \leq \Gamma_{max}$. With proper choice of Γ, the parameter estimate θ and the estimation error e are jointly convergent, regardless of the other state variables. After e vanishes, the input dynamics resemble a pure oscillator. Therefore, the multiple eigenvalues of unity cause a bounded and persistence oscillatory behavior. This oscillatory input in turn causes the open-loop stable drug delivery model to approach a limit cycle. Lastly, the oscillation in the states of the drug delivery model induces an oscillation in the evolution of y.

The above argument suggests that whereas the motion along some modes of the system vanish, there are perturbations in other directions that oscillate indefinitely. More specifically, this analysis tells us that for small enough estimation gains: (i) if the system is initiated from a point close but not on the optimal solution cycle, it will asymptotically converge to it; and (ii) if the system is initiated somewhere on the optimal solution cycle but with a phase shift, then the system stays on the cycle, but the phase shift remains unchanged. Needless to say, this phase shift is immaterial and does not affect the objective value of the problem. Hence, this proves that the closed-loop system is locally asymptotically convergent to the optimal solution cycle.

4.4 Note on Generalization of the Scheme to Other Problems

This section briefly discusses how the proposed controllers can be employed for solving OPC problems other than the drug delivery problem. Both the presented control architectures rely on the assumption of open loop stability of the plant's limit cycles. In other words, for each piecewise continuous periodic input trajectory, the stable LTI drug delivery model "forgets" its initial condition and eventually converges to a corresponding limit cycle. The drug delivery model is just an example of a much larger class of dynamical systems known as "Convergent Systems" that

show this property (see [88]).

Assuming that the estimator block in the STOP controller has asymptotically stable dynamics, [88] outlines the conditions under which the bidirectional interconnection of the estimator's and plant's dynamics is itself a convergent system. However, a rigorous proof of stability of the algorithm for a broader class of convergent nonlinear systems is beyond the scope of this work.

4.5 Simulation Results

This section shows the results of each of the two online OPC strategies when applied the drug delivery problem. In the STOP control scheme, the parameter k_a, from Eq. (4.1), is treated as unknown. To maintain consistency with the offline solution obtained in Section 4.2.3, we use $n = 4$.

4.5.1 STOP Control Results

For the simulation of the performance of this controller, we assume that the patient has not been exposed to the drug for a long time. Therefore, the drug and antogonist

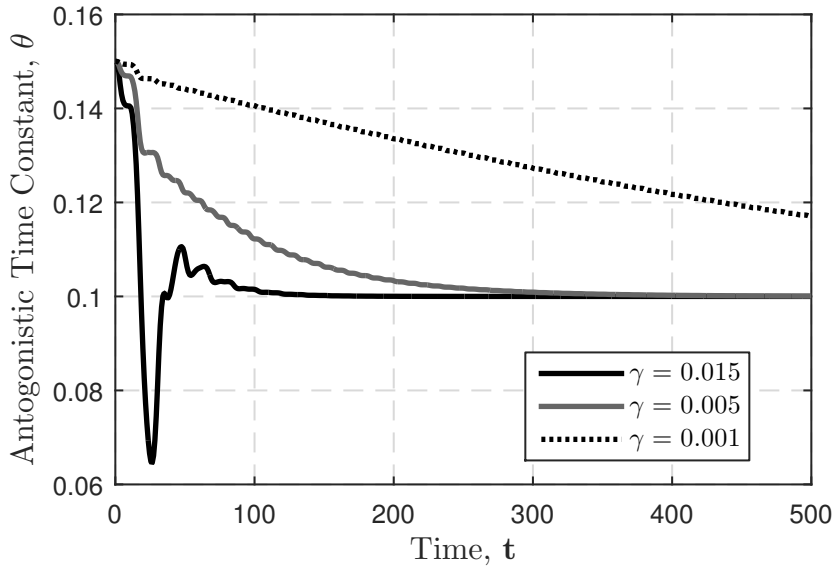

Figure 4.5. Estimated time constant of the antagonistic reaction k_a for different estimation gain values.

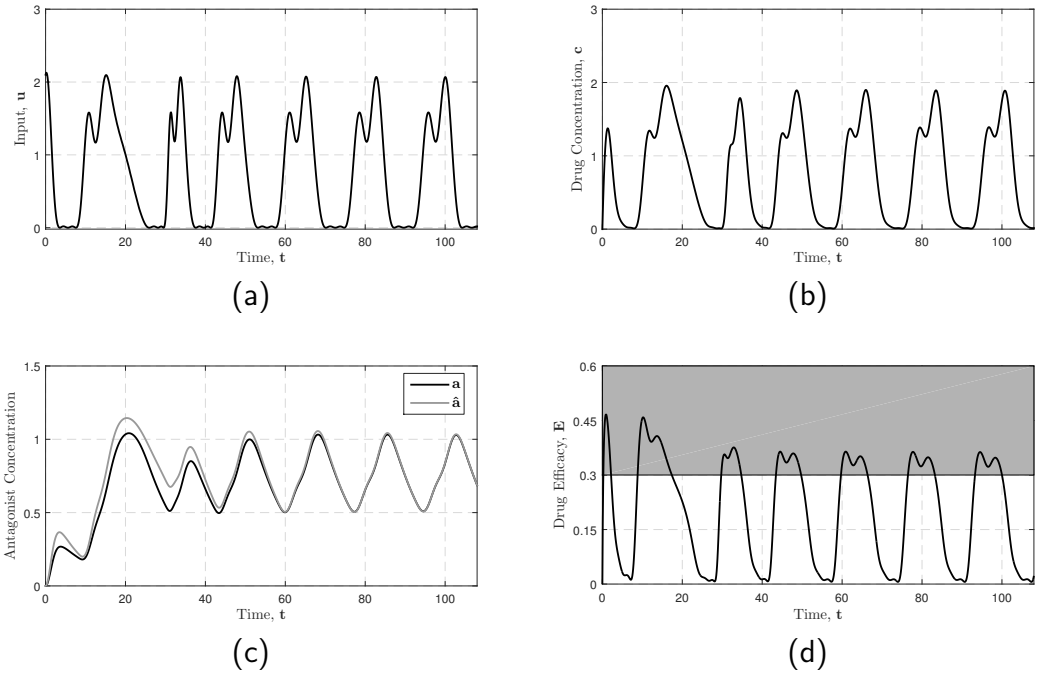

Figure 4.6. Convergence of (a) drug infusion rate, (b) drug concentration, (c) antagonist concentration, and (d) drug efficacy trajectories to their associated optimum in the self-tuning regulation scheme.

concentration as well as y are all initially set to zero. In addition, the initial guess for the uncertain parameter, k_a, is chosen to be 50% greater than its nominal value (i.e. $\theta^* = 0.1, \theta(0) = 0.15$).

Fig. 4.5 shows the convergence of the estimated parameter for 3 different stabilizing (i.e. less than Γ_{max}) values of the estimation gain. As seen in this figure, with increasing this gain the convergence rate also increases. However, this adversely affects the stability of the estimation dynamics resulting in the underdamped behavior for the case with $\Gamma = 0.013$. Fig. 4.6 depicts all the other trajectories of the closed-loop system when $\Gamma = 0.013$ is selected. Notice that the initial estimate of the unknown parameter is far from the truth and the initial position of the system far from its optimal orbit. However, within only a few cycles, all the trajectories shown in Fig. 4.6 converge to their optimum given in Fig. 4.2.

In Fig. 4.6d, the average drug's efficacy in the second cycle seems to be higher than its optimal value. Nevertheless, this acute response to the drug is caused by the initial absence of the antagonist. The behavior is only temporary and impossible

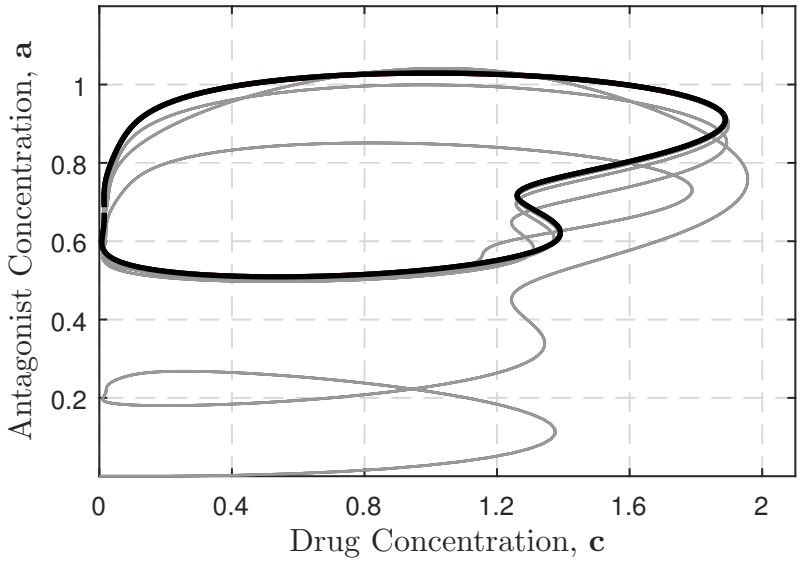

Figure 4.7. Convergence of state trajectory of the system to its optimal periodic trajectory in the self-tuning regulation scheme.

to maintain over time.

Fig. 4.7 shows the phase plot of the system as the state trajectories converge to the optimal periodic solution of the problem. This convergence to the optimum trajectory corresponds to the increasing accuracy of the estimation of k_a. As shown in Fig. 4.5, the system latches on to the correct k_a value quickly. As the estimate of k_a evolves, increasingly optimal input trajectories are implemented.

4.5.2 Comparison with the Literature

Both algorithms converge to near optimal solutions. The self-tuning regulation solution results in an average objective function of $J = 0.33$, and the ES solution results in an average value of $J = 0.31$. The values achieved in this work (without assuming an accurate model of the plant) are comparable to the values obtained elsewhere in the literature, as shown in Table 4.1. As explained before, slightly higher values of the objective function could have been achieved if more Fourier expansion terms and smaller constraint penalty weights were used.

Table 4.1. Different solutions of the drug delivery problem

Method		Avg. Obj. Fn.	No. of Cycles	No. of Parameters
Self-tuning optimal periodic regulator		0.33	4	10
Offline solution using parameterization of flat output	[56]	0.35	—	42
Online solution using parameterization of flat output	[45]	0.35	1	22
Online solution using model predictive control	[85]	0.2	15	1
Online solution using parameterization of Hamiltonian system	[46]	0.19	4	3

4.6 Discussion and Conclusions

This chapter presented an online OPC method for optimization of nicotine's periodic delivery schedule. First, an offline solution method is proposed that discretizes the nicotine's infusion trajectory as a truncated Fourier series, and then optimizes the time period and Fourier coefficients online. Building on the offline solution, an online method proposed that employs a model-reference, gradient-descent based rule to estimate parameters, and then uses the estimates to adapt the shape of the optimal trajectory. When applied to the drug delivery problem, the optimal objective function value ($J = 0.33$) and the convergence time are comparable to other deterministic schemes in the literature (see Table 4.1). This method is applicable to problems where an uncertain parameter within the plant is included but the structure of the plant is known.

Chapter 5
An Adaptive Control Algorithm for Tracking Parametric Reference Trajectories in Feedback Linearizable Systems[1]

5.1 Introduction

This chapter proposes an adaptive feedback linearizing (FBL) control algorithm for tracking reference trajectories dependent on uncertain plant model parameters. This chapter is motivated by the need for online controllers that can achieve periodic optimality in the presence of uncertain and potentially unstable open-loop plant dynamics. This represents a significant step forward from the online periodic optimal control approach of Chapter 4, which assumes open-loop plant stability. Our goal in this chapter is to solve a robust online tracking problem for a reference trajectory that may or may not be periodic. The application of the resulting approach to periodic optimal control is explored in Chapter 6.

The convergence and boundedness of the closed-loop dynamics generated by our tracking controller are studied in the presence of persistently exciting estimation regressors and assuming linear parameterization of the plant model. By allowing the target trajectory to be not fully deterministic *a priori*, our control algorithm creates an opportunity for undertaking challenging applications such as adaptive

[1]The work of this chapter has been submitted to Automatica and is currently in review [99].

model reference control where the reference model inherits some uncertain plant models or self-tuning optimal controller design.

Over the past four decades, many researchers have exploited feedback linearzation for solving regulation and tracking problems in the presence of plant model uncertainties. The work in this area can be divided into two categories. The first body of work relies on the "certainty equivalence principle". These controllers involve a static state/output feedback rule which simplifies to the deterministic FBL rule when the plant model parameters are all known. Sastry and Isidori, for instance, use an augmented error scheme together with a gradient-type identification algorithm to propose a parameter adaptive control algorithm for minimum phase nonlinear systems [59]. They prove closed-loop convergence under Lipschitz continuity assumptions on the nonlinearities for systems of varying relative degrees. Taylor *et al.* focus on the regulation problem and assume the "uncertainty matching condition" is met, but consider asymptotically stable unmodeled dynamics in addition to parametric uncertainties [60]. They also provide an estimate of the region of attraction for the overall system, when the singular perturbation parameter of the parasitic dynamics is small enough. Kanellakopoulos *et al.* derive the "extended matching condition" and develop an adaptive regulation scheme suitable for a broader class of parametric uncertainties [61]. Mrino *et al.* propose the tracking counterpart of the aforementioned algorithm by designing a nonlinear filter which converts the reference output signal to a reference state vector trajectory for the feedback linearized system [62].

The second category of parameter adaptive FBL controllers, in contrasts, develop a dynamic feedback rule using back-stepping techniques. The design procedure for these dynamic FBL controllers is usually more involved, but they can offer better transient behavior, handle a larger class of modeling uncertainties, and provide more robustness to unmodeled uncertainties. The seminal work by Kanellakopoulos *et al.* presents a dynamic-feedback-based approach for adaptive tracking of nonlinear systems transformable into the parametric-pure feedback form (a.k.a. triangular form) [63]. This work significantly broadens the class of permissible parametric uncertainties without imposing any growth condition on the allowable type of nonlinearities. Shortly after, Krstić *et al.* address the overparameterization issue of this scheme by introducing tuning functions [64]. Marino and Tomei study the problem of existence of adaptive FBL controllers robust to unknown disturbances

under the assumption of "strict triangularity condition". They allow the uncertain plant parameters to be time-varying and also enter the dynamics in a nonlinear fashion [65]. The work by Polycarpou and Ioannou design an adaptive stabilizing controller for systems in "semi-strict-feedback form" which are affected by unknown nonlinearties with partially known bounds. Assuming the triangular bounds on the nonlinearities, they prove the system trajectories are globally uniformly ultimately bounded [66]. Yao and Tomizukaia offer an alternative approach for design of adaptive robust controllers for systems transformable to the semi-strict-feedback form. Assuming known bounds on the uncertain plant parameters and using a smooth projection algorithm, their method modifies the control scheme in [64], derives an adjustable upper bound for the tracking error, and guarantees exponentially decaying transient behavior [67].

While the existing body of literature on adaptive feedback linearization is quite mature, there is an implicit restricting assumption present in all of the above algorithms when they are applied to tracking applications. The reference trajectory in tracking problems must be fully known and independent of the uncertain plant model parameters. The work in this chapter relaxes this assumption and accounts for the appearance of uncertain parameters in the target trajectory. Our scheme falls into the first category of parameter adaptive FBL controllers discussed above and requires the structure of the parameter uncertainties to be consistent with the strict matching condition.

The reminder of this chapter is organized as follows. Section 5.2 gives a quick overview of exact and adaptive feedback linearization as some basic knowledge is required for development of the chapter main's contribution. This section also explains the modeling uncertainty types considered in this dissertation. Section 5.3, next, provides a formal statement of the adaptive tracking problem for which our FBL control algorithm is designed. Subsequently, Section 5.4 covers the control synthesis and stability analysis. The chapter concludes with numerically demonstrating the performance of the control algorithm for an active vehicle suspension example in Section 5.5.

5.2 Background

There are many nonlinear dynamic systems which are "feedback equivalent" to controllable linear systems. Through a change of coordinates and use of state/output feedback, dynamic systems belonging to this class can be converted to a chain of integrators. In this section, we provide a quick background of feedback linearization theory. First, this section shows how using feedback one can exactly remove nonlinear dynamics, when a feedback linearizable plant model is fully known. The section goes over adaptive feedback linearization next, and discusses the type of structural uncertainties considered in the analysis of this chapter.

5.2.1 Exact Feedback Linearization

Feedback linearization is a very powerful tool in nonlinear systems theory, as it allows for systematic design of controllers for the entire class of feedback linearizable systems. A complete characterization of this class of dynamic systems is therefore very critical. Necessary and sufficient conditions for existence of local and global FBL transformations and control laws can be found in [102–105].

Consider a time-invariant input-affine nonlinear system given by:

$$\dot{\vec{z}} = F(\vec{z}) + G(\vec{z})\vec{u} \tag{5.1}$$

where $\vec{z} \in \mathbb{R}^n, \vec{u} \in \mathbb{R}^m$ and F and G are smooth vector fields with $F(\vec{0}) = \vec{0}$ and $G(\vec{0}) \neq \vec{0}$. For the sake of simplicity, this chapter focuses on the single-input systems (i.e., $m = 1$), but the analysis can be generalized to multi-input examples as well. Geometric control theory and Lie algebra can be employed to derive conditions for existence of a transformation and a feedback control law linearizing Eq. (5.1).

To outline the necessary and sufficient conditions for feedback linearizability, we need to first introduce some notations. The Lie bracket of two vector fields is itself a vector field defined as follows.

$$[F, G] = \frac{\partial F}{\partial \vec{z}} G - \frac{\partial G}{\partial \vec{z}} F \tag{5.2}$$

Moreover, the adjoint action $ad_F^k G$ is a repeated Lie bracket operation defined as:

$$ad_F^k G = [F \ , \ ad_F^{k-1} G] \tag{5.3}$$

for any integer $k \geq 1$ with the convention that $ad_F^0 G = G$. Furthermore, define the distribution $D^k(\vec{z})$:=span$\{G, ad_F G, \cdots, ad_F^{k-1} G\}$.

The input-affine system (5.1) is feedback equivalent to n^{th} order controllable LTI systems if and only if the following two conditions are met.

(i) ***Accessibility Condition:*** D^n is of dimension n.

(ii) ***Feedback Linearizability Condition:*** D^{n-1} is closed under the Lie bracket operation (i.e. $[F, G] \in D^{n-1} \ \ \forall F, G \in D^{n-1}$).

Refer to [105] for the multi-input (i.e. $m > 1$) version of the above differential geometry conditions. In the case of LTI systems, accessibility and controllability are equivalent concepts and Condition (i) simplifies to having a full rank controllability test matrix. Additionally, Condition (ii) is trivially satisfied for an LTI system, as the Lie bracket of any two constant vector field is zero.

Satisfaction of Conditions (i) and (ii) guarantees the existence of a diffeomorphism $\vec{x} = T(\vec{z})$ which transforms the system (5.1) into the following form.

$$\begin{aligned} \dot{x}_i &= x_{i+1}, i = 1, \cdots, n-1 \\ \dot{x}_n &= f(\vec{x}) + g(\vec{x})u \end{aligned} \tag{5.4}$$

with $f(\vec{0}) = 0$ and $g(\vec{0}) \neq 0$ [102, 105, 106]. Eq. (5.4) can be thought of as the controllable canonical form of the nonlinear system (5.1). The above system can now be easily converted to a chain of n integrators through selecting u according to the following feedback law.

$$u = g(\vec{x})^{-1}(-f(\vec{x}) + v) \tag{5.5}$$

with v as the new free control variable.

5.2.2 Adaptive Feedback Linearization

The feedback linearization procedure outlined in Section 5.2.1 relies on the exact cancellation of the plant model's nonlinearities. Adaptive feedback linearization techniques, in contrast, asymptotically eliminate the unknown nonlinearities in the plant dynamics by identifying the plant model and adapting the FBL rule accordingly.

Consistent to the majority of the adaptive literature, the work in this chapter allows parametric uncertainties to enter into the plant model, but restricts them to appear only in a linear fashion. In other words, it is assumed that the vector field F, and G in Eq. (5.1) are of the form:

$$\begin{aligned} F &= F_0 + \sum_{i=1}^{p} \theta_i^* F_i \\ G &= G_0 + \sum_{i=1}^{p} \theta_i^* G_i \end{aligned} \tag{5.6}$$

where F_i's and G_i's, $i = 0, \cdots, p$, are smooth and known vector fields and $\vec{\theta}^* \in \mathbb{R}^p$ is the vector of constant unknown plant parameters.

When F,G meet the feedback linearizability conditions outlined in Section 5.2, there exists a $\vec{\theta}^*-$dependent diffeomorphism $\vec{x} = T(\vec{z}, \vec{\theta}^*)$ that transforms the system into the standard feedback linearization form as follows:

$$\begin{aligned} \dot{x}_i &= x_{i+1}, i = 1, \cdots, n-1 \\ \dot{x}_n &= f_0(\vec{x}) + \vec{f}_1(\vec{x})^T \vec{\theta}^* + \left(g_0(\vec{x}) + \vec{g}_1(\vec{x})^T \vec{\theta}^* \right) u \end{aligned} \tag{5.7}$$

Since the controller utilizes feedback for linearization, the knowledge of the state vector $\vec{x}$ in the above representation is essential. The following two conditions explain two different possibilities in this regard.

(iii) ***Measurability of Linearized State Vector:*** the state vector of the system in its standard feedback linearization form can be directly measured.

(iv) ***Strict Uncertainty Matching Condition:*** $F_i, G_i \in D^0 = \text{span}\{G_0\}$, for $i = 1, \cdots, p$ and the original state vector $\vec{z}$ is measurable.

For many mechanical systems, for instance, the state vector $\vec{x}$ consists of some generalized coordinates of motion and can be physically measured. Condition (iii), in contrast, ensures that the diffeomorphism T is independent of $\vec{\theta}^*$ and therefore $\vec{x}$ can be indirectly calculated from the measurement of the system's original state vector, $\vec{z}$ [60, 61]. In simple words, Condition (iv) means that the input signal is directly present in those state equations which include parametric uncertainties.

5.3 Problem Statement

This chapter tackles the adaptive tracking problem for uncertain dynamic systems defined by Eq. (5.1) and (5.6). We assume the conditions (i),(ii) and either (iii) or (iv) are met. These assumptions collectively allow us to work directly with the standard representation of the system as given in (5.7). Moreover, the given parametric target trajectory is assumed to be C^n in time and C^1 in the uncertain parameter vector, where C^k is the space of functions with continuous first k derivatives.

Note that using the smooth FBL transformation T, the input and the original state vector can all be expressed purely as a function of x_1 and its first n time-derivatives. Therefore, any tracking objective for the original system dynamics can be translated into tracking a corresponding target trajectory for x_1 in the x coordinates.

In summary, for the purpose of controller design, the adaptive tracking problem can be restated in the following simplified form: find a control law and an adaptation law such that the output of the system

$$\begin{aligned} \dot{x}_i &= x_{i+1}, i = 1, \cdots, n-1 \\ \dot{x}_n &= f_0(\vec{x}) + \vec{f}_1(\vec{x})^T\vec{\theta}^* + \left(g_0(\vec{x}) + \vec{g}_1(\vec{x})^T\vec{\theta}^*\right) u \\ y &= x_1 \end{aligned} \tag{5.8}$$

is enforced to track a given reference signal $y_r(t, \vec{\theta}^*)$, where y_r is C^n in t and C^1 in $\vec{\theta}^*$.

5.4 Controller Design and Stability Analysis

This section first presents our adaptive tracking algorithm designed for the system (5.8). This algorithm uses an estimate of the uncertain plant parameters to adapt an FBL control law. Next, Lyapunov stability analysis is employed to prove the system's output always asymptotically tracks an estimate of the reference output signal. The section concludes with showing that meeting a persistence of excitation condition leads to convergence to the true target output trajectory.

5.4.1 Adaptive Control Scheme

Let us denote by $\vec{\theta}$ an estimate of the uncertain plant parameter vector $\vec{\theta}^*$. Moreover, introduce a tracking error vector $\vec{e}$ whose components are defined as follows:

$$\begin{aligned} e_1 &= y - y_r(t, \vec{\theta}) \\ &\vdots \\ e_n &= y^{(n)} - \frac{\partial^{n-1} y_r(t, \vec{\theta})}{\partial t^{n-1}} \end{aligned} \tag{5.9}$$

where $y^{(n)}$ represents the n^{th} time-derivative of the output signal, y. Using Eq. (5.7), the time dynamics of this error signal are obtained as:

$$\begin{aligned} \dot{e}_1 &= e_2 - \frac{\partial y_r(t, \vec{\theta})}{\partial \vec{\theta}}^T \dot{\vec{\theta}} \\ \dot{e}_2 &= e_3 - \frac{\partial^2 y_r(t, \vec{\theta})}{\partial t \partial \vec{\theta}}^T \dot{\vec{\theta}} \\ &\vdots \\ \dot{e}_n &= f_0(\vec{x}) + \vec{f}_1(\vec{x})^T \vec{\theta}^* + \left(g_0(\vec{x}) + \vec{g}_1(\vec{x})^T \vec{\theta}^* \right) u - \frac{\partial^n y_r(t, \vec{\theta})}{\partial t^n} - \frac{\partial^n y_r(t, \vec{\theta})}{\partial t^{n-1} \partial \vec{\theta}}^T \dot{\vec{\theta}} \end{aligned} \tag{5.10}$$

Note that, due to the smoothness requirements on y_r, system (5.10) is well-defined. Now, select the real numbers $\alpha_1, \cdots, \alpha_n$ such that $H(s) = s^n + \alpha_1 s^{n-1} + \cdots + \alpha_n$ is a Hurwitz polynomial and let A be the state matrix of $1/H(s)$ in its "controllable canonical form". Furthermore, choose an arbitrary positive definite

matrix $Q \in \mathbb{R}^{n\times n}$ and let $P > 0$ be the solution to the Lyapunov equation given below.

$$A^T P + PA = -Q \tag{5.11}$$

The adaptive FBL control law can now be expressed as follows.

$$u = \left(g_0(\vec{x}) + \vec{g}_1(\vec{x})^T \vec{s}\right)^{-1} \left(\frac{\partial^n y_r(t,\vec{\theta})}{\partial t^n} - \alpha_n e_1 - \cdots - \alpha_1 e_n - f_0(\vec{x}) - \vec{f}_1(\vec{x})^T \vec{s}\right) \tag{5.12}$$

where $\vec{s}$ is defined as:

$$\vec{s}(\vec{e},\vec{\theta}) = \vec{\theta} - \Gamma \left[\frac{\partial y_r}{\partial \vec{\theta}} \;\; \frac{\partial^2 y_r}{\partial t \partial \vec{\theta}} \;\; \cdots \;\; \frac{\partial^n y_r}{\partial t^{n-1} \partial \vec{\theta}}\right] P\vec{e} \tag{5.13}$$

with $\Gamma > 0$ as the estimation gain used to update the parameter estimate vector according to the following adaptation law.

$$\dot{\vec{\theta}} = \Gamma \left(\vec{f}_1(\vec{x}) + \vec{g}_1(\vec{x})u\right) [0 \;\; \cdots \;\; 0 \;\; 1] P\vec{e} \tag{5.14}$$

Note that without the parametric uncertainties in the plant model (i.e., $\vec{f}_1 = \vec{g}_1 = \vec{0}$), Eq. (5.12) simplifies to an exact FBL tracking control law for the system in (5.4). Also, the roots of $H(s)$, in that case, become the tracking poles for the system. Figure 5.1 is a control flow diagram depicting the interactions between the controls architecture designed above and the plant.

5.4.2 Lyapunov stability analysis

We show that our choice of the control and estimation law given by Eq. (5.12)-(5.14) makes the error dynamics in Eq. (5.10) asymptotically stable. Let us first introduce $\vec{\phi} = \vec{\theta} - \vec{\theta}^*$ as the estimation error vector. Also, for notational convenience, define the following two matrices.

$$W(t) = \left(\vec{f}_1(\vec{x}) + \vec{g}_1(\vec{x})u\right) [0 \;\; \cdots \;\; 0 \;\; 1] \in \mathbb{R}^{p\times n} \tag{5.15}$$

$$M(t,\vec{\theta}) = W(t)^T \Gamma \left[\frac{\partial y_r}{\partial \vec{\theta}} \;\; \frac{\partial^2 y_r}{\partial t \partial \vec{\theta}} \;\; \cdots \;\; \frac{\partial^n y_r}{\partial t^{n-1} \partial \vec{\theta}}\right] \in \mathbb{R}^{n\times n} \tag{5.16}$$

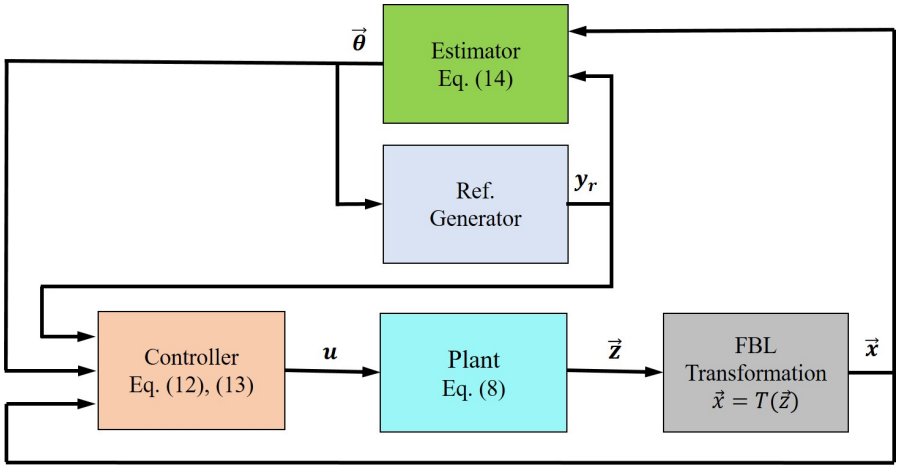

Figure 5.1. Closed-loop block diagram illustrating the interactions between the true plant and the adaptive feedback linearizing controller.

Substituting the control law from Eq. (5.12) into the error dynamics given in Eq. (5.10) and after some algebraic simplifications, one obtains the closed loop tracking and estimation error dynamics to be given by:

$$\begin{aligned} \dot{\vec{\phi}} &= \Gamma W P \vec{e} \\ \dot{\vec{e}} &= A\vec{e} - W^T \vec{\phi} + (M - M^T) P \vec{e} \end{aligned} \tag{5.17}$$

Now, consider the following positive definite expression as a candidate Lyapunov function for stabilization of system (5.17).

$$V(\vec{e}, \vec{\phi}) = \frac{1}{2} \vec{e}^T P \vec{e} + \frac{1}{2} \vec{\phi}^T \Gamma^{-1} \vec{\phi} \tag{5.18}$$

Differentiating V with respect to time and using the closed loop dynamics of Eq. (5.17) yields:

$$\dot{V}(\vec{e}, \vec{\phi}) = -\frac{1}{2} \vec{e}^T Q \vec{e} \leq 0 \tag{5.19}$$

The expression for $\dot{V}$ in Eq. (5.19) is only negative semidefinite in $(\vec{e}, \vec{\phi})$ and further analysis is needed to determines stability of the closed loop dynamics. Since V is bounded and nonincreasing $\lim_{t \to \infty} V(t)$ exists. Also, integrating $\dot{V}$ from 0 to t, one obtains:

$$0 \leq V(t) = V(0) + \int_0^t \dot{V}(\tau) d\tau \leq V(0) \tag{5.20}$$

Therefore, $\vec{e}(t), \vec{\phi}(t) \in L^\infty$, where $L^p, p \in [1, \infty]$ is the space of $p-$integrable functions. Equation (5.20) can also be rewritten as:

$$\int_0^t \vec{e}^T(\tau) Q \vec{e}(\tau) d\tau = 2(V(0) - V(t)) \tag{5.21}$$

from which it follows $\vec{e}(t) \in L^2 \cap L^\infty$. Taking the time derivative of Eq. (5.19) and using Eq. (5.17), one concludes that $\ddot{V}$ is also bounded. It then follows from the application of Barbalat's lemma to the Lyapunov candidate function V that $\lim_{t\to\infty} \dot{V}(t) = 0$, and as a result, $\lim_{t\to\infty} \vec{e}(t) = 0$. This proves that the system's output, $y(t)$, asymptotically approaches the estimate of the reference output trajectory, $y_r(t, \theta)$. Hence, the control and adaption rules derived in Section 5.4.1 guarantee bounded and asymptotic tracking of an estimate of the parametric target trajectory.

5.4.3 Convergence to the true reference output

As is typical in the adaptive control literature, the above Lyapunov analysis is inconclusive about parameter estimation convergence. When the signal used in the estimation law Eq. (5.17) are persistently exciting, the parameter estimate vector also converges to its true value. Denote by $\|\vec{e}_t(t)\|$ the distance from the true reference signal, with $e_t(t) := y(t) - y_r(t, \vec{\theta}^*)$. Next, use the triangular inequality for the Euclidean norm to conclude:

$$0 \leq \|\vec{e}_t\| \leq \|\vec{e}\| + \|\delta \vec{y}_r\| \tag{5.22}$$

where $\delta \vec{y}_r$ is an $n-$dimensional vector representing the difference between the estimate and true target trajectories and is defined as follows.

$$\delta \vec{y}_r^T = \left[y_r(t, \vec{\theta}) - y_r(t, \vec{\theta}^*),\ \cdots,\ \frac{\partial^{n-1} y_r(t, \vec{\theta})}{\partial t^{n-1}} - \frac{\partial^{n-1} y_r(t, \vec{\theta}^*)}{\partial t^{n-1}} \right] \tag{5.23}$$

However, the smoothness requirement on the target trajectory implies that y_r and its first n time derivatives are all continuous in $\vec{\theta}$. Consequently, $\delta \vec{y}_r$ approaches zero as $\vec{\theta}$ approaches $\vec{\theta}^*$. Finally, taking the limits of the inequalities in (5.22) as t tends to infinity implies that $\lim_{t\to\infty} \vec{e}_t = \vec{0}$. Hence, when the estimation

regressor vector W defined in Eq. (5.15) is “sufficiently rich", the system's output is guaranteed to asymptotically track the true realization of the target reference trajectory in a bounded fashion.

5.5 Active Vehicle Suspension Example

This section employs the Lyapunov-based adaptive control algorithm developed in Section 5.4 to design an active vehicle suspension system. Assuming uncertainty in the damping and stiffness characteristics of the suspension system, we use this numerical example to explain the implementation details of our control strategy and showcase its performance. More specifically, the problem's objective is using active control to enable percentagewise modification of the damping and stiffness parameters of the suspension model, without knowing their exact values.

5.5.1 Plant model

We use a quarter-car suspension model to explain the dynamic interaction between the vehicle's mass and the road surface. Figure 5.2 gives a graphical representation of the different components of this model together with the reference coordinate systems used to fully describe the state of the system. The variable z in this diagram represents the vehicle's vertical displacement from its reference positioning where the nonlinear spring is undeflected. Acting as an exogenous input to the suspension system, w represents the road surface roughness profile as a function of time. The following differential equation governs the vertical motion of the vehicle.

$$M\ddot{z} + C(\dot{z} - \dot{w}) + K_1(z - w)z + K_2(z - w)^3 + Mg = u \tag{5.24}$$

where g represents the gravitational acceleration and the suspension spring is assumed to be stiffening (and therefore nonlinear). Suppose there is uncertainty associated with our knowledge of the model parameters C, K_1, K_2 and only their nominal values are known.

Selecting the displacement and velocity of the mass as the state variables (i.e., $x_1 = z, x_2 = \dot{z}$) puts the system in its standard adaptive feedback linearization

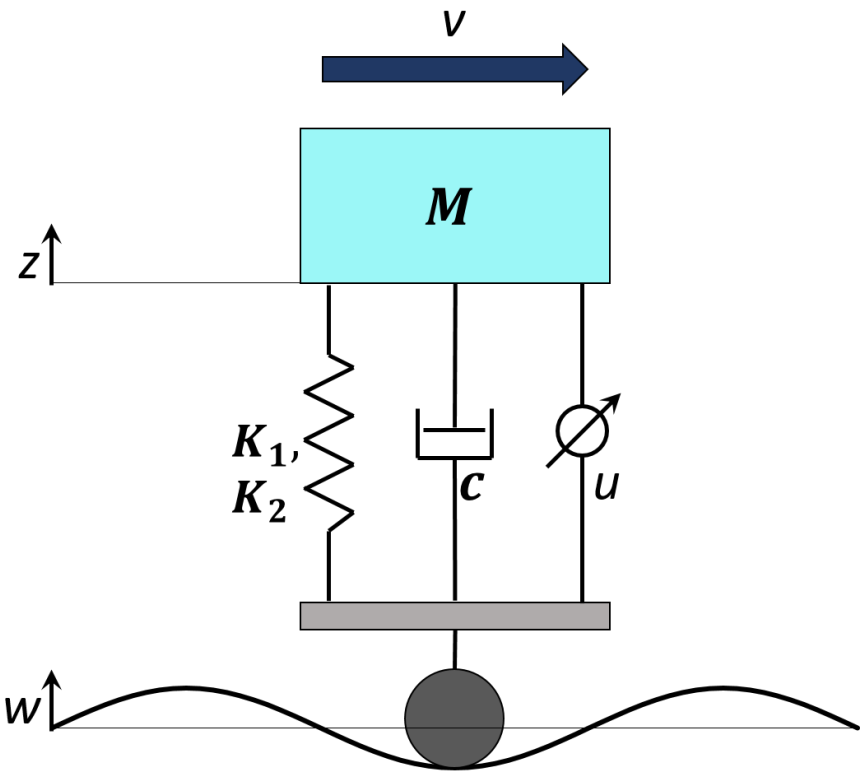

Figure 5.2. A quarter-car suspension model.

form as follows.

$$\begin{aligned}\dot{x}_1 &= x_2 \\ \dot{x}_2 &= -g + \theta_1^* \frac{K_{n,1}}{M}(w - x_1) + \theta_2^* \frac{K_{n,2}}{M}(w - x_1)^3 + \theta_3^* \frac{C_n}{M}(\dot{w} - x_2) + \frac{1}{M}u\end{aligned} \tag{5.25}$$

where $\vec{\theta}^* = [\frac{K1}{K_{n,1}}, \frac{K2}{K_{n,2}}, \frac{C}{C_n}]^T$ and the subscript n is used to denote the nominal values of the damping and stiffness parameters. The state vector $\vec{x}$ can be physically measured for this mechanical system. Table 5.1 lists the quarter-car suspension model's true and nominal parameter values in this simulation study.

5.5.2 Reference output trajectory

The reference displacement trajectory for this problem, is the output of a parameter-dependent reference model. This reference model replicates the the unforced dynamics plant, but includes additional knobs enabling modification of the damping

Table 5.1. Numerical values of the vehicle suspension model

Parameter	Value	Unit
M	1400/4	Kg
g	9.81	m/s^2
C	5300	N.s/m
C_n	8000	N.s/m
K_1	20000	N/m
$K_{n,1}$	10000	N/m
K_2	10000	N/m^3
$K_{n,2}$	8000	N/m^3

and stiffness constants. Equation 5.26 gives a state-space representation of this model.

$$\begin{aligned} \dot{x}_{r,1} &= x_{r,2} \\ \dot{x}_{r,2} &= -g + \theta_1\mu_1(w - x_{r,1}) + \theta_2\mu_2(w - x_{r,1})^3 + \theta_3\mu_3(\dot{w} - x_{r,2}) \\ y_r(t, \vec{\theta}) &= x_{r,1} \end{aligned} \tag{5.26}$$

where $\vec{\mu} = 1/M[A_1K_{n,1}, A_2K_{n,2}, A_3C_n]^T$ and A_1, A_2, A_3 are respectively the amplification coefficients for the linear spring, stiffening spring, and damping constants.

The vector $\vec{s}$ in the FBL control law of Eq. (5.12) requires computation of the parameter sensitivities of the reference output trajectory and its time derivative. Taking partial derivatives of Eq. (5.26) with respect to the uncertain parameter vector yields:

$$\begin{aligned} \dot{\vec{n}}_1 &= \vec{n}_2 \\ \dot{\vec{n}}_2 &= -\theta_1\mu_1\vec{n}_1 - 3\theta_2\mu_2(w - x_{r,1})^2\vec{n}_1 - \theta_3\mu_3\vec{n}_2 + \begin{bmatrix} \mu_1(w - x_{r,1}) \\ \mu_2(w - x_{r,1})^3 \\ \mu_3(\dot{w} - x_{r,2}) \end{bmatrix} \end{aligned} \tag{5.27}$$

with $\vec{n}_1 = \frac{\partial y_r}{\partial \vec{\theta}}, \vec{n}_2 = \frac{\partial^2 y_r}{\partial t \partial \vec{\theta}}$. It is evident that the reference trajectory $y_r(t, \vec{\theta})$ possesses the smooth properties required for the stability analysis of Section 5.4.2.

5.5.3 Selection of control parameters

The vehicle is assumed to have a constant speed of $v = 50$ mph (≈ 80.47 kph) over a sinusoidal road profile with an amplitude and period equal to 0.1 ft (≈ 0.03 m) and 20 ft (≈ 6.1 m), respectively. This amounts to base excitations with a frequency of roughly 23 rad/s affecting the chassis. Setting $\alpha_1 = \alpha_2 = 4$ leads to $H(s) = (s+2)^2$, making the "tracking poles" an order of magnitude slower than the excitation frequency.

As seen from the estimation update law given in Eq. (5.14), the estimation speed is proportional to the product of the P and Γ matrices. Additionally, from the definition of the Lyapunov function in Eq. (5.18), the matrices P and Γ^{-1} determine the relative significance of the tracking error and parameter estimation error. Therefore, ensuring that P and Γ^{-1} are of comparable sizes is important. Moreover, a large size difference between the diagonal elements of Q makes the condition number $\kappa(P)$ smaller, which puts similar emphasis on the elements of the tracking error vector, $\vec{e}$. We achieve all these objectives by selecting Q and Γ as follows:

$$Q = \begin{bmatrix} 1 & 0 \\ 0 & 10 \end{bmatrix}, \Gamma = \begin{bmatrix} 1 & 0 & 0 \\ 0 & 1000 & 0 \\ 0 & 0 & 1 \end{bmatrix}$$

Solving Eq. (5.11) for P gives $\kappa(P) \approx 4, \|P\| \approx 5$. Thus, size of P is of the same order of magnitude as $\|\Gamma^{-1}\| = 1$. The second diagonal element of Γ is selected to be much larger than the others, as it gets multiplied by e_1^3 in the estimation update law (5.14). This choice leads to a consistent rate of change for all three estimation parameters.

5.5.4 Numerical simulation results

The closed-loop response of the suspension model is simulated for the control parameters selected above. This simulation study uses the nominal values of the uncertain plant parameters as the initial guess for the estimator. The plant model itself is initiated from the equilibrium state corresponding to the weight of the vehicle. The reference model is selected to have a 25% decrease in its linear spring constant (i.e., $A_1 = 0.75$) and a 100% increase in its stiffening spring constant (i.e., $A_2 = 2$). The desired damping constant of the reference model is also double its

original value (i.e., $A_3 = 2$).

Figure 5.3 shows how the actuation force adapts as a function of time to steer the car towards its target displacement trajectory. The plotted input trajectory is normalized by the weight of the vehicle. Figure 5.4 depicts how this forcing function affects the displacement trajectory and the estimate of the target trajectory and make them approach the true target displacement trajectory. All the displacement trajectories are plotted relative to the equilibrium vertical positioning of the car. Finally, Fig. 5.5 demonstrates the evolution of the uncertain plant parameter estimates with time. The estimated parameters are normalized by their true value. Simultaneous scaling of Q and Γ by the same factor leaves the simulation results almost unchanged. Keeping Q fixed and making Γ smaller, however, can remove the overshoots in the parameter estimate trajectories at the cost of a longer convergence time.

5.6 Conclusion

This chapter presents an adaptive tracking algorithm for a class of state feedback linearizable systems with linear and constant parametric plant model uncertainties.

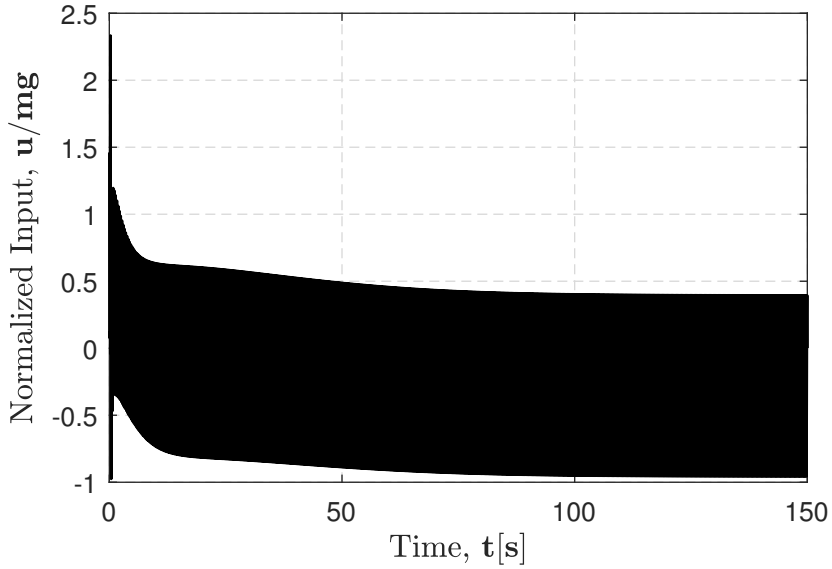

Figure 5.3. The input actuation force driving the suspension system to its reference model. The input force is normalized by the weight of the vehicle.

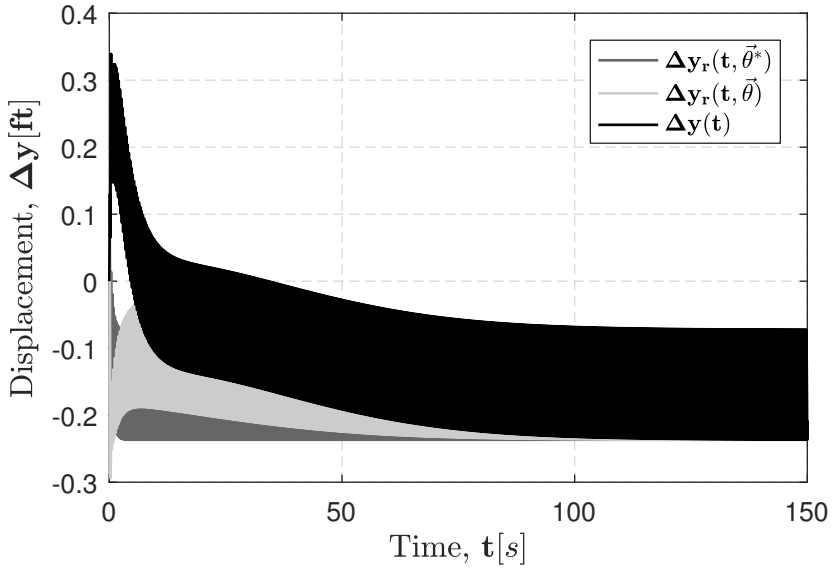

Figure 5.4. Convergence of the displacement to its target trajectory. Black is the plant's output, whereas light and dark gray represent the estimate and true target displacement trajectories, respectively.

The literature is abundant with adaptive feedback linearization strategies to design tracking controller for many nonlinear systems with varying degrees of parametric and unmodeled uncertainties. However, all the existing methods require that the target trajectory to be deterministic and fully known *a priori*. In contrast, the control algorithm developed in this chapter allows the plant's target trajectory to be dependent on the uncertain plant model parameters. Through a Lyapunov stability analysis, we prove that the controller guarantees bounded and asymptotic tracking of an estimate of the target trajectory. In the presence of persistence of excitation for the parameter identification problem, we additionally prove bounded and asymptotic convergence to the true target trajectory. The performance of the controller is demonstrated using an active car suspension example. The real plant model and the reference model share the same set of uncertain parameters in this example. The chapter concludes with a numerical simulation of the closed-loop system dynamics and explaining how different control parameters affect the convergence properties of the algorithm.

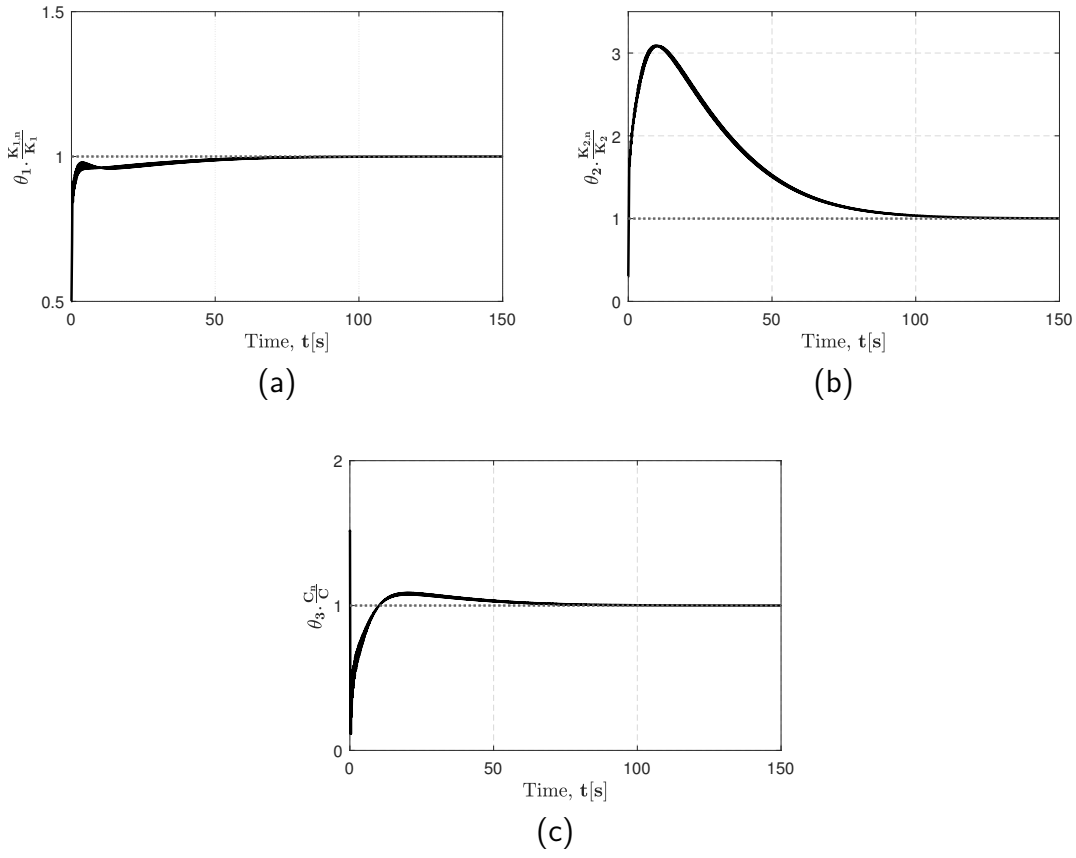

Figure 5.5. Convergence of (a) linear spring constant, (b) stiffening spring constant, and (c) damping constant estimates to their true values.

Chapter 6
An Adaptive Framework for the Online Optimal Periodic Control of Feedback Linearizable Systems with Unknown Parameters[1]

6.1 Introduction

This chapter presents a framework for solving Optimal Periodic Control (OPC) problems for feedback linearizable systems in the presence of unknown plant model parameters. As discussed in Chapter 1, it is a well-established fact in the literature that periodic operations of some dynamic systems can offer an improvement in time-averaged performance over the best steady-state behavior [1–28].

There has also been a substantial amount of work in the literature to develop offline [37–43, 84] as well as online [44–46, 85] solution strategies for OPC problems. However, all these online solution algorithms assume perfect knowledge of the underlying plant model and ensure robust tracking of the optimal solution. The online OPC controller developed in Chapter 4 and the corresponding publications [86, 87] allow for the appearance of unknown parameters in the plant model but rely on the plant's open-loop stability for implementation of the optimal solution. In other words, to the best of our knowledge, the problem of developing online control

[1]The work of this chapter has been submitted to the American Control Conference 2018 and is currently in review [107].

policies capable of converging to the true optimal periodic trajectories of open-loop unstable plants with parameter uncertainties remain relatively less-explored. The goal of this chapter is to address this shortcoming of the existing solution algorithms by employing the adaptive tracking algorithm developed in Chapter 5. More specifically, the work in this chapter assumes that the OPC solution is available for different realizations of uncertain plant parameters, and utilizes an adaptive feedback linearization technique to simultaneously estimate and track the parameter-dependent solution of the online OPC problem.

The remainder of this chapter is organized as follows. Section 6.2 formulates the online OPC problem, explains the basics of our adaptive framework, and outlines the assumptions required for its successful implementation. The next section goes over the design of the adaptive tracking algorithm central to this control framework and discusses the guaranteed convergence of the closed-loop system to its optimal periodic path (Section 6.3). Lastly, Section 6.4 employs the adaptive framework of this chapter for solving the periodic drug delivery example and provides some numerical results.

6.2 Problem Statement

This section presents the OPC problem, for which the online control framework of this chapter is developed. The section begins with introducing an OPC problem for general nonlinear plant models which include unknown parameters. Next, some simplifying assumptions on the plant model and the OPC solution trajectories are outlined. These assumptions are essential to the development of the closed-loop control scheme of the next section.

The dynamic systems considered in this chapter are assumed to be time-invariant and affine in their inputs. We specifically study optimization of the averaged cyclic performance of plant models given by:

$$\dot{\vec{z}} = F(\vec{z}, \vec{\theta}^*) + G(\vec{z}, \vec{\theta}^*)\vec{u} \tag{6.1}$$

where $\vec{z} \in \mathcal{R}^n$,$\vec{u} \in \mathcal{R}^m$, and constant $\vec{\theta}^* \in \mathcal{R}^p$ are the state, input, and uncertain parameter vectors, respectively. Additionally, F, G are assumed to be smooth vector fields of proper dimensions with $F(\vec{0}^*, \vec{\theta}^*) = \vec{0}, G(\vec{0}, \vec{0}) \neq \vec{0}$, which makes the origin

a parameter-independent equilibrium point of the dynamic system.

Given a smooth performance index functional L, an OPC problem for system (6.1) is formulated as follows:

$$\begin{aligned} &\max_{\vec{z},\vec{u},T} \left\{ J = \tfrac{1}{T} \int_0^T L(\vec{z},\vec{u})\, dt \right\} \\ &\\ &\text{subject to:} \\ &H_i(\vec{z},\vec{u}) \leq 0, i = 1, \cdots, q \qquad \textit{(Path Constraints)} \\ &\vec{z}(0) = \vec{z}(T) \qquad\qquad\qquad \textit{(Periodicity Constraint)} \end{aligned} \tag{6.2}$$

where T, the time period of the system, is to be optimized and H_i's are smooth constraints specifying the feasible region of the optimization problem.

The overarching goal of the adaptive control scheme of this chapter is to drive the state trajectories of system (6.1) towards, and force them to track, the extremal periodic path solving the OPC problem in Eq. (6.2). This optimal solution trajectory is (i) not known *a priori*, as it depends on the true values of the uncertain plant parameters, and (ii) not necessarily a globally stable orbit. We simplify the online control problem by assuming that the solution to Eq. (6.2) is available offline for any given realization of the unknown plant parameter vector $\vec{\theta}^*$. Therefore, the specific objective of the adaptive framework of this chapter is the online discovery and robust implementation of the true optimal solution trajectory among a family of parameter-dependent solutions.

For simplicity, this chapter focuses on the case of $m = 1$ (i.e., single-input dynamic systems), but generalization of the scheme to $m \geq 2$ is possible and achieved by following similar steps. The framework proposed in this chapter requires further assumptions on both the plant dynamics and the parametric solution of the OPC problem of (6.2), to guarantee stable tracking of its true solution. The dynamic system (6.1) must meet the following set of assumptions:

Assumption 1. *There exist a continuous and bijective transformation $\vec{x} = T_z(\vec{z}, \vec{\theta}^*)$ together with a state feedback law, which converts the nonlinear dynamics of Eq. (6.1) to a chain of integrators.*

The differential geometry literature derives necessary and sufficient conditions on the vector fields F, G in Eq. (6.1), for which this assumption is guaranteed [102]. Under these conditions, the nonlinear dynamics can be rendered linear through

state feedback. Specifically, a change of variables induced by the transformation T_z puts the dynamic system given in Eq. (6.2) into the following form:

$$\begin{aligned} \dot{x}_i &= x_{i+1}, i = 1, \cdots, n-1 \\ \dot{x}_n &= f(\vec{x}, \vec{\theta}^*) + g(\vec{x}, \vec{\theta}^*)u \end{aligned} \tag{6.3}$$

where f, g are scalar-valued functions with $f(\vec{0}, \vec{\theta}^*) = \vec{0}, g(\vec{0}, \vec{0}) \neq 0$. Consequently, the origin remains unchanged under this mapping (i.e., $\vec{0} = T_z(\vec{0}, \vec{\theta}^*)$).

Assumption 2. *The system dynamics are affine in the uncertain plant parameter vector, i.e., $F = F_0 + \Sigma_{i=1}^{p} \theta_i^* F_i$ and $G = G_0 + \Sigma_{i=1}^{p} \theta_i^* G_i$.*

It follows from this assumption that the functions f, g are also affine in the uncertain parameter vector and can be expressed as:

$$\begin{aligned} f(\vec{x}, \vec{\theta}^*) &= f_0(\vec{x}) + \vec{f}_1^T(\vec{x})\vec{\theta}^* \\ g(\vec{x}, \vec{\theta}^*) &= g_0(\vec{x}) + \vec{g}_1^T(\vec{x})\vec{\theta}^* \end{aligned} \tag{6.4}$$

Assumption 3. *The strict uncertainty matching condition is met, or equivalently $F_i, G_i \in span\{G_0\}$ for $i = 1, \cdots, p$.*

As explained in Chapter 5, satisfaction of this assumption ensures that the feedback linearizing transformation T_z is deterministic and independent of the unknown plant parameters. This assumption is important, as it allows for calculation of the new state vector $\vec{x}$ from the original state vector $\vec{z}$, when $\vec{x}$ in the system's linear representation may not be directly available for feedback.

In Eq. (6.1), let $\vec{\theta}$ be a variable representing an estimate of the unknown plant parameter vector $\vec{\theta}^*$. As explained before, this chapter assumes that the OPC problem formulated in Eq. (2.1) can be solved offline as a function of $\vec{\theta}$. Our adaptive control scheme additionally requires this parametric solution trajectory to vary continuously with time and $\vec{\theta}$. More specifically, for a given $\vec{\theta}$, let $x_{1,opc}(t, \vec{\theta})$ represent the x_1 trajectory corresponding to the solution of the OPC problem. Then, the following assumption must be met.

Assumption 4. *$x_{1,opc}(t, \vec{\theta})$ is C^n in t and C^1 in $\vec{\theta}$, where C^k is the class of $k-$times continuously differentiable functions.*

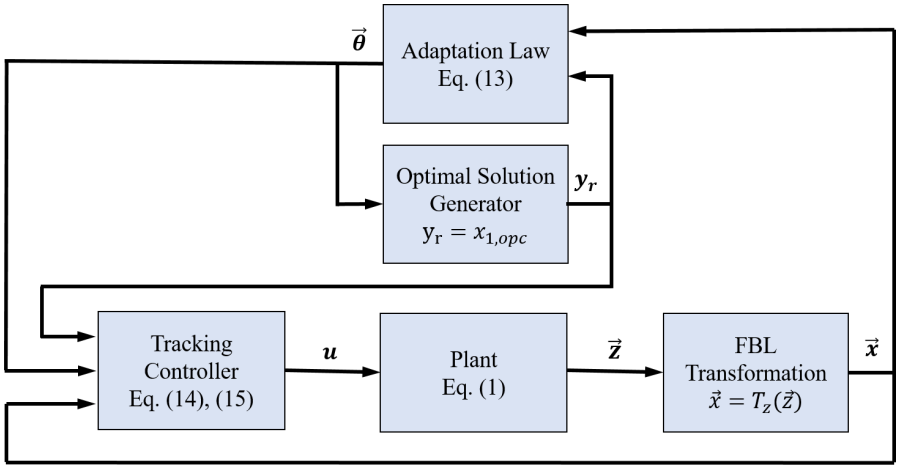

Figure 6.1. An adaptive control framework for finding, and stable tracking, of solutions of OPC problems including unknown plant parameters.

The above assumption may admittedly be somewhat restrictive. The solution to many optimal control problems involves discrete jumps or may show bifurcation behaviors with some parametric variations. In such cases, an approximate solution can be used which meets the differentiability requirements of our adaptive control scheme. In that case, our analysis guarantees convergence to an arbitrary, user-selected, smooth approximation of the optimal periodic trajectory, rather than convergence to the true optimal trajectory.

Section 6.3 show how Assumptions 1-4 allow us to accomplish the objective of this chapter. The adaptive feedback linearization control algorithm from Chapter 5 is exploited to simultaneously estimate $\vec{\theta}^*$ and track its corresponding optimal solution path computed offline. Figure 6.1 presents a schematic diagram of the adaptive control framework and demonstrates the interactions of the different elements of the closed-loop scheme.

6.3 Adaptive Tracking Algorithm

This section aims to develop an adaptive control scheme which (i) provides an online estimate of the unknown plant parameter vector, and (ii) ensures asymptotic and stable tracking of the OPC solution corresponding to this parameter estimate.

Assumption 3 of Section 6.2 allows one to use the original and the feedback linearized state-space representations of the plant model interchangeably. This

section selects $y = x_1$ as the output of the linearized representation given in Eq. (6.3). We next employ our previously-developed adaptive output tracking algorithm from Chapter 5 and [99], with the parametric optimal solution trajectory $x_{1,opc}$ designated as its reference trajectory y_r.

For ease of access, a summary of the design procedure of the adaptive tracking controller is given as follows. First, define the tracking error vector, $\vec{e}$, as in the following.

$$\begin{aligned} e_1 &= y - y_r(t, \vec{\theta}) \\ &\vdots \\ e_n &= y^{(n-1)} - \frac{\partial^{n-1} y_r(t, \vec{\theta})}{\partial t^{n-1}} \end{aligned} \tag{6.5}$$

where $y^{(n)}$ denotes the n^{th} time-derivative of the output signal, y. Recall that, from Assumption 4, $y_r = x_{1,opc}$ is C^n in time and the error vector of Eq. (6.5) is well-defined.

Next, select the real numbers $p_1, \cdots, p_n$ such that the transfer function defined by $1/H(s)$ with $H(s) = s^n + p_1 s^{n-1} + \cdots + p_n$ has all its poles in the left half complex plane. Furthermore, denote by A the state matrix of $1/H(s)$ in its controllable canonical state-space representation as shown below.

$$A = \begin{bmatrix} 0 & 1 & \cdots & 0 \\ \vdots & \vdots & \ddots & \vdots \\ 0 & 0 & \cdots & 1 \\ -p_n & -p_{n-1} & \cdots & p_1 \end{bmatrix} \tag{6.6}$$

Additionally, choose an arbitrary positive definite matrix $Q \in \mathbf{R}^{n \times n}$, and solve for the positive definite matrix $P \in \mathbf{R}^{n \times n}$ satisfying the following Lyapunov equation.

$$A^T P + PA = -Q \tag{6.7}$$

Now, the parameter estimate vector is updated according to the following equation.

$$\dot{\vec{\theta}} = \Gamma \left(\vec{f}_1(\vec{x}) + \vec{g}_1(\vec{x}) u \right) [0 \ \cdots \ 0 \ 1] P \vec{e} \tag{6.8}$$

where $\Gamma \in \mathbf{R}^{p \times p}, \Gamma > 0$ is the estimation gain matrix.

Lastly, the following equation dictates the adaptive output tracking control signal.

$$\begin{aligned} u &= \left(g_0(\vec{x}) + \vec{g}_1(\vec{x})^T \vec{s}\right)^{-1} \\ &.(\frac{\partial^n y_r(t,\vec{\theta})}{\partial t^n} - p_n e_1 - \cdots - p_1 e_n - f_0(\vec{x}) - \vec{f}_1(\vec{x})^T \vec{s}) \end{aligned} \tag{6.9}$$

with $\vec{s}$ defined as:

$$\vec{s}(\vec{e},\vec{\theta}) = \vec{\theta} - \Gamma \left[\frac{\partial y_r}{\partial \vec{\theta}} \;\; \frac{\partial^2 y_r}{\partial t \partial \vec{\theta}} \;\; \cdots \;\; \frac{\partial^n y_r}{\partial t^{n-1} \partial \vec{\theta}}\right] P\vec{e} \tag{6.10}$$

Note that when the plant model is fully known (i.e., $\vec{\theta} = \vec{\theta^*}$) and the estimator is turned off (i.e., $\Gamma = 0$), we obtain $\vec{s} = \vec{\theta^*}$ and the tracking control signal simplifies to the following expression:

$$\begin{aligned} u_{\theta^*} &= \left(g_0(\vec{x}) + \vec{g}_1(\vec{x})^T \vec{\theta^*}\right)^{-1} \\ &.(\frac{\partial^n y_r(t,\vec{\theta^*})}{\partial t^n} - p_n e_1 - \cdots - p_1 e_n - f_0(\vec{x}) - \vec{f}_1(\vec{x})^T \vec{\theta^*}) \end{aligned} \tag{6.11}$$

It can readily be seen that substituting this control law in the error dynamics cancels out all the system's nonlinearities and results in the following homogeneous LTI dynamics.

$$\dot{\vec{e}} = A\vec{e} \tag{6.12}$$

Hence, the roots of the Laplace-domain polynomial $H(s)$ are indeed the poles of the tracking error dynamics, when our knowledge of the plant model is perfect.

The Lyapunov analysis of Section 5.4.2 shows that the tracking control law of Eq. (6.9) and the estimation rule given by Eq. (6.8) collectively make the error dynamics asymptotically stable. This implies convergence to an estimate of the optimal periodic trajectory. Moreover, from the discussion in Section 5.4.3, when the plant parameter also converges to its true value, the system approaches its true optimal periodic path. This combined with the Lyapunov analysis above guarantees global convergence of system (6.1) to its true optimal periodic path.

6.4 Application to the Drug Delivery Problem

This section applies the proposed online adaptive framework to the drug delivery problem. As a reminder, nicotine affects the body through elevating the heartbeat rate: an effect which grows with the drug's concentration, but eventually diminishes as the body accumulates a tolerance to nicotine over time. The rate of nicotine absorption in the blood is much faster than the build-up of this tolerance effect. Because of this time-scale difference, there exist periodic administration trajectories which on average achieve an efficacy level much higher than the best time-invariant administration trajectory [56].

Our variational calculus analysis in Chapter 3 showed that the optimal solution trajectory has a bang-singular-bang structure. Relying on the intrinsic *open-loop stability* of the model, Chapter 4 proposed an adaptive controller for implementing the optimal solution in the presence of parametric uncertainties in the plant model. Chapter 4 also employed Floquet analysis to show the local closed-loop stability of the true periodic solution trajectory with this controller. The control scheme presented in this chapter offers another online method for implementing the solution of this benchmark OPC problem in the presence of unknown plant parameters. This implementation method has two main advantages over the existing solutions in the literature: (i) it does not depend on the open-loop stability of the drug delivery model; (ii) convergence to the optimal solution is global, assuming persistence of excitation.

6.4.1 Plant Model and Optimization Objective

This Section uses a slightly modified formulation of the drug concentration dynamics from [56]:

$$\begin{aligned} \dot{c} &= k_c(u - c) \\ \dot{a} &= k_a(c - a) \end{aligned} \tag{6.13}$$

where the new parameter k_c in this model determines the elimination rate of the agonist concentration with $k_c = 1 \gg k_a = 0.1$. The dimensionless drug efficacy

metric capturing the drug's interaction with the body is again given by:

$$E(c,a) = \frac{c}{(1+c)(1+a)} \tag{6.14}$$

and the smoothed indicator function for the desired efficacy interval $[E_1, E_2]$ is:

$$I(E) = \frac{(E/E_1)}{(1+(E/E_1)^{10})(1+(E/E_2)^{20})} \tag{6.15}$$

Similar to the problem statement of Chapter 3 and Chapter 4, the optimal periodic treatment regimen is the solution to the following optimal control problem.

$$\begin{aligned}
&\max_{a,c,u,T} \left\{ J = \tfrac{1}{T}\int_0^T I(t)\,dt \right\} \\
&\\
&\text{subject to:} \\
&a(0) = a(T), c(0) = c(T) \quad \textit{(Periodicity Constraints)} \\
&0 \le u \le 10 \quad \textit{(Input Constraints)} \\
&a(t) \ge 0, c(t) \ge 0 \;\; \forall t \in [0,T] \quad \textit{(State Constraints)}
\end{aligned} \tag{6.16}$$

and the drug delivery dynamics given in Eq. (6.13).

To showcase the performance of our adaptive optimal control framework for this problem, suppose that the antagonist elimination rate, k_c, is unknown. Note that an unknown k_a violates the uncertainty matching condition and therefore our adaptive tracking algorithm would require the direct measurement of $\vec{x}$ which may not be feasible. We demand to find and track the optimal solution of Eq. (6.16), where only an initial estimate of the plant model parameter k_c is available. Choosing $x_1 = a$, $x_2 = \dot{a} = k_a(c-a)$ transforms Eq. (6.13) into the standard feedback linearization form as follows:

$$\begin{aligned}
\dot{x}_1 &= x_2 \\
\dot{x}_2 &= -k_a x_2 + \theta^*(-k_a x_1 - x_2) + \theta^* k_a u \\
y &= x_1
\end{aligned} \tag{6.17}$$

with $\theta^* = k_c$. Note that $\vec{x}$ can be calculated from the measurement of the agonist and antagonist concentrations. Thus, Assumptions 1-3 are all met and the adaptive scheme of this chapter is applicable. Although the drug delivery model has already linear dynamics, the adaptive tracking controller of this chapter can be used for any

feedback linearizable system. An application of this controller in a model reference adaptive control scheme for a nonlinear car suspension system can be found in [99].

6.4.2 Parametric Optimal Solutions

As shown in Chapter 3, the optimal drug injection rate solving Eq. (6.13) is only piecewise-continuous and has a bang-singular-bang structure [84]. Therefore, Assumption 4 is not met for the true optimal periodic solution path and we instead use an smooth approximation of the optimal solution trajectory similar to the analysis of Chapter 4.

The smoothed approximation of the solution to the optimal drug delivery problem is obtained as follows. First, introduce the change of variable $t = T\tau$ and incorporate the input constraints using shifted log-barrier penalty functions. This yields an augmented OPC objective function given by:

$$\tilde{J} = \int_0^1 \{I + \rho_1 \log(\epsilon_1 + u_{max} - u) + \rho_2 \log(\epsilon_2 + u)\}\, d\tau \tag{6.18}$$

The state nonnegativity constraints are automatically satisfied when the input bounds are respected [84]. Next, approximate the periodic x_1 trajectory with its truncated Fourier expansion as follows.

$$\begin{aligned} x_{1,opc}(\tau, \vec{\theta}) \approx\ & \alpha_0(\vec{\theta}) \\ & + \Sigma_{k=1}^{N} \left(\alpha_k(\vec{\theta}) \cos(\omega_k \tau) + \beta_k(\vec{\theta}) \sin(\omega_k \tau)\right) \end{aligned} \tag{6.19}$$

where $\omega_k = 2k\pi, k = 1, \cdots, N$. Lastly, use Eq. (6.17) to express the original state and input trajectories in terms of x_1 as follows:

$$\begin{aligned} a &= x_1 \\ c &= \frac{T}{k_a} x_1' + x_1 \\ u &= \frac{T^2 x_1'' + T(k_a + \theta) x_1' + \theta k_a x_1}{k_a \theta} \end{aligned} \tag{6.20}$$

where x_1' and x_1'' represent first and second derivatives with respect to the new time variable τ. It is clear from Eq. (6.19) and (6.20) that all the system trajectories are made $T-$periodic by construction.

The infinite dimensional OPC problem of Eq. (6.13) has reduced to a $2 \times (N+1)$ dimensional NLP problem in terms of the coefficients and time period of a truncated Fourier series for the antagonist concentration trajectory. This NLP problem is solved for a discrete mesh of the interval spanning the likely realizations of the uncertain plant parameter vector. This bank of optimal solutions constitutes the desired parameter-dependent target trajectory, $y_r(t, \theta)$, for our adaptive tracking algorithm.

6.4.3 Adaptation and Control Laws

From Section 6.3, the tracking error vector is defined as:

$$\begin{aligned} e_1 &= a - y_r \\ e_2 &= k_a(c - a) - \frac{\partial y_r(t, \theta)}{\partial t} \end{aligned} \tag{6.21}$$

The parameter update rule then becomes:

$$\dot{\theta} = \Gamma k_a (u - c)[0\ 1] P \vec{e} \tag{6.22}$$

and the tracking control law is written as follows:

$$u = \frac{\frac{\partial^2 y_r}{\partial t^2} - p_2 e_1 - p_1 e_2 + k_a^2 (c - a)}{ka(\theta - \Gamma[\frac{\partial y_r}{\partial \theta}\ \ \frac{\partial^2 y_r}{\partial t \partial \theta}] P \vec{e})} + c \tag{6.23}$$

Assuming that the agonist and antagonist concentrations are available for measurement, Eq. (6.22) and (6.23) together must guarantee convergence of the tracking error dynamics.

6.4.4 Numerical Results and Discussions

Table 6.1 lists all the parameter values used in this study. Similar to the numerical study of Chapter 3 and 4, the model parameters are all adopted from [56]. The simulation is performed with zero initial states, assuming that the body has not been exposed to the drug for a sufficiently long time period. The initial guess of the uncertain parameter value is set to be %50 larger than its true value.

All the parameters of the shifted log-barrier penalty functions are set equal to

0.01. With these soft penalty terms, the approximate solution to the OPC problem of Eq. (6.16) yields an objective value of $J_{OPC} = 0.33$. This is fairly close to the true theoretical optimal objective value of $J_{OPC} = 0.36$ obtained in Chapter 3. Figure 6.2a and 6.2b depict variations of select optimal parameters of Eq. (6.19) as a function of the uncertain plant parameter, where the first four harmonics of the Fourier expansion is used (i.e., $N = 4$). The optimization was carried out using the MATLAB's interface of the NLP solver SNOPT [100, 101], for θ values spanning from $0.5k_c$ to $2k_c$ with a step size equal to %5 of k_c. The optimal values are marked by circles, whereas the solid lines represent the best 5^{th} order polynomials fits. These smooth polynomials are then used to construct the target optimal antagonist trajectory for the simulation study.

The selected p_1, p_2 values from Table 6.1 places both the poles of tracking error dynamics at -0.5. Faster poles can also be used at the expense of more aggressive control behavior. From the discussion in Chapter 5, the matrices P and Γ^{-1} determine the relative importance of the tracking and estimation errors, respectively. Also, the estimation convergence speed is proportional to the product of norms of P and Γ. Selecting Q as the 2-by-2 identity matrix, we solve Eq. (6.7) for P. The choice of $\Gamma = 2$ puts the norms of P and Γ^{-1} within the same order of magnitude and achieves fast convergence.

Table 6.1. Numerical parameter values for the drug delivery example

Parameter	Value
k_c	1
k_a	0.1
E_1	0.3
E_2	0.6
u_{max}	10
$\vec{x}(0)$	$[0,\ 0]^T$
$\theta(0)$	$1.5k_c$
ϵ_1, ϵ_2	0.01
ρ_1, ρ_2	0.01
p_1	1
p_2	0.25
Q	I_2
Γ	2

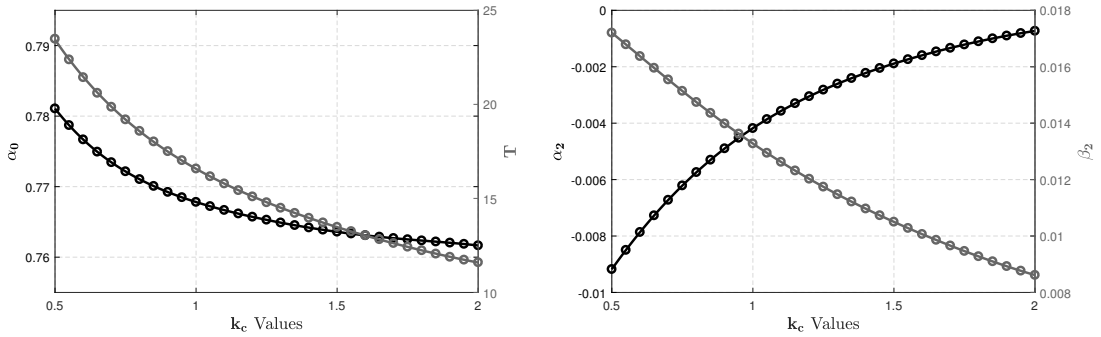

Figure 6.2. Continuous dependence of select reference signal's parameters on the uncertain model parameter, k_a.

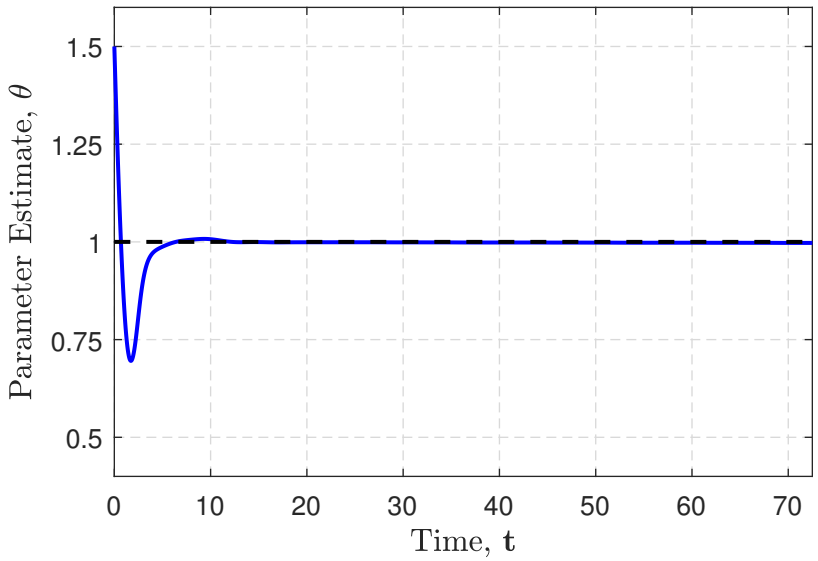

Figure 6.3. Convergence of the uncertain plant parameter estimates to its true value.

Figure 6.3 shows that the unknown parameter estimate quickly converges to its true value. Figure 6.4 depicts time variations of the control input and adaptation of its shape as the unknown parameter estimate changes. The drug's injection rate approaches its final periodic trajectory after roughly two cycles. The measured output antagonist concentration trajectory as well as its estimate and true target optimal trajectories are demonstrated in Fig. 6.5. Despite the %50 error in the initial guess for the uncertain parameter, it can be seen that the estimate and true

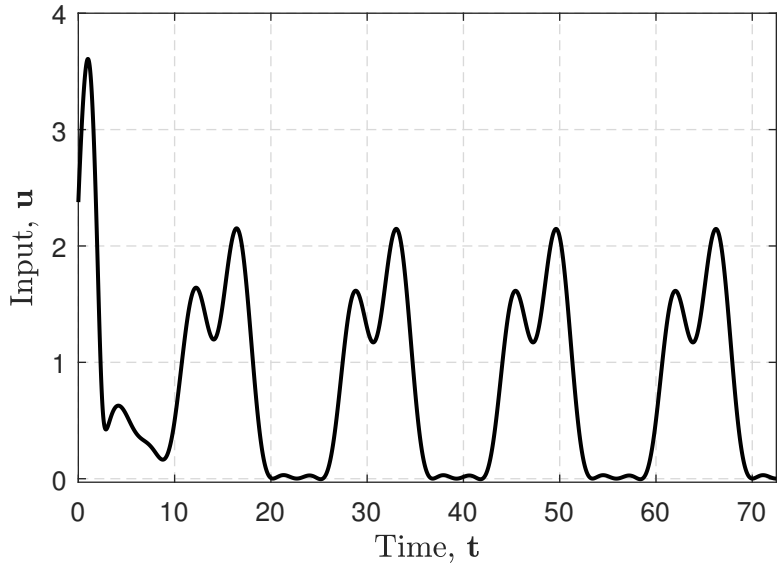

Figure 6.4. The drug infusion rate steering the system towards its maximal efficacy trajectory in the presence of parametric modeling uncertainties.

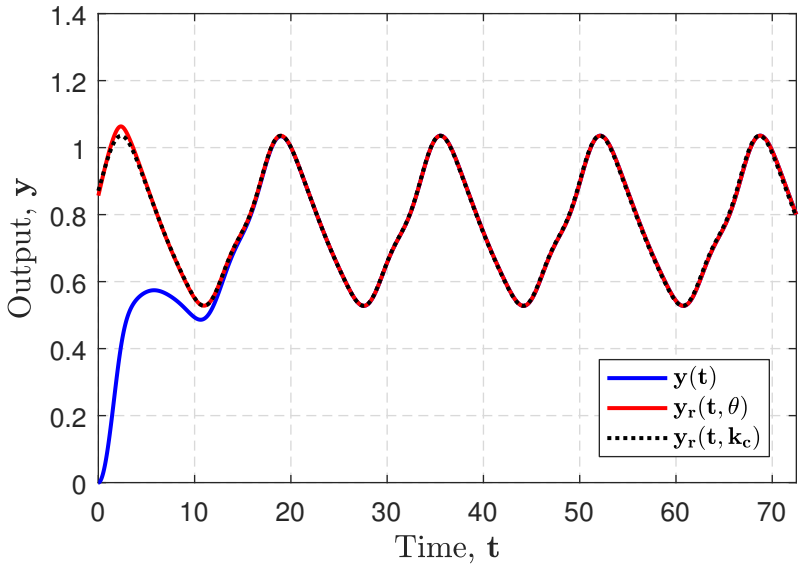

Figure 6.5. Convergence of antagonist concentration to its true optimal trajectory. Solid blue is the measured agonist concentration, whereas solid red and dashed black respectively represent the estimate and true efficacy maximizing trajectories.

reference optimal trajectories start off very close to each other. With the unknown plant parameter estimate quickly converging, the estimate optimal trajectory soon

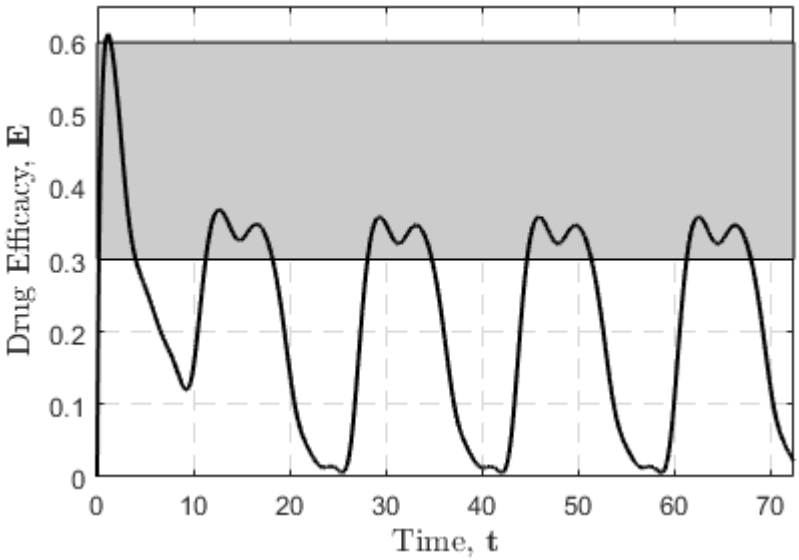

Figure 6.6. Convergence of the drug efficacy to its maximal periodic trajectory. The gray shaded area represents the desired efficacy range.

approaches its true counterpart. This drives the measured antagonist concentration to its optimal periodic destination after roughly two cycles. Finally, Fig. 6.6 depicts convergence of the drug's efficacy to its optimal periodic path. As seen from this figure, on the optimal periodic path, the drug's efficacy remains in its desired effective range for almost a third of each cycle. The average drug efficacy in the first cycle seems to be higher than its optimal value. Nevertheless, this acute response to the drug is caused by the initial absence of the antagonist and the behavior is only temporary and not sustainable over time.

6.5 Conclusions

This chapter proposes an adaptive control framework designed for online solution of a large class of OPC problems. The underlying plant models in these OPC problems are assumed to have feedback linearizable dynamics, which potentially include some unknown parameters. The exact shape of the optimal periodic solution of the problem is typically dependent on those unknown plant parameter and therefore the target optimal periodic path may not be known *a priori*. A common practice in optimal control is to find the solution to the nominal formulation

of an optimal control problem and ensure its robust tracking for the real plant model. This technique, however, is often not justified in periodic operation regimes. As insignificant as the loss associated with implementation of the nominal optimal solution might be, the repetition of the cycle could lead to a substantial accrual of performance deterioration over time. This creates a critical need for an online framework capable of discovering the true optimal periodic path of the system and ensuring its stable tracking in the presence of unknown plant parameters.

The adaptive optimal control algorithm of this chapter addresses this need by (i) assuming that the optimal solution trajectory is available as a function of the uncertain plant parameters and (ii) developing an adaptive feedback-linearizing control algorithm that simultaneously estimates and tracks the optimal solution trajectory. Through a Lyapunov analysis, we show that the tracking error signal is always bounded and asymptotically approaches zero. Furthermore, a persistently exciting estimation regressor signal guarantees global and asymptotic convergence of the system's trajectories to their true optimal periodic paths. The chapter concludes with numerically showcasing the performance of the proposed control framework in a periodic drug delivery application problem.

Chapter 7
Conclusions

This dissertation presents a framework to achieve periodic optimality for dynamic systems in the presence of unknown plant models. It is well established in the literature that periodic operations can improve the average performance beyond the standard steady-state design paradigm in many engineering systems. However, the adoption of optimal control methods in practice has been hindered due to the challenges associated with the online implementation of these algorithms.

The realization of a robust online periodic controller is tied to addressing the following sequence of questions in the order they are posed: (i) How one can determine if an engineering application can benefit from periodic operation? (ii) What is the structure of the optimal periodic controller for a given application problem and can one use this structure for efficient computation of the optimal periodic trajectories? (iii) How does one implement these optimal periodic solutions in a stable manner in the presence of plant parameters/model uncertainties, when these optimal solutions are not known *a priori* because if these uncertainties?

This dissertation addresses the above questions in the context of different application problems from the literature. The end results, based on the answers to the above questions, is an adaptive optimal periodic controller which accounts for the existence of unknown plant parameters and offers guaranteed stability properties. The work in this dissertation is composed of 7 chapters each taking a further step towards the design of this above online periodic controller. More specifically, the main body of this dissertation is organized as follows.

- Chapter 1 presents the motivation for the work of this dissertation and the state-of-art in the OPC literature. The benefits and the shortcoming of the

existing bodies of work in the literature are discussed followed by a list of contributions of this dissertation to address those limitations.

- Chapter 2 introduces a test from the OPC literature in response to the first research question posed above. Through this test one can determine whether periodic operations can outperform the best steady-state behavior. The application of this tool is demonstrated on a flapping flight model of the fruit fly.

- Chapter 3 addresses the second research question by incorporating variational calculus methods to discover the structure of the solution trajectory of a periodic drug delivery application. Two different discretization approaches based on the discovered structure are presented and shown to reduce the computational requirements of solving the offline OPC problem.

- Chapter 4 takes the first step towards answering the third research question by developing an online adaptive OPC controller for the drug delivery application in the presence of unknown plant parameters. This controller is dependent on the innate open-loop stability of the drug absorption dynamics. The local convergence of the closed-loop scheme is shown using Floquet analysis.

- Chapter 5 designs a novel adaptive tracking algorithm grounded in the principles of feedback linearization theory as an attempt to relax the stability requirement of the controller developed in Chapter 4. A Lyapunov stability analysis establishes global convergence to any smooth target trajectory dependent on unknown plant parameters. A numerical active vehicle suspension example is employed to showcase the performance of the algorithm.

- Chapter 6 finally presents the online robust OPC framework of this dissertation with the adaptive tracking controller of Chapter 5 incorporated at its heart. The performance of the closed-loop scheme is demonstrated through a numerical simulation of the benchmark drug delivery application.

Appendix A
The Π matrix as a function of the flight kinematics and aerodynamic coefficients

In this appendix, the $\Pi(\omega, \lambda)$ matrix introduced in Section 2.4.3 is expressed as an explicit function of the flight kinematics and the model's lift and power coefficients.

Table A.1 provides a summary of the components of the $P = H_{xx}$ and $Q = h_{xu}$ matrices in terms of the flight model's variables and parameters, where the pair of subindices ij denotes the element sitting in i^{th} row and j^{th} column of the

Table A.1. Components of P, Q matrices used in the definition of the Π matrix

Matrix Entry	Expression
P_{11}	$2(1-\gamma)K_t \sin(2\alpha_{oss}) - 6\gamma(T_{t1} - T_{t2}\cos(2\alpha_{oss}))\dot{\phi}_{oss}$
P_{12}, P_{21}	$(1-\gamma)(K_{a1}\cos(\alpha_{oss})^2 + K_r\cos(\alpha_{oss})) - \gamma(2T_r\sin(\alpha_{oss}) + T_{a1}\sin(2\alpha_{oss}))\dot{\phi}_{oss}$
P_{13}, P_{31}	$4(1-\gamma)K_t\cos(2\alpha_{oss})\dot{\phi}_{oss} - 6\gamma T_{t2}\sin(\alpha_{oss})\dot{\phi}_{oss}^2$
P_{22}	$-2\gamma T_{a4}\cos(\alpha_{oss})\dot{\phi}_{oss}$
P_{23}, P_{32}	$-(1-\gamma)(\sin(2\alpha_{oss}) + K_r\sin(\alpha_{oss}))\dot{\phi}_{oss} - \gamma(T_{a1}\cos(2\alpha_{oss}) + T_r\cos(\alpha_{oss}))\dot{\phi}_{oss}^2$
P_{33}	$-4(1-\gamma)K_t\sin(2\alpha_{oss})\dot{\phi}_{oss}^2 - 4\gamma\cos(2\alpha_{oss}))\dot{\phi}_{oss}^3$
Q_{11}	$-\gamma T_{a1}\sin(\alpha_{oss})^2$
Q_{12}	$-\gamma T_{a2}\sin(\alpha_{oss})$
Q_{21}	0
Q_{22}	0
Q_{31}	$(1-\gamma)K_{a1}\cos(2\alpha_{oss}) - \gamma T_{a1}\sin(2\alpha_{oss})\dot{\phi}_{oss}$
Q_{32}	$-(1-\gamma)K_{a2}\sin(\alpha_{oss}) - \gamma T_{a2}\cos(\alpha_{oss})\dot{\phi}_{oss}$

corresponding matrix.

Also, as mentioned in Section 4.2.2, the $R = H_{uu}$ matrix is zero due to the linearity of the lift and force expressions in $\ddot{\phi}, \ddot{\alpha}$. The Π matrix is then calculated by the substitution of P, Q, R, and results in the expression given in Eq. (2.36).

Appendix B
Existence of A Bijective Map between the Periodic Input and State Trajectories of an LTI System

This appendix proves the statements made in Section 3.3 regarding the existence of a bijective map between the periodic input and state trajectories of a given LTI system. The proofs are presented in the order in which the statements are given as follows.

Proof of Statement 1: Let x_u be a $\tau-$periodic orbit induced by the $T-$periodic input u. We first show that $\tau = nT$ for some $n \in \mathbb{N}$.

$x_u(t)$ is a solution to Eq. (3.6) and therefore

$$\dot{x}_u(t) = [A]x_u(t) + [B]u(t)\ \forall t \tag{B.1}$$

Since x_u is $\tau-$periodic one can also show that

$$\dot{x}_u(t) = [A]x_u(t) + [B]u(t+\tau)\ \forall t \tag{B.2}$$

Subcontracting Eq. (B.2) from Eq. (B.1), one obtains $[B](u(t+\tau) - u(t)) = 0\ \forall t$. This in turn implies that τ is also a period of u, as the columns of $[B]$ are assumed to be linearly independent. Therefore, $\tau = nT$ for some $n \in \mathbb{N}$.

Let us by contradiction assume $n \geq 2$. Integrate Eq. (B.1) from $t = s + T$ to

$s + nT$ and use the periodicity property of u to obtain

$$\begin{aligned} x_u(s+nT) = &\int_{s+T}^{s+nT} e^{[A](s+nT-t)}[B]u(t)\ dt \\ &+ e^{[A](n-1)T}x_u(s+T) \\ &= \sum_{k=0}^{n-2} e^{[A]kT}\left(\int_s^{s+T} e^{[A](s+T-t)}[B]u(t)\ dt\right) \\ &+ e^{[A](n-1)T}x_u(s+T) \end{aligned} \tag{B.3}$$

Also, integrating Eq. (B.1) from $t = s$ to $s + T$ gives

$$x_u(s+T) = \int_s^{s+T} e^{[A](s+T-t)}[B]u(t)\ dt + e^{[A]T}x_u(s) \tag{B.4}$$

Combining Eq. (B.3) and Eq. (B.4) with the fact that $x_u(s + nT) = x_u(s + T)$ results in the following equality.

$$\left(\sum_{k=0}^{n-1} e^{[A]kT}\right)(x_u(s+T) - x_u(s)) = 0 \tag{B.5}$$

Denote by [J] the Jordan form of matrix [A] and define the similarity transformation matrix $[P]$ such that $[A] = [P][J]P^{-1}$. Then,

$$\begin{aligned} det\left(\sum_{k=0}^{n-1} e^{[A]kT}\right) &= det\left([P]\left(\sum_{k=0}^{n-1} e^{[J]kT}\right)[P]^{-1}\right) \\ &= \prod_{\lambda\in\Lambda}\left(\sum_{k=0}^{n-1} e^{k\lambda T}\right) \end{aligned} \tag{B.6}$$

Since $\lambda \notin R$, one has $e^{\lambda T} \neq 1$. Hence, $\sum_{k=0}^{n-1} e^{k\lambda T} = \frac{1-e^{n\lambda T}}{1-e^{\lambda T}} \neq 0$. Therefore, $\sum_{k=0}^{n-1} e^{[A]kT}$ is always a nonsingular matrix and it follows form Eq. (B.5) that

$$x_u(s+T) = x_u(s), \forall s \in \mathbb{R} \tag{B.7}$$

This is contradictory with the assumption of $n \geq 2$ and hence $\tau = T$.

Proof of Statement 2: Suppose there exists a unique periodic state trajectory, x_u, corresponding to the periodic input trajectory, u. Set s in Eq. (B.4) equal to

zero and use the result of Statement 1 to obtain the following.

$$[E]x_u(0) = \int_0^T e^{[A](T-t)}[B]u(t)\,dt \tag{B.8}$$

where $[E] = [I] - e^{[A]T}$, and [I] is the identity matrix of proper dimension. Since x_u is assumed to be unique, the solution of Eq. (B.8) must be a singleton, implying that $[E]$ is an invertible matrix.

Conversely, assume $[E]$ is invertible. Then, $x_u(0)$ is uniquely determined from Eq. (B.8) for any given u. The knowledge of $x_u(0)$ and u together, leads to the unique determination of a periodic state trajectory, x_u.

Define $R = \{\lambda : \lambda = \frac{2k\pi i}{T}, k \in \mathbb{Z}\}$. Now, what is left to show is that the invertibility of $[E]$ is equivalent to saying that the set of eigenvalues of $[A]$ and R are two disjoint sets. For that, we need to see what the invertibility of $[E]$ imposes on the configuration of the eigenvalues of $[A]$ in the complex plane. Transforming $[A]$ into its Jordan form, one obtains:

$$\begin{aligned} det([E]) &= det\left([P]\left([I] - e^{[J]T}\right)[P]^{-1}\right) \\ &= det\left([I] - e^{[J]T}\right) \end{aligned} \tag{B.9}$$

Thus, $[E]$ is singular if and only if $[A]$ has an eigenvalue λ such that $e^{\lambda T} = 1$. Finally, it is readily seen that the set R is nothing but the collection of all the roots of the equation $e^{\lambda T} = 1$ in the complex plane.

Proof of Statement 3: The input matrix, $[B]$, is assumed to be full column rank. Therefore, the Eq. (B.1) can be uniquely solved for u and Eq. (3.8) is obtained.

Bibliography

[1] Horn, F. and R. Lin (1967) "Periodic processes: a variational approach," *Industrial & Engineering Chemistry Process Design and Development*, **6**(1), pp. 21–30.

[2] Horn, F. and J. Bailey (1968) "An application of the theorem of relaxed control to the problem of increasing catalyst selectivity," *Journal of Optimization Theory and Applications*, **2**(6), pp. 441–449.

[3] Douglas, J. (1967) "Periodic reactor operation," *Industrial & Engineering Chemistry Process Design and Development*, **6**(1), pp. 43–48.

[4] Furzer, I. (1973) "Periodic cycling of plate columns," *Chemical Engineering Science*, **28**(1), pp. 296–299.

[5] Parulekar, S. J., R. S. Waghmare, and H. C. Lim (1988) "Yield optimization for multiple reactions," *Chemical engineering science*, **43**(11), pp. 3077–3091.

[6] Watanabe, N., K. Onogi, and M. Matsubara (1981) "Periodic control of continuous stirred tank reactors–I: The pi criterion and its applications to isothermal cases," *Chemical Engineering Science*, **36**(5), pp. 809–818.

[7] De Klerk, P. and M. Gatto (1981) "Some remarks on periodic harvesting of a fish population," *Mathematical Biosciences*, **56**(1-2), pp. 47–69.

[8] Park, E.-J., M. Iannelli, M.-Y. Kim, and S. Anita (1998) "Optimal harvesting for periodic age-dependent population dynamics," *SIAM Journal on Applied Mathematics*, **58**(5), pp. 1648–1666.

[9] Luo, Z., W.-T. Li, and M. Wang (2004) "Optimal harvesting control problem for linear periodic age-dependent population dynamics," *Applied mathematics and computation*, **151**(3), pp. 789–800.

[10] Xiao, Y., D. Cheng, and H. Qin (2006) "Optimal impulsive control in periodic ecosystem," *Systems & Control Letters*, **55**(7), pp. 558–565.

[11] Speyer, J. L. (1976) "Nonoptimality of the steady-state cruise for aircraft," *AIAA Journal*, **14**(11), pp. 1604–1610.

[12] Grimm, W., K. Well, and H. Oberle (1986) "Periodic Control for Minimum Fuel Aircraft Trajectories," *Journal of Guidance, Control, and Dynamics*, **9**(2), pp. 169–174.

[13] Chuang, C.-H. and J. L. Speyer (1987) "Periodic optimal hypersonic scramjet cruise," *Optimal Control Applications and Methods*, **8**(3), pp. 231–242.

[14] Dewell, L. D. and J. L. Speyer (1997) "Fuel-optimal periodic control and regulation in constrained hypersonic flight," *Journal of guidance, control, and dynamics*, **20**(5), pp. 923–932.

[15] Chuang, C. and H. Morimoto (1997) "Periodic optimal cruise for a hypersonic vehicle with constraints," *Journal of Spacecraft and Rockets*, **34**(2), pp. 165–171.

[16] Gilbert, E. G. (1976) "Vehicle cruise: Improved fuel economy by periodic control," *Automatica*, **12**(2), pp. 159–166.

[17] Li, S. E., S. Xu, G. Li, and B. Cheng (2014) "Periodicity based cruising control of passenger cars for optimized fuel consumption," in *Intelligent Vehicles Symposium Proceedings, 2014 IEEE*, IEEE, pp. 1097–1102.

[18] Xu, S., S. E. Li, X. Zhang, B. Cheng, and H. Peng (2015) "Fuel-optimal cruising strategy for road vehicles with step-gear mechanical transmission," *IEEE Transactions on Intelligent Transportation Systems*, **16**(6), pp. 3496–3507.

[19] Goswami, A., B. Espiau, and A. Keramane (1996) "Limit cycles and their stability in a passive bipedal gait," in *Robotics and Automation, 1996. Proceedings., 1996 IEEE International Conference on*, vol. 1, IEEE, pp. 246–251.

[20] Grizzle, J. W., F. Plestan, and G. Abba (1999) "Poincare's method for systems with impulse effects: application to mechanical biped locomotion," in *Decision and Control, 1999. Proceedings of the 38th IEEE Conference on*, vol. 4, IEEE, pp. 3869–3876.

[21] Mombaur, K. D., H. G. Bock, J. P. Schlöder, and R. W. Longman (2005) "Open-loop stable solutions of periodic optimal control problems in robotics," *ZAMM-Journal of Applied Mathematics and Mechanics/Zeitschrift für Angewandte Mathematik und Mechanik*, **85**(7), pp. 499–515.

[22] Han, M., G. Feichtinger, and R. F. Hartl (1994) "Nonconcavity and proper optimal periodic control," *Journal of Economic Dynamics and Control*, **18**(5), pp. 975–990.

[23] Maurer, H., C. Büskens, and G. Feichtinger (1998) "Solution techniques for periodic control problems: A case study in production planning," *Optimal Control Applications and Methods*, **19**(3), pp. 185–203.

[24] Canale, M., L. Fagiano, and M. Milanese (2010) "High altitude wind energy generation using controlled power kites," *IEEE Transactions on Control Systems Technology*, **18**(2), pp. 279–293.

[25] Kehs, M. A., C. Vermillion, and H. K. Fathy (2015) "Maximizing average power output of an airborne wind energy generator under parametric uncertainties," in *ASME 2015 Dynamic Systems and Control Conference*, American Society of Mechanical Engineers, pp. V002T21A001–V002T21A001.

[26] Sager, S., C. Kirches, and H. G. Bock (2008) "Fast solution of periodic optimal control problems in automobile test-driving with gear shifts," in *Decision and Control, 2008. CDC 2008. 47th IEEE Conference on*, IEEE, pp. 1563–1568.

[27] Zhao, Y. J. (2004) "Optimal patterns of glider dynamic soaring," *Optimal control applications and methods*, **25**(2), pp. 67–89.

[28] Traugott, J., A. Nesterova, and G. Sachs (2013) "The flight of the albatross," *IEEE Spectrum*, **50**(7), pp. 46–54.

[29] Bailey, J. and F. Horn (1971) "Comparison between two sufficient conditions for improvement of an optimal steady-state process by periodic operation," *Journal of Optimization Theory and Applications*, **7**(5), pp. 378–384.

[30] Bittanti, S., A. Locatelli, and C. Maffezzoni (1974) "Second-variation methods in periodic optimization," *Journal of Optimization Theory and Applications*, **14**(1), pp. 31–49.

[31] Speyer, J. and R. Evans (1984) "A second variational theory for optimal periodic processes," *IEEE Transactions on Automatic Control*, **29**(2), pp. 138–148.

[32] Gilbert, E. G. (1977) "Optimal periodic control: A general theory of necessary conditions," *SIAM Journal on Control and Optimization*, **15**(5), pp. 717–746.

[33] Barbu, V. and N. Pavel (1996) "Periodic optimal control in Hilbert space," *Applied mathematics & optimization*, **33**(2), pp. 169–188.

[34] Bittanti, S., G. Fronza, and G. Guardabassi (1973) "Periodic control: A frequency domain approach," *IEEE Transactions on Automatic Control*, **18**(1), pp. 33–38.

[35] Bernstein, D. and E. Gilbert (1980) "Optimal periodic control: The π test revisited," *IEEE Transactions on Automatic Control*, **25**(4), pp. 673–684.

[36] Bernstein, D. (1985) "Control constraints, abnormality, and improved performance by periodic control," *IEEE transactions on automatic control*, **30**(4), pp. 367–376.

[37] Varga, A. and S. Pieters (1998) "Gradient-based approach to solve optimal periodic output feedback control problems," *Automatica*, **34**(4), pp. 477–481.

[38] Chen, C.-C., C. Hwang, and R. Y. Yang (1994) "Optimal periodic forcing of nonlinear chemical processes for performance improvements," *The Canadian Journal of Chemical Engineering*, **72**(4), pp. 672–682.

[39] Evans, R., J. Speyer, and C. Chuang (1987) "Solution of a periodic optimal control problem by asymptotic series," *Journal of optimization Theory and Applications*, **52**(3), pp. 343–364.

[40] Speyer, J. L. and R. T. Evans (1981) "A shooting method for the numerical solution of optimal periodic control problems," in *Decision and Control including the Symposium on Adaptive Processes, 1981 20th IEEE Conference on*, vol. 20, IEEE, pp. 168–174.

[41] van Noorden, T. L., S. V. Lunel, and A. Bliek (2003) "Optimization of cyclically operated reactors and separators," *Chemical engineering science*, **58**(18), pp. 4115–4127.

[42] Varigonda, S., T. T. Georgiou, and P. Daoutidis (2001) "A flatness based algorithm for optimal periodic control problems," in *American Control Conference, 2001. Proceedings of the 2001*, vol. 2, IEEE, pp. 831–836.

[43] ——— (2004) "Numerical solution of the optimal periodic control problem using differential flatness," *IEEE Transactions on Automatic Control*, **49**(2), pp. 271–275.

[44] Guay, M., D. Dochain, M. Perrier, and N. Hudon (2005) "Extremum-seeking control over periodic orbits," *IFAC Proceedings Volumes*, **38**(1), pp. 206–211.

[45] ——— (2007) "Flatness-based extremum-seeking control over periodic orbits," *IEEE Transactions on Automatic Control*, **52**(10), pp. 2005–2012.

[46] Höffner, K., N. Hudon, and M. Guay (2007) "On-Line Feedback Control for Optimal Periodic Control Problems," *The Canadian Journal of Chemical Engineering*, **85**(4), pp. 479–489.

[47] Azzato, J. and J. B. Krawczyk (2008) "Applying a finite-horizon numerical optimization method to a periodic optimal control problem," *Automatica*, **44**(6), pp. 1642–1651.

[48] Dickinson, M. H., F.-O. Lehmann, and S. P. Sane (1999) "Wing rotation and the aerodynamic basis of insect flight," *Science*, **284**(5422), pp. 1954–1960.

[49] Sane, S. P. and M. H. Dickinson (2001) "The control of flight force by a flapping wing: lift and drag production," *Journal of experimental biology*, **204**(15), pp. 2607–2626.

[50] Lentink, D. and M. H. Dickinson (2009) "Rotational accelerations stabilize leading edge vortices on revolving fly wings," *Journal of the American Helicopter Society*, **212**(16), pp. 2705–2719.

[51] Mayo, D. B. and J. G. Leishman (2010) "Comparison of the hovering efficiency of rotating wing and flapping wing micro air vehicles," *Journal of Fluid Mechanics*, **55**(2), pp. 25001–25001.

[52] Berman, G. J. and Z. J. Wang (2007) "Energy-minimizing kinematics in hovering insect flight," *Journal of Fluid Mechanics*, **582**, pp. 153–168.

[53] Nabawy, M. R. and W. J. Crowther (2015) "Aero-optimum hovering kinematics," *Bioinspiration & biomimetics*, **10**(4), p. 044002.

[54] Pesavento, U. and Z. J. Wang (2009) "Flapping wing flight can save aerodynamic power compared to steady flight," *Physical review letters*, **103**(11), p. 118102.

[55] Zheng, L., T. Hedrick, and R. Mittal (2013) "A comparative study of the hovering efficiency of flapping and revolving wings," *Bioinspiration & biomimetics*, **8**(3), p. 036001.

[56] Varigonda, S., T. T. Georgiou, R. A. Siegel, and P. Daoutidis (2008) "Optimal periodic control of a drug delivery system," *Computers and Chemical Engineering*, **32**(10), pp. 2256–2262.

[57] Hudon, N., K. Höffner, and M. Guay (2008) "Existence of optimal homoclinic orbits," in *Proceedings of the American Control Conference*, pp. 3829–3833.

[58] Porchet, H. C., N. L. Benowitz, and L. B. Sheiner (1988) "Pharmacodynamic Model of Tolerance: Application to Nicotine," *The Journal of Pharmacology and Experimental Therapeutics*, **244**(1), pp. 231–236.

[59] Sastry, S. S. and A. Isidori (1989) "Adaptive control of linearizable systems," *IEEE Transactions on Automatic Control*, **34**(11), pp. 1123–1131.

[60] Taylor, D. G., P. V. Kokotovic, R. Marino, and I. Kannellakopoulos (1989) "Adaptive regulation of nonlinear systems with unmodeled dynamics," *IEEE Transactions on Automatic Control*, **34**(4), pp. 405–412.

[61] Kanellakopoulos, I., P. V. Kokotovic, and R. Marino (1991) "An extended direct scheme for robust adaptive nonlinear control," *Automatica*, **27**(2), pp. 247–255.

[62] Mrino, R., I. Kanellakopoulos, and P. Kokotovic (1989) "Adaptive tracking for feedback linearizable SISO systems," in *Decision and Control, 1989., Proceedings of the 28th IEEE Conference on*, IEEE, pp. 1002–1007.

[63] Kanellakopoulos, I., P. V. Kokotovic, and A. S. Morse (1991) "Systematic design of adaptive controllers for feedback linearizable systems," in *American Control Conference, 1991*, IEEE, pp. 649–654.

[64] Krstić, M., I. Kanellakopoulos, and P. Kokotović (1992) "Adaptive nonlinear control without overparametrization," *Systems & Control Letters*, **19**(3), pp. 177–185.

[65] Marino, R. and P. Tomei (1993) "Robust stabilization of feedback linearizable time-varying uncertain nonlinear systems," *Automatica*, **29**(1), pp. 181–189.

[66] Polycarpou, M. M. and P. A. Ioannou (1996) "A robust adaptive nonlinear control design," *Automatica*, **32**(3), pp. 423–427.

[67] Yao, B. and M. Tomizuka (1997) "Adaptive robust control of SISO nonlinear systems in a semi-strict feedback form," *Automatica*, **33**(5), pp. 893–900.

[68] Ellington, C. P., C. Van Den Berg, A. P. Willmott, and A. L. Thomas (1996) "Leading-edge vortices in insect flight," *Nature*, **384**(6610), p. 626.

[69] Fry, S. N., R. Sayaman, and M. H. Dickinson (2003) "The aerodynamics of free-flight maneuvers in Drosophila," *Science*, **300**(5618), pp. 495–498.

[70] Zheng, L., T. Hedrick, and R. Mittal (2013) "A comparative study of the hovering efficiency of flapping and revolving wings," *Bioinspiration & biomimetics*, **8**(3), p. 036001.

[71] Colonius, F. (1988) *Optimal periodic control*, Springer.

[72] Sane, S. P. (2003) "The aerodynamics of insect flight," *Journal of experimental biology*, **206**(23), pp. 4191–4208.

[73] Sun, M. and J. Tang (2002) "Unsteady aerodynamic force generation by a model fruit fly wing in flapping motion," *Journal of experimental biology*, **205**(1), pp. 55–70.

[74] Lee, Y., K. Lua, T. Lim, and K. Yeo (2016) "A quasi-steady aerodynamic model for flapping flight with improved adaptability," *Bioinspiration & biomimetics*, **11**(3), p. 036005.

[75] Dudley, R. and C. Ellington (1990) "Mechanics of forward flight in bumblebees: I. Kinematics and morphology," *Journal of Experimental Biology*, **148**(1), pp. 19–52.

[76] ——— (1990) "Mechanics of forward flight in bumblebees: II. Quasi-steady lift and power requirements," *Journal of Experimental Biology*, **148**(1), pp. 53–88.

[77] Willmott, A. P. and C. P. Ellington (1997) "The mechanics of flight in the hawkmoth Manduca sexta. II. Aerodynamic consequences of kinematic and morphological variation." *Journal of Experimental Biology*, **200**(21), pp. 2723–2745.

[78] Usherwood, J. R. and C. P. Ellington (2002) "The aerodynamics of revolving wings I. Model hawkmoth wings," *Journal of Experimental biology*, **205**(11), pp. 1547–1564.

[79] ——— (2002) "The aerodynamics of revolving wings II. Propeller force coefficients from mayfly to quail," *Journal of Experimental Biology*, **205**(11), pp. 1565–1576.

[80] Sane, S. P. and M. H. Dickinson (2002) "The aerodynamic effects of wing rotation and a revised quasi-steady model of flapping flight," *Journal of experimental biology*, **205**(8), pp. 1087–1096.

[81] Whitney, J. and R. Wood (2010) "Aeromechanics of passive rotation in flapping flight," *Journal of Fluid Mechanics*, **660**, pp. 197–220.

[82] Sedov, L. and P. A. Libby (1966) "Two-dimensional problems in hydrodynamics and aerodynamics," *Journal of Applied Mechanics*, **33**, p. 237.

[83] Fahroo, F. and I. M. Ross (2001) "Costate estimation by a Legendre pseudospectral method," *Journal of Guidance, Control, and Dynamics*, **24**(2), pp. 270–277.

[84] Ghanaatpishe, M. and H. K. Fathy (2017) "On the Structure of the Optimal Solution to a Periodic Drug-Delivery Problem," *Journal of Dynamic Systems, Measurement, and Control*, **139**(7), p. 071001.

[85] Hudon, N., M. Guay, M. Perrier, and D. Dochain (2006) "Nonlinear Model Predictive Control for Optimal Discontinuous Drug Delivery," in *Proceedings of the 2006 IFAC ADCHEM Conference*, pp. 527–532.

[86] Ghanaatpishe, M., M. Kehs, and H. K. Fathy (2015) "Development of online solution algorithms for optimal periodic control problems with plant uncertainties," in *2015 American Control Conference (ACC)*, IEEE, pp. 3576–3582.

[87] Ghanaatpishe, M., M. A. Kehs, and H. K. Fathy (2017) "Online Shaping of a Drug's Periodic Administration Trajectory for Efficacy Maximization," *IEEE Transactions on Control Systems Technology*.

[88] Pavlov, A. V., N. Wouw, and H. Nijmeijer (2006) *Uniform output regulation of nonlinear systems: a convergent dynamics approach*, Springer Science & Business Media.

[89] De Leenheer, P. and D. Aeyels (2001) "Stabilization of positive linear systems," *Systems & Control Letters*, **44**(4), pp. 259–271.

[90] Angeli, D. and E. D. Sontag (2003) "Monotone control systems," *IEEE Transactions on Automatic Control*, **48**(10), pp. 1684–1698, 0206133.

[91] Robbins, H. (1967) "A generalized Legendre-Clebsch condition for the singular cases of optimal control," *IBM Journal of Research and Development*, **11**(4), pp. 361–372.

[92] Powers, W. (1980) "On the order of singular optimal control problems," *Journal of optimization theory and applications*, **32**(4), pp. 479–489.

[93] Kopp, R. E. and H. G. MoYER (1965) "Necessary conditions for singular extremals," *AIAA Journal*, **3**(8), pp. 1439–1444.

[94] Kelley, H. J. (1964) "A second variation test for singular extremals," *AIAA Journal*, **2**(8), pp. 1380–1382.

[95] Bliss, G. A. (1946) *Lectures on the Calculus of Variations*, Chicago Univ. Press, Chicago, IL.

[96] Kamien, M. I. and N. L. Schwartz (2012) *Dynamic optimization: the calculus of variations and optimal control in economics and management*, Courier Corporation.

[97] Hull, D. G. (2013) *Optimal control theory for applications*, Springer Science & Business Media.

[98] Sussmann, H. J. and J. C. Willems (1997) "300 years of optimal control: from the brachystochrone to the maximum principle," *IEEE Control Systems*, **17**(3), pp. 32–44.

[99] Ghanaatpishe, M. and H. K. Fathy (in review) "An Adaptive Control Algorithm for Tracking Parametric Reference Trajectories in Feedback Linearizable Systems," *Automatica*.

[100] Philip, E., W. Murray, and M. A. Saunders (2015) "UserâĂŹs Guide for SNOPT Version 7: Software for Large-Scale Nonlinear Programming," .

[101] Gill, P. E., W. Murray, and M. A. Saunders (2005) "SNOPT: An SQP algorithm for large-scale constrained optimization," *SIAM review*, **47**(1), pp. 99–131.

[102] Su, R. (1982) "On the linear equivalents of nonlinear systems," *Systems & control letters*, **2**(1), pp. 48–52.

[103] Isidori, A. and A. Krener (1982) "On feedback equivalence of nonlinear systems," *Systems & Control Letters*, **2**(2), pp. 118–121.

[104] Hunt, L., R. Su, and G. Meyer (1983) "Global transformations of nonlinear systems," *IEEE Transactions on automatic control*, **28**(1), pp. 24–31.

[105] Mitter, S., J. B. Baillieul, and J. Willems (2012) *Mathematical control theory*, Springer Science & Business Media.

[106] Jakubczyk, B. (1980) "On linearization of control systems," *Bull. Acad. Polonaise Sci. Ser. Sci. Math.*, **28**, pp. 517–522.

[107] Ghanaatpishe, M. and H. K. Fathy (in review) "An Adaptive Framework for the Online Optimal Periodic Control of Feedback Linearizable Systems with Unknown Parameters," in *2018 American Control Conference (ACC)*, IEEE.

Vita

Mohammad Ghanaatpishe

Education:
Pennsylvania State University, Ph.D. Mechanical Engineering, Dec. 2017.
Pennsylvania State University, M.Sc. Mechanical Engineering, Dec. 2015.
Sharif University of Technology, B.Sc. Mechanical Engineering, June 2012.

Experience:
Research Assistant, Pennsylvania State University, Aug. 2012 - Jul. 2017.
Research Intern, GE Global Research Center, May 2016 - Aug. 2016.
Teaching Assistant, Pennsylvania State University, Aug. 2016 - Dec 2016.

Personal Website:
https://www.linkedin.com/in/ghanaatpishe/

Selected Publications:

1. Ghanaatpishe, M., & Fathy, H. K. (2017). On the Structure of the Optimal Solution to a Periodic Drug-Delivery Problem. *Journal of Dynamic Systems, Measurement, and Control,* 139(7), 071001.

2. Ghanaatpishe, M., Kehs, M. A., & Fathy, H. K. (2017). Online Shaping of a Drug's Periodic Administration Trajectory for Efficacy Maximization. *IEEE Transactions on Control Systems Technology.*

3. Docimo, D. J., Ghanaatpishe, M., & Mamun, A. (2017). Extended Kalman Filtering to estimate temperature and irradiation for maximum power point tracking of a photovoltaic module. *Energy,* 120, 47-57.

4. Ghanaatpishe, M., Kehs, M., & Fathy, H. K. (2015, July). Development of online solution algorithms for optimal periodic control problems with plant uncertainties. *In American Control Conference (ACC),* 2015 (pp. 3576-3582). IEEE.

5. Docimo, D. J., Ghanaatpishe, M., Rothenberger, M. J., Rahn, C. D., & Fathy, H. K. (2014). The lithium-ion battery modeling challenge: a dynamic systems and control perspective. *Mechanical Engineering,* 136(6), S7.

6. Docimo, D., Ghanaatpishe, M., & Fathy, H. K. (2014). Development and experimental parameterization of a physics-based second-order lithium-ion battery model. *ASME Paper No. DSCC2014-6270.*